Department of Aeronautics and Astronautics
Stanford University
Stanford, California

THE DISPERSION AND DISSIPATION OF WAVES IN BLOOD VESSELS

by

James A. Maxwell and Max Anliker

SUDAAR No. 312

May 1967

This work was performed at Stanford University
with the sponsorship of the
U. S. Army Research Office under Contract No. DA-31-124-ARO-D-223
and the National Science Foundation under Grant No. GK-47

ACKNOWLEDGEMENT

The author would like to express his deep appreciation to Professor Max Anliker for his invaluable guidance and advice both before and during the course of this study. Thanks are also due to Professors I-Dee Chang and Maurice L. Rasmussen for reading the preliminary manuscript and for their criticisms and suggestions.

The work presented here was supported in part by the National Science Foundation under grant NSF GK-47, the Army Research Office under ARO-D-223 and the Ames Research Center, NASA.

Finally, the author wishes to thank his wife, Trudy, for her patience and encouragement.

ABSTRACT

Dispersion and dissipation phenomena associated with waves propagating in blood vessels are potential measures of the distensibility of the vessels and other cardiovascular parameters. In this investigation we assume the vessels to behave like thin-walled circular cylindrical shells filled with an inviscid compressible fluid. The vessel wall is assumed to have isotropic and homogeneous viscoelastic properties. The waves are described by small three-dimensional displacements of the middle surface of the shell from an equilibrium configuration defined by a mean transmural pressure and an initial axial strain. The fluid motion associated with the waves is considered as irrotational. The linearized differential equations of motion are based on the shell equations derived by Flügge.

While all previous work on wave propagation in blood vessels has been restricted to axisymmetric waves, we include in our consideration waves which exhibit a circumferential dependence of the corresponding displacements of the vessel wall. For each circumferential wave number we find infinitely many waves with individual speeds of propagation, of which only the three slowest waves are not due to the compressibility of the fluid. In this study we disregard all but the three slowest waves, and denote these as waves of type I, II and III. In waves of type I the radial displacement component is dominant at high frequencies, while in waves of type II the circumferential and in waves of type III the axial displacement component dominate at high frequencies. Of these three types of waves, those of type II and III are less important from the practical point of view, since only type I waves are associated with significant internal pressure fluctuations.

The results of a parametric analysis assuming a purely elastic model for the vessel wall indicate that axisymmetric waves are only mildly dispersive while non-axisymmetric waves are highly dispersive and exhibit cut-off phenomena. The transmural pressure and the initial axial stretch can have a marked effect on phase velocities, mode shapes and cut-off frequencies of waves of all three types.

The viscoelastic properties of the vessel wall are treated by assuming that the wall material is incompressible but behaves as a Voigt solid in shear. Using such a viscoelastic model it is found that the decrease per wavelength in wave amplitudes is essentially independent of frequency over a wide range of high frequencies. This result is in qualitative agreement with recent experiments on the dissipation of high frequency waves in the thoracic aorta of anesthetized dogs. Axisymmetric waves of type II and type III exhibit stronger dispersion as compared with the elastic case, while those of type I remain only slightly dispersive. In contrast to the elastic case, non-axisymmetric waves are propagated at all frequencies, although the damping per wavelength of such waves is very strong at frequencies below the elastic cut-off point. For viscoelastic walls the dissipation of waves shows a high sensitivity to changes in the transmural pressure and initial axial stretch. Consequently, the reliable estimation of the viscoelastic parameters of the vessel wall from experiments involving high frequency wave propagation must take into consideration the effects of axial stretch and transmural pressure.

TABLE OF CONTENTS

Table of Contents (Continued)

LIST OF ILLUSTRATIONS

List of Illustrations (Continued)

List of Illustrations (Continued)

List of Illustrations (Continued)

List of Illustrations (Continued)

NOMENCLATURE

a = equilibrium radius of the middle surface of the vessel wall

A_λ = wave amplitude at a distance of one wavelength from origin

A_o = wave amplitude at origin

A_{sc}, B_{sc}, C_{sc} = mode amplitudes for circumferential wave number s, phase velocity c

$c = \frac{\omega}{k_R}$ = axial phase velocity

$c_b = (3E_o/\rho_w)^{1/2}$ = normalizing phase velocity (viscoelastic shell)

c_f = speed of sound in blood

$c_p = [E/\rho_w(1-\nu^2)]^{1/2}$ = normalizing phase velocity (elastic shell)

$\bar{c} = c/c_p$ = dimensionless phase velocity (elastic shell)

$\hat{c} = c/c_b$ = dimensionless phase velocity (viscoelastic shell)

$c^* = c_f/c_p$ = dimensionless speed of sound in blood (elastic shell)

$\hat{c}^* = c_f/c_b$ = dimensionless speed of sound in blood (viscoelastic shell)

$D = \partial/\partial t$ = differential operator

D_{sc} = constant related to initial conditions of fluid

$e^2 = h^2/(12a^2)$ = dimensionless parameter

E = Young's modulus of vessel wall

E_o = zero frequency modulus, viscoelastic shell

$\hat{E}$ = complex Young's modulus

G = elastic shear modulus

h = thickness of vessel wall

i = $\sqrt{-1}$

$I_s(\xi)$ = modified Bessel function of the first kind, argument ξ

ka = $(k_R + ik_I)a$ = complex axial wave number

k_R = $Re(ka/a)$

k_I = $Im(ka/a)$

K = elastic bulk modulus

L_{ij} = differential operators

m_f = radial apparent mass of blood contained in the vessel

p_e = external pressure applied to vessel

p_i = perturbed internal pressure applied to vessel

p_{io} = unperturbed internal pressure

P,P' = viscoelastic operators

q_1 = $T_{1O}(1-\nu^2)/Eh$ = dimensionless axial stress resultant

q_2 = $a\Delta p(1-\nu^2)/Eh$ = dimensionless radial stress resultant

q_1 = $T_{1O}/(3E_o h)$ = dimensionless axial stress resultant (viscoelastic shell)

q_2 = $a\Delta p/(3E_o h)$ = dimensionless radial stress resultant (viscoelastic shell)

Q,Q' = viscoelastic operators

r = coordinate in radial direction

s = circumferential wave number

t = time

T_{lo} = initial axial tension of vessel

u,v,w = displacements of vessel middle surface in axial, circumferential and radial directions, respectively

$\bar{v}$ = fluid velocity

x = coordinate in axial direction

α = x/a = dimensionless axial coordinate

β = coordinate in circumferential direction

Δp = $p_{io} - p_e$ = transmural pressure

η = vessel wall coefficient of viscosity

$\hat{\eta}$ = $\eta/(a\rho_w\sqrt{E_o/\rho_w})$ = dimensionless vessel wall coefficient of viscosity

μ_f = fluid inertia parameter

μ_w = $(1-\nu^2)a^2(\rho_w h)/Eh$ = wall inertia parameter

ν = Poisson's ratio

$\hat{\nu}$ = Complex Poisson's ratio (viscoelastic shell)

$\bar{\rho}$ = ρ_f/ρ_w = dimensionless density ratio

ρ_f = blood density

ρ_w = vessel wall density

Φ = fluid velocity potential

ξ = $\frac{\omega a}{c}(1 - c^2/c_p^2)^{1/2}$ = dimensionless parameter

ω = angular frequency

$\bar{\omega}$ = $\omega a/c_p$ = dimensionless angular frequency (elastic shell)

$\hat{\omega}$ = $\omega a/c_b$ = dimensionless angular frequency (viscoelastic shell)

∇ = gradient operator

∇^2 = Laplacian operator

INTRODUCTION

The transmission velocity of the natural pulse wave in an artery of given diameter and wall thickness has long been recognized as an approximate measure of the elasticity or distensibility of that artery.[1] A rough estimate of the elasticity in the form of an effective Young's modulus can be obtained through the Moens-Korteweg equation:

$$c^2 = \frac{Eh}{2\rho_f a}$$

in which c denotes the signal velocity, E Young's modulus, h the wall thickness, a the radius of the vessel, and ρ_f the density of the blood.

For a comparative study of different physiological situations or a study of the effects of various stresses such as prolonged weightlessness or acceleration on the elastic properties of blood vessels, we need a more precise quantitative description than that afforded by the natural pulse wave and the Moens-Korteweg equation.

If we consider the propagation of a pulse wave in the vascular system as a problem of applied mechanics, we expect the pulse wave velocity to be a function of the following properties and parameters:

Elastic properties of vessel wall

Diameter of vessel (geometry of vessel)

Thickness of vessel wall

Transmural pressure (blood pressure)

Shape of wave

Longitudinal stretch (tension) of vessel

Density of vessel wall

Density of blood

Mean flow and nature of flow

Viscous properties of vessel wall

Compressibility of blood

Viscosity of blood

Properties of vascular bed

The variability of these parameters and properties differs greatly and probably also their significance in affecting the pulse wave velocity. For example, the variations in the densities of the vessel wall and the blood will hardly ever be more than a few percent, while the transmural pressure may vary within seconds by as much as a factor of two or more.

In any attempt to predict theoretically the manner in which a given signal in the form of a pressure fluctuation or vessel wall displacement propagates through the vascular system we have, of course, to resort to approximations by introducing models for the dynamic behavior of the blood, the complex geometry of the vessels, their elastic behavior and the properties of the vascular bed. An incisive review of various earlier approaches in the mathematical analysis of blood flow was published by Fox and Saibel[2] in 1963.

To assess the significance of each of the properties and parameters listed above we have begun a systematic theoretical study taking into consideration the results of recent investigations.[3-10] In the initial phase of our analysis we have introduced the following assumptions:

1. The waves (signals) considered have the form of sinusoidal displacements of the vessel wall.

2. The signals are sufficiently small to allow linearization of the equations.

3. In equilibrium the vessels have the form of a circular cylindrical shell of constant diameter and wall thickness.

4. The vessel wall has uniform and isotropic elastic or viscoelastic properties.

5. The blood behaves like a compressible inviscid fluid.

6. The effects of the vascular bed can be neglected.

It is convenient to divide the analysis into two distinct parts. In the first, the wall is assumed to be purely elastic in nature, obeying Hooke's law for small displacements. In the second part, the wall is assumed to have linear viscoelastic properties for small displacements. In each case, the displacements represent deviations from an equilibrium configuration which is defined by an initial axial stretch and an initial transmural pressure.

Our approach differs from earlier studies in that we do not restrict ourselves to axisymmetric waves, but include in our considerations waves which exhibit a circumferential dependence of the corresponding displacements of the vessel wall. Also, we include the effects on the phase velocities of an initial axial stretch and transmural pressure, which have only recently been considered for low frequency axisymmetric waves by Atabek and Lew.[10] Besides this, our model for the elastic behavior of the vessel incorporates the effects of bending rigidity, which are of importance at all but low frequencies. The influence of blood viscosity on dispersion has been analyzed to some extent by several investigators.[3,4,10] Their results indicate that dispersion due to the viscosity of the blood

appears to be pronounced only at very low frequencies. We have therefore neglected blood viscosity in this first analysis.

PART I - ELASTIC SHELL ANALYSIS

BASIC EQUATIONS

The signals considered are defined by the displacement components u, v, w of an arbitrary point of the middle surface of the vessel in the axial, circumferential and radial direction respectively. As illustrated in Fig. 1, the vessel is referred to a set of cylindrical coordinates x, r, β such that $r = a$ represents the middle surface of the vessel wall. The displacement components u, v, w are thus functions of the two coordinates x and β, implying that the waves to be studied are two-dimensional in character.

The fluid contained within the vessel is assumed to be compressible and inviscid. Besides this we assume that the flow associated with the signals is irrotational and that the effects of a mean flow and of gravity can be neglected. The fluid velocity $\vec{v}$ is then given by

$$\vec{v} = - \nabla\Phi \ . \tag{1}$$

Within the realm of a linearized theory the velocity potential Φ satisfies the three-dimensional continuity equation

$$\nabla^2\Phi = \frac{1}{c_f^2} \frac{\partial^2\Phi}{\partial t^2} \tag{2}$$

with c_f denoting the speed of sound in the fluid. If we let p_i denote the perturbed intra-arterial pressure, p_{io} the internal pressure in the absence of a signal and ρ_f the fluid density, the linearized Euler equation can be written in the form

$$p_i = \rho_f \frac{\partial\Phi}{\partial t} + p_{io} \ . \tag{3}$$

The velocity potential Φ and the radial displacement component w are interconnected through the kinematic boundary condition

$$\frac{\partial w}{\partial t} = - \left(\frac{\partial \Phi}{\partial r}\right)_{r=a} . \tag{4}$$

We now consider solutions to the continuity equation (2) of the form

$$\Phi_{sc} = D_{sc} I_s(\xi \frac{r}{a}) \exp[i \frac{\omega}{c}(x-ct) + is\beta] \tag{5}$$

where D_{sc} is an amplitude defined by initial conditions, s is the circumferential wave number, ω the circular frequency, c the wave velocity, I_s the modified Bessel function of the first kind of order s and

$$\xi = \left(\frac{\omega a}{c}\right)\left(1 - \frac{c^2}{c_f^2}\right)^{1/2} . \tag{6}$$

The vessel is assumed to behave like an elastic, homogeneous, isotropic and thin-walled circular cylindrical shell, its wall thickness is denoted by h, its Young's modulus by E and its Poisson's ratio by ν. The axial stretch of the vessel gives rise to an initial axial tension T_{10} and in the presence of an external pressure p_e the transmural pressure Δp is given by

$$\Delta p = p_{io} - p_e . \tag{7}$$

For convenience we introduce the dimensionless stress resultants in the axial and circumferential directions

$$q_1 = \frac{T_{10}(1-\nu^2)}{Eh} , \tag{8}$$

$$q_2 = \frac{a\Delta p(1-\nu^2)}{Eh} \tag{9}$$

and the two-dimensional Laplacian operator by

$$\nabla^2 = \frac{\partial^2}{\partial\alpha^2} + \frac{\partial^2}{\partial\beta^2} \tag{10}$$

with the non-dimensional axial coordinate α defined by

$$\alpha = \frac{x}{a} \, . \tag{11}$$

The elastic behavior of the vessel wall is assumed to be governed by the linearized equations for circular cylindrical shells derived by W. Flügge[11] which have been shown to be useful also in analyzing the vibrations of cylindrical shells that can no longer be considered as thin-walled.[8] Hence for small displacements from the equilibrium configuration and for shells whose length remains unchanged after the initial axial stretch has been applied we have the following differential equations for the displacement components u, v, w:

$$\begin{aligned} &L_{11}(u) + L_{12}(v) + L_{13}(w) + (q_1 + \nu q_2)\frac{\partial^2 u}{\partial\alpha^2} \\ &\quad + q_2\left(\frac{\partial^2 u}{\partial\beta^2} - \frac{\partial w}{\partial\alpha}\right) - \mu_w \frac{\partial^2 u}{\partial t^2} = 0 \, , \\ &L_{21}(u) + L_{22}(v) + L_{23}(w) + (q_1 + \nu q_2)\frac{\partial^2 v}{\partial\alpha^2} \\ &\quad + q_2\left(\frac{\partial^2 v}{\partial\beta^2} + \frac{\partial w}{\partial\beta}\right) - \mu_w \frac{\partial^2 v}{\partial t^2} = 0 \, , \end{aligned} \tag{12}$$

$$L_{31}(u) + L_{32}(v) + L_{33}(w) - (q_1 + \nu q_2)\frac{\partial^2 w}{\partial \alpha^2} - q_2\left(\frac{\partial u}{\partial \alpha} - \frac{\partial v}{\partial \beta} + \frac{\partial^2 w}{\partial \beta^2}\right)$$

$$+ (\mu_w + \mu_f)\frac{\partial^2 w}{\partial t^2} = 0 \ .$$

The differential operators L_{ij} are defined as

$$L_{11} = \frac{\partial^2}{\partial \alpha^2} + \frac{(1-\nu)}{2}\frac{\partial^2}{\partial \beta^2}(1 + e^2)$$

$$L_{22} = \frac{\partial^2}{\partial \beta^2} + \frac{(1-\nu)}{2}\frac{\partial^2}{\partial \alpha^2}(1 + e^2)$$

$$L_{33} = 1 + e^2\left(\nabla^2\nabla^2 + 2\frac{\partial^2}{\partial \beta^2} + 1\right) \qquad (13)$$

$$L_{12} = L_{21} = \frac{(1+\nu)}{2}\frac{\partial^2}{\partial \alpha \partial \beta}$$

$$L_{13} = L_{31} = \nu\frac{\partial}{\partial \alpha} - e^2\left[\frac{\partial^3}{\partial \alpha^3} - \frac{(1-\nu)}{2}\frac{\partial^3}{\partial \alpha \partial \beta^2}\right]$$

$$L_{23} = L_{32} = \frac{\partial}{\partial \beta} - e^2\left(\frac{3-\nu}{2}\right)\frac{\partial^3}{\partial \alpha^2 \partial \beta}$$

where

$$e^2 = \frac{h^2}{12a^2} \ . \qquad (14)$$

μ_w and μ_f are inertia quantities associated with the wall and the fluid:

$$\mu_w = \frac{(1-\nu^2)}{Eh}a^2(\rho_w h) \qquad (15)$$

$$\mu_f = \frac{(1-\nu^2)}{Eh}a^2 m_f \qquad (16)$$

with m_f denoting the apparent mass of the fluid. By definition, we have

$$- m_f \frac{\partial^2 w}{\partial t^2} = (p_i - p_{io})_{r=a} \tag{17}$$

while from the Euler equation we obtain

$$- m_f \frac{\partial^2 w}{\partial t^2} = \rho_f \left(\frac{\partial \Phi}{\partial t}\right)_{r=a} . \tag{18}$$

We assume solutions to Eqns. (12) of the form

$$u = A_{sc} \exp[i \tfrac{\omega}{c}(x - ct) + is\beta]$$

$$v = B_{sc} \exp[i \tfrac{\omega}{c}(x-ct) + is\beta] \tag{19}$$

$$w = C_{sc} \exp[i \tfrac{\omega}{c}(x-ct) + is\beta + i \tfrac{\pi}{2}] .$$

Combining Eqns. (4), (5), (17) and (18), we find for the apparent mass

$$m_f = \rho_f a \frac{I_s(\xi)}{\xi I_s'(\xi)} . \tag{20}$$

The substitution of (19) into (12) leads to a set of three linear homogeneous equations for the coefficients A_{sc}, B_{sc} and C_{sc}. The requirement that non-trivial solutions exist for A_{sc}, B_{sc} and C_{sc} then leads to the frequency equation of the system. To reduce the frequency equation to a convenient form we introduce the following dimensionless parameters:

$$c_p^2 = E/[\rho_w(1-\nu^2)], \quad \bar{c}^2 = c^2/c_p^2, \quad \bar{\omega}^2 = \omega^2 a^2/c_p^2, \quad \bar{\rho} = \rho_f/\rho_w,$$

$$c^{*2} = c_f^2/c_p^2 . \tag{21}$$

Then

$$\xi = \frac{\bar{\omega}}{\bar{c}}\left(1 - \frac{\bar{c}^2}{c^{*2}}\right)^{1/2} \tag{22}$$

and the frequency equation can be written as

$$\begin{vmatrix} \frac{\bar{\omega}^2}{\bar{c}^2}(1+q_1+\nu q_2)+q_2 s^2 & -\frac{(1+\nu)}{2}\frac{\bar{\omega}}{\bar{c}}\,s & \frac{\bar{\omega}}{\bar{c}}(\nu - q_2)+e^2\left[\frac{\bar{\omega}^3}{\bar{c}^3} \right. \\ + \frac{(1-\nu)}{2}s^2(1+e^2)-\bar{\omega}^2 & & \left. - \frac{(1-\nu)}{2}\frac{\bar{\omega}}{\bar{c}}\,s^2\right]. \\ \hline & \frac{\bar{\omega}^2}{\bar{c}^2}\left[(q_1+\nu q_2)+\frac{(1-\nu)}{2}(1+3e^2)\right] & -e^2\frac{(3-\nu)}{2}\frac{\bar{\omega}^2}{\bar{c}^2}\,s \\ \text{SYMMETRIC} & + (1+q_2)s^2 - \bar{\omega}^2 & -(1+q_2)s \\ \hline & & 1+e^2\left[\left(\frac{\bar{\omega}^2}{\bar{c}^2}+s^2\right)^2\right. \\ & & \left. -2s^2+1\right] + \frac{\bar{\omega}^2}{\bar{c}^2}(q_1+\nu q_2) \\ & & + q_2 s^2 - \left[1+\bar{\rho}\,\frac{a}{h}\,\frac{I_s(\xi)}{\xi I_s'(\xi)}\right]\bar{\omega}^2 \end{vmatrix} = 0 \tag{23}$$

GENERAL RESULTS OF ELASTIC SHELL ANALYSIS

The frequency equation (23) interrelates nine dimensionless parameters: q_1, q_2, ν, s, h/a, $\bar{\rho}$, $\bar{\omega}$, $\bar{c}$ and c*. Young's modulus E, the wall density ρ_w and the radius of the middle surface a do not enter into the equation explicity, but affect the solutions as scale factors through $\bar{\omega}$, $\bar{c}$ and c*. With the aid of an IBM 7094 digital computer we have determined $\bar{c}$ and the corresponding mode shape defined by A_{sc}, B_{sc} and C_{sc} as a function of the 8 other nondimensional parameters.

For each circumferential wave number s we find infinitely many waves with individual speeds of propagation. Within the parameter ranges pertaining to physiological problems all but the three slowest waves of each infinite set of waves for a given s are a direct consequence of the compressibility of the fluid. The results given as graphs in Figures 2 to 54 are based on c_f = 1500 meters/sec and are in agreement within the drawing accuracy with the results for an incompressible fluid ($c_f = \infty$). We shall identify the three slowest waves as waves of type I, II and III. In waves of type I the radial displacement component is dominant at high frequencies, while in waves of type II the circumferential and in waves of type III the axial displacement components dominate at high frequencies. All of the faster waves exhibit cut-off frequencies (frequencies at which the phase velocity is infinite) and are transmitted only at frequencies above 1000 cycles/sec for physiologically meaningful parameter values. In this investigation we shall disregard these waves and consider only waves of type I, II and III.

The general dispersive nature of the waves of type I, II and III is illustrated in Figure 2, which depicts the non-dimensional axial phase

velocity $\bar{c} = c/c_p$ as a function of the frequency parameter $\bar{\omega} = \omega a/c_p$ for $s = 0$ through $s = 5$ and for zero transmural pressure $(q_2 = 0)$ and zero tethering $(q_1 = 0)$. The amplitude patterns corresponding to these waves are shown in Figures 3, 4 and 5 in which the relative magnitudes of the radial, circumferential and axial displacement components are plotted versus $\bar{\omega}$. As is evident from Figures 2 to 5, we find that for $q_1 = 0$ and $q_2 = 0$ the waves of type I, II and III also exhibit cut-off frequencies below which no waves of the kind considered are being propagated. For waves of type II and III the cut-off frequencies are consistently much higher than those of the type I waves. From this we conclude that waves of type II and III can be disregarded in non-axisymmetric signals with predominantly low frequency components. We also note that irrespective of the number of circumferential lobes the amplitude pattern of a given wave generally depends strongly on the frequency, which emphasizes the significance of allowing for the interaction of the three displacement components in the analysis.

Discussion of Type I Waves

The characterization of the type I waves as having a large radial displacement component is in a strict sense only valid for high frequencies. We see from Figure 3 that for $s = 0$ and a decreasing $\bar{\omega}$ the mode shape changes from one with a predominant radial displacement component into one with a predominant axial component. Also, for $s = 1$ we note that for decreasing $\bar{\omega}$ the circumferential component $v1$ begins to exceed

slightly the radial displacement component $w1$. A change of the mode shape for $s = 0$ with decreasing $\bar{\omega}$ is also observed when the density of the fluid is taken as zero. However, this change is more pronounced and takes place at higher frequencies when the shell is filled with a liquid since the apparent mass of the fluid in the radial direction for small $\bar{\omega}$ and $s = 0$ can be written as

$$m_f = 2\rho_f a \frac{\bar{c}^2}{\bar{\omega}^2} \tag{24}$$

and thus becomes unbounded as $\bar{\omega}$ approaches zero. When $\bar{\rho} \approx 1$ and $\bar{\omega}$, q_1, q_2 and h/a are small compared to 1 the displacement components for $s = 0$ are given approximately by

$$\left|\frac{w}{u}\right| \approx \frac{\bar{\omega}(1 + q_2 + \nu q_2)}{\bar{c}(\nu - q_2)}$$

$$\nu = 0 \tag{25}$$

and as $\bar{\omega} \to 0$ the phase velocity approaches

$$\bar{c}^2 \approx \frac{h}{2\bar{\rho}a} + \frac{(\nu - q_2)^2}{1 - 2\bar{\rho}\frac{a}{h}(1 + q_1 + \nu q_2)} \tag{26}$$

When the transmural pressure and the axial stretch are zero ($q_1 = 0$, $q_2 = 0$) and $h/\bar{\rho}a \ll 1$, equation (26) reduces to

$$\bar{c}^2 = \frac{h(1-\nu^2)}{2\bar{\rho}a}$$

or (27)

$$c^2 = \frac{Eh}{2\rho_f a},$$

the familiar Moens-Korteweg equation. It is of interest to note that when the couping between the axial and radial displacement components is neglected, one obtains in lieu of (27)

$$c^2 = \frac{Eh}{2\rho_f a(1-\nu^2)} \tag{28}$$

For $s = 1$ and $\bar{\omega} \to 0$ the limiting phase velocity is zero while the limiting displacement pattern is given by $u = 0$ and $v/w = 1$ which corresponds to a rigid body displacement of the cylinder in the lateral direction.

If we let the wave number ka approach zero in the frequency equation (23) and take $s \geq 1$, we find nontrivial solutions for $\bar{\omega}$, i.e., frequencies at which the phase velocity is infinite. Adhering to the established nomenclature, we call these frequencies cut-off frequencies since no waves of the kind considered are being propagated whenever the frequency is below the cut-off value. Expanding the determinant in (23) for small values of ka and letting $ka \to 0$ we obtain for type I waves the following approximate expression for the cut-off frequencies:

$$\bar{\omega}^2 \approx \frac{s^2(s^2-1)(1+q_2)[e^2(s^2-1) + q_2]}{1 + e^2(s^2-1)^2 + q_2 s^2 + (1+q_2)s(s+\bar{\rho}\,\frac{a}{h})} \tag{29}$$

which is based on the assumptions that $\bar{\rho} \approx 1$, $s \leq 5$, and that q_1, q_2 and h/a are small compared to 1. From (29) we conclude that the cut-off frequencies are independent of the axial stretch q_1. Poisson's ratio ν, Young's modulus E and the wall density ρ_w do not appear in equation (29) but come into play through the reference velocity c_p. For $q_2 \gg e^2(s^2 - 1)$ the cut-off frequency is approximately proportional to

$\sqrt{q_2}$. This dependence of the cut-off frequency on the transmural pressure is clearly illustrated in the lower half of Figure 6, which gives the phase velocity for $s = 2$ and various values of q_2. When we let the transmural pressure assume negative values we find that at a critical value corresponding to $q_2 = -e^2(s^2 - 1)$ the cut-off frequency becomes zero and the system reaches a limiting stability boundary.

On the basis of the same approximations leading to (29) we find that the mode shapes of type I waves at the cut-off frequencies are given by

$$\left|\frac{v}{w}\right| \approx \frac{1}{s} + \frac{e^2(s^2-1)^2 + q_2(s^2 - 1)}{s(1+q_2)[1 + s(s+\bar{\rho}\frac{a}{h})]} \qquad (30)$$

$$u = 0 .$$

Within the realm of physiologically meaningful parameter values, including the case when the transmural pressure is near the critical pressure, we can replace (30) by

$$\left|\frac{v}{w}\right| = \frac{1}{s} , \qquad u = 0 \qquad (31)$$

without introducing a substantial error.

Discussion of Type II Waves

Axisymmetric type II waves ($s = 0$) have no displacement components in the axial and radial direction. They are nondispersive and their propagation velocity is given by

$$\bar{c}^2 = \frac{1-\nu}{2}(1 + 3e^2) + q_1 + \nu q_2 . \qquad (32)$$

These waves are obviously identical with the axisymmetric torsional waves of an empty cylindrical shell since there is no coupling between an inviscid fluid and such a wave motion. For $s \neq 0$ all type II waves have cut-off frequencies at

$$\bar{\omega}^2 = \frac{1-\nu}{2} s^2(1 + e^2) + q_2 s^2. \tag{33}$$

Also, as shown in Figure 4, at cut-off the mode shapes have only an axial displacement component, but at higher frequencies they become almost purely circumferential. The phase velocity of the nonaxisymmetric type II waves approach asymptotically that of the symmetric wave as indicated in Figure 2.

Discussion of Type III Waves

Unlike the case of an empty cylindrical shell, we do not find a cut-off frequency for axisymmetric type II waves[6] but obtain with $\bar{\omega} \to 0$ a limiting phase velocity given approximately by

$$\bar{c}^2 \approx 1 + q_1 + \nu q_2 - \frac{(\nu - q_2)^2}{1 - 2\bar{\rho}\frac{a}{h}(1 + q_1 + \nu q_2)} \tag{34}$$

when $\bar{\rho} \approx 1$ and q_1, q_2 and h/a are small compared to 1. However, when we let the density of the fluid approach zero, the frequency equation (23) yields the established value for the cut-off frequency of such waves:

$$\bar{\omega}^2 = 1 + e^2 . \tag{35}$$

Non-axisymmetric waves of type III exhibit cut-off frequencies as indicated in Figure 2. The expansion of the determinant in (23) for

small wave numbers ka leads to the following approximate expression for the cut-off frequencies:

$$\bar{\omega}^2 \approx \frac{s}{s+\bar{\rho}\frac{a}{h}} [1 + e^2(s^2-1)^2 + q_2 s^2 + s(1+q_2)(s + \bar{\rho}\frac{a}{h})] \qquad (36)$$

while we find for the displacement pattern at cut-off

$$\left|\frac{v}{w}\right| \approx \frac{(1 + q_2)(s + \bar{\rho}\frac{a}{h})}{1 + e^2(s^2-1)^2 + q_2 s^2} \qquad (37)$$

$$u = 0 .$$

Relations (36) and (37) are again based on the assumptions that $\bar{\rho} \approx 1$, $s \leq 5$ and that q_1, q_2 and h/a are small compared to 1. The mode shapes become predominantly radial in nature at high frequencies as shown in Figure 5 and the phase velocities all approach asymptotically

$$\bar{c}^2 = 1 + q_1 + \nu q_2 - e^2 . \qquad (38)$$

PARAMETRIC STUDY OF TYPE I WAVES

The mode shapes of type II and III waves consistently have small displacement components in the radial direction and thus are associated with much smaller fluctuations of the intraluminal pressure than are type I waves. Since we are primarily interested in the propagation of pressure waves we focus our attention initially to a parametric study of type I waves. However, for the sake of completeness, we later also examine the effects of certain parameters on the properties of type II and III waves.

Effects of Transmural Pressure and Axial Stretch

The effects of a transmural pressure and an axial stretch on the phase velocities and mode shapes of type I waves are illustrated in Figures 6 to 9 for $s = 0$ and $s = 2$. The phase velocities and mode shapes have been computed for a set of transmural pressures corresponding to $q_2 = 0.1, 0.2, 0.5$ and 0.8 and a set of axial stretch values corresponding to $q_1 = 0.1$ and 0.2. The selected parameter values can be given physiologically meaningful interpretation. We have for example $q_2 = 0.1$ if $E = 10^6$ dynes/cm^2, $\nu = 0.5$, $h/a = 0.1$, and $\Delta p = 10$ mm Hg, while $q_1 = 0.1$ represents an initial axial strain of 13.3% at zero transmural pressure and $\nu = 0.5$. From Figures 6 and 7 we note that with increasing transmural pressure the phase velocity generally increases for both axisymmetric and nonasixymmetric waves. For $\bar{\omega} < 0.2$ the nondimensional phase velocity $\bar{c}$ of the axisymmetric waves increases less than 30% when q_2 is increased form 0 to 0.8, while for $0.2 \leq \bar{\omega} \leq 1.0$ the corresponding increase is at most 125%. In stating this result it should be mentioned that the shell equations used in this analysis require q_1 and q_2 to be "small" in comparison to 1.0, which implies that the curves for $q_2 = 0.8$ should be considered only as rough approximations.

While the phase velocities and mode shapes of axisymmetric waves are not drastically changed by moderate transmural pressures, we find that the non-axisymmetric waves $s = 2$ are significantly affected. Since in the illustrated example $q_2 \gg e^2(s^2 - 1)$, the cut-off frequencies increase approximately as $\sqrt{q_2}$, which may mean the complete disappearance of waves of this type from the frequency interval $0 \leq \omega \leq 1000$

cycles/second with a sufficient increase in transmural pressure. As indicated earlier, the cut-off frequency for $s = 2$ approaches zero and the system becomes unstable if we let the transmural pressure fall below certain negative values. If we have again $E = 10^6$ dynes/cm^2, $\nu = 0.5$, $h/a = 0.1$ and $q_1 = 0$ we find as critical pressure at which the system becomes instable $\Delta p = -0.25$ mm Hg.

For axisymmetric waves of type I the effect of tethering or axial stretch is small at low frequencies but becomes reasonably significant at higher frequencies where an increase in stretch corresponding to a change of q_1 from 0 to 0.2 causes an increase in wave velocity of almost 100%, as illustrated in Figure 8. For $s = 2$ the wave velocity is markedly increased at all frequencies by essentially a constant amount while the cut-off frequency is independent of q_1. As may be seen from Figure 9, an increase in axial stretch has only little effect on the mode shapes of the waves.

Effects of Geometry, Poisson's Ratio and the Density Ratio

The effect of geometry is examined by comparing phase velocities and mode shapes for $h/a = 0.01$, 0.03, 0.1 and 0.2. The range $0.01 \leq h/a \leq 0.1$ is of interest for veins, while h/a values between 0.1 and 0.3 pertain to arteries. It appears from the graphs in Figures 10 and 11 that the phase velocities and mode shapes of type I waves for $s = 0$, $s = 2$ are greatly affected by changes in h/a and that arteries and veins of like diameter should have distinctly different wave propagation characteristics if they have identical Young's moduli. It should be noted that the radius of the middle surface of the vessel has merely a

scaling effect through the nondimensional frequency parameter $\bar{\omega} = \omega a/c_p$.

According to the graphs in Figures 12 and 13 we find that a change of Poisson's ratio from 0.5 to 0.3 practically does not alter the wave velocity but affects the mode shape to some extent through the reference wave velocity c_p. Finally we conclude from the dispersion curves given in Figures 14 and 15 that minor variations in blood density or wall density should have little effect on the propagation of type I waves since a 10% change of $\bar{\rho}$ leads to less than 10% change in the phase velocities.

PARAMETRIC STUDY OF TYPE II AND TYPE III WAVES

Effects of Transmural Pressure and Axial Stretch

Figure 16 illustrates the effects of a transmural pressure on axisymmetric type II and type III waves, with a type I wave for $q_2 = 0$ presented for purposes of comparison. As in the type I case, type II and III phase velocities increase with increasing transmural pressure. However, while type I waves nearly double their phase velocities when q_2 is increased from 0 to 0.2, those of type II increase less than 20% and those of type III less than 5%. Type II waves remain non-dispersive. Type III waves exhibit dispersion of less than 0.5% for $\bar{\omega} \leq 5.0$, which is so small that it falls within the plotting accuracy of the curves in Figure 16. The mode shapes corresponding to type II waves remain purely circumferential, while the radial component of type III waves, which are small for $q_2 = 0$, become even small with increasing transmural pressure, as can be seen in Figure 17.

Nonaxisymmetric $s = 2$ waves change their phase velocities and cut-off frequencies markedly with transmural pressure. Figure 16 indicates that the relative shift of the cut-off frequencies with increasing q_2 is not as great as in the case of type I waves. From Figure 18, it is evident that mode shapes are not significantly altered by the presence of a transmural pressure, except that the cut-off frequencies are increased.

Figures 19, 20 and 21 illustrate the effect of an axial stretch for values of q_1 between 0 and 0.4. For $s = 0$ and $s = 2$ the phase velocities generally increase with increasing q_1. The type II and type III cut-off frequencies for nonaxisymmetric waves remain independent of q_1. Comparing Figures 16 and 19, it can be seen that the changes in the phase velocities of axisymmetric waves produced by an axial stretch with given q_1 is essentially the same as those changes produced by a transmural pressure corresponding to a value of $q_2 = q_1/\nu$. Mode shapes again are not significantly altered by the presence of an axial stretch. A review of the results given for axisymmetric type III waves indicates that the phase velocities appear to be more sensitive to small changes in the axial stretch parameter q_1 than to small changes in the transmural pressure parameter q_2. Conversely, the amplitude pattern of such waves shows a greater sensitivity to changes in the parameter q_2 than to q_1.

Effects of Geometry, Poisson's Ratio and the Density Ratio

Unlike the case of type I waves, the phase velocities of waves of type II and III are only mildly affected by changes in the thickness ratio h/a, as shown in Figures 22, 23 and 24. In the axisymmetric case, this result for type II waves is well-known and follows immediately from equation (32). As is evident from equations (33) and (36) the cut-

off frequencies for $s = 2$ waves are shifted to slightly higher values as h/a is increased. The axial and circumferential mode shapes of type II and III waves remain practically unchanged as h/a is varied. In the radial direction, however, the displacement is approximately proportional to h/a. This last result could be of experimental significance, since a larger radial displacement implies a larger pressure, which in turn suggests that non-axisymmetric waves of type II and III should be more readily observed in thick walled tubes.

Figures 25, 26 and 27 show that the non-dimensional phase velocities of type II waves are strongly affected by changes in Poisson's ratio for the $s = 0$ and $s = 2$ waves. The type II mode shape remains circumferential when $s = 0$. When $s = 2$, mode shapes of type II waves are essentially unchanged when ν is varied, except that the cut-off frequencies are increased. Likewise, phase velocities and mode shapes of type III waves for both $s = 0$ and $s = 2$ remain nearly unaltered by variations in ν. However, it should be emphasized at this point that Poisson's ratio enters into the reference speed c_p utilized in the normalization of both the phase velocities and frequencies, so that the dimensionalized type III phase velocities and mode shapes will be strong functions of ν.

The phase velocities of axisymmetric type II waves are independent of the density ratio $\bar{\rho}$, as is evident from equation (32). Changes in type III axisymmetric waves are less than 0.15% for $0.9 \leq \bar{\rho} \leq 1.1$, when $h/a = 0.1$, $q_1 = q_2 = 0$ and $\nu = 0.5$, and are therefore entirely insignificant for studying the propagation of such waves in blood vessels. Similarly, when $s = 2$, density ratio variations for $0.9 \leq \bar{\rho} \leq 1.1$

have no pronounced effect on type II waves but a noticeable effect on type III waves near the cut-off frequencies. From equation (36) it follows that the type III cut-off frequencies increase only 0.7% as $\bar{\rho}$ decreases from 1.1 to 0.9, and the values for h/a, q_1, q_2 and ν are the same as those given above. Mode shapes are all virtually identical to those for $\bar{\rho} = 1.0$ except for the small variation in the cut-off frequency of type III waves.

PART II - VISCOELASTIC SHELL ANALYSIS

EFFECTS OF VISCOELASTICITY OF THE VESSEL WALL ON THE DISPERSION AND DISSIPATION OF WAVES

Introduction

The propagation of sounds and pulse waves within the cardiovascular system is subject to strong dissipative mechanisms. The dissipation of waves in blood vessels can be attributed to three main causes: viscosity of the blood, viscoelastic behavior of the wall, and radiation of energy into the surrounding medium. Some data on the combined effect of the various dissipative mechanisms in arteries under in vivo conditions has been deduced from simultaneous recordings of the natural pulse wave at various points along the aorta and other arteries of anesthetized dogs. The data take into account the effects of reflections and dispersion and are based on the assumption that the propagation of pressure pulses generated by the heart is governed by linear laws that permit a harmonic analysis.

Several mathematical models have been postulated for dissipative mechanisms[14,15,16,17] which take into consideration the viscosity of the fluid and viscoelastic properties of the vessel wall, but which largely adhere to a membrane analysis and exclusively consider only axisymmetric waves of type I. Also, these models have neglected the presence of an axial stretch and a transmural pressure, both of which play a significant role.

Recently, techniques have been developed which make possible the direct measurement of dissipation in veins as well as in arteries.[18] These direct methods are not subject to certain of the inaccuracies inherent in the indirect techniques which have been previously employed. Results from direct arterial and venous experiments on anesthetized dogs reveal a strong frequency dependence of the dissipation at frequencies between 50 and 200 cycles per second. The magnitude of the dissipation, however, is markedly less than one might expect from the data obtained through the indirect methods.

It has been shown theoretically[19] that for the frequency range covered in the direct dissipation measurements described in Reference 18 the effects of fluid viscosity are unimportant as far as the dispersion and dissipation of symmetric type I waves are concerned. Therefore, in this section, the fluid will again be treated as inviscid. Even though the contribution of the surrounding medium to the dissipation of waves will most likely be of importance, it will not be investigated in this study.

VISCOELASTIC SHELL EQUATIONS

In the three-dimensional theory of linear viscoelasticity, an isotropic viscoelastic material is described by means of relationships specifying the material's behavior in shear and in dilitation; i.e.,

$$P(\tau_{ij}) = Q(\gamma_{ij}) \quad i,j = 1,2,3; \; i \neq j \tag{39}$$

and

$$\frac{1}{3} P'(\sigma_{ii}) = Q'(\epsilon_{ii}) \tag{40}$$

where P, Q, P' and Q' are linear differential operators of the form

$$L(D) = a_0 + a_1 D + a_2 D^2 + \ldots + a_n D^n \tag{41}$$

with $D \equiv \partial/\partial t$. The coefficients a_i are constants, and the operators P and Q may be chosen independent of P' and Q'. The viscoelastic equations are analogous to the elastic relations

$$\tau_{ij} = G(\gamma_{ij}) \quad i,j = 1,2,3; \; i \neq j \tag{42}$$

and

$$\frac{1}{3}\sigma_{ii} = K\epsilon_{ii} \tag{43}$$

in which G and K are the shear modulus and bulk modulus, respectively. From the elastic relationships

$$G = \frac{E}{2(1+\nu)} \quad , \qquad K = \frac{E}{3(1-2\nu)} \tag{44}$$

and from the formal equivalences

$$Q/P = \tilde{G} \; , \qquad Q'/P' = \tilde{K} \tag{45}$$

one may, by algebraic manipulations, define operators $\tilde{E}$ and $\tilde{\nu}$ in terms of the viscoelastic operators P, Q, P' and Q'. One obtains

$$\tilde{E} = \frac{9QQ'}{3Q'P + QP'} \tag{46}$$

and

$$\tilde{\nu} = \frac{3Q'P - 2QP'}{2(3Q'P + QP')} \; . \tag{47}$$

Replacing the Young's modulus E and Poisson's ratio ν in the differential equations of motion for the fluid filled elastic vessel

(equations (12) and (13)) by the operators $\tilde{E}$ and $\tilde{\nu}$ as defined by equations (46) and (47), one arrives at the differential equations of motion corresponding to a linearly viscoelastic vessel wall. The fluid equations of motion and kinematic boundary conditions are clearly unaffected by the assumptions made on the vessel wall material, so that the apparent mass term remains unchanged.

As in the case of the elastic shell, solutions of the form

$$\begin{aligned} u &= A \exp[i(kx - \omega t + s\beta)] \\ v &= B \exp[i(kx - \omega t + s\beta)] \\ w &= C \exp[i(kx - \omega t + s\beta + \frac{\pi}{2}] \end{aligned} \tag{48}$$

are assumed. In the corresponding frequency equation the wave number $k = k_R + ik_I$ must have a positive imaginary part if attenuation is to be present. The phase velocity of signals with an angular frequency ω is given by $c = \omega/k_R$, while the signal is attenuated by a factor of $\exp(-k_I x)$ after travelling a distance x.

It should be noted that for the trial solution (48) the frequency equation can be obtained by formally substituting $-i\omega$ for D in the operators $\tilde{E}$ and $\tilde{\nu}$ given by equations (46) and (47) and by replacing E and ν in the elastic frequency equation (23) by $\tilde{E}$ and $\tilde{\nu}$. Therefore, it is possible to arrive directly at the viscoelastic frequency equation without formally deriving the viscoelastic differential equations of motion. It is clear that the viscoelastic parameters corresponding to E and ν will be complex, and for the sake of clarity, they will be denoted $\hat{E}$ and $\hat{\nu}$, respectively:

$$\hat{E} = \frac{9\hat{Q}\hat{Q}'}{3\hat{Q}'\hat{P} + \hat{Q}\hat{P}'} \tag{49}$$

$$\hat{\nu} = \frac{3\hat{Q}'\hat{P} - 2\hat{Q}\hat{P}'}{2(3\hat{Q}'\hat{P} + \hat{Q}\hat{P}')} \tag{50}$$

with

$$\begin{aligned} \hat{P}(\omega) &\equiv P\Big/_{D \to -i\omega} \\ \hat{Q}(\omega) &\equiv P\Big/_{D \to -i\omega} \\ \hat{P}'(\omega) &\equiv P'\Big/_{D \to -i\omega} \\ \hat{Q}'(\omega) &\equiv Q'\Big/_{D \to -i\omega} . \end{aligned} \tag{51}$$

VISCOELASTIC MODELS

In one-dimensional linear viscoelasticity it is convenient to interpret expressions of the form $P\sigma = Q\epsilon$ as a mathematical model of a mechanical system consisting of springs and dashpots. Because of mathematical complexities, this mechanical system is usually restricted to three simple models: the standard linear solid, the Maxwell fluid, and the Voigt solid. In the three-dimensional case the problem may become completely intractable when independent models for both the shear and dilitational behavior of the material must be selected. A major simplification can be achieved if the material is assumed to be incompressible. Utilizing the fact that most biological materials, including blood vessels, are nearly incompressible, we assume that

$$\frac{\hat{P}'}{\hat{Q}'} = 0. \tag{52}$$

From this it follows that

$$\hat{E} = 3\hat{Q}/\hat{P} \tag{53}$$

and

$$\hat{\nu} = \frac{1}{2}. \tag{54}$$

Thus the viscoelastic properties of the material are now completely determined by its behavior in shear and a single viscoelastic model suffices to describe the behavior of the material. In the case of the three simple models mentioned above, $\hat{E}$ becomes:

$$\begin{aligned} &\text{Standard linear solid} && \hat{E} = \frac{E_1 E_2}{E_1 + E_2} \; \frac{1 - i\eta\omega/E_2}{1 - i\eta\omega/(E_1+E_2)} \\ &\text{Maxwell fluid} && \hat{E} = \frac{-3i\eta\omega}{(1 - i\eta\omega/E_o)} \\ &\text{Voigt solid} && \hat{E} = 3(E_o - i\eta\omega). \end{aligned} \tag{55}$$

Irrespective of the viscoelastic behavior, $\hat{E}$ may be written in the form

$$\hat{E} = \hat{E}_R(\omega) + i\hat{E}_I(\omega). \tag{56}$$

In fact, equations (56) and (54) may be taken as the starting point for an analysis of waves in a viscoelastic vessel, with the functions $\hat{E}_R(\omega)$ and $\hat{E}_I(\omega)$ selected so as to exhibit certain properties determined from experimental data. Such an approach has been employed in References 15, 16 and 17. However, these investigations have been restricted to

axisymmetric vibrations using an unrealistic mechanical model for the vessel, since initial axial stretch and a transmural pressure were neglected. Of interest is a systematic analysis of the effects of a viscoelastic behavior of the vessel wall including the influence of initial loading, bending rigidity, and also allowing for non-symmetrical waves.

Of the three simple viscoelastic models considered here, it is clear that the standard linear solid allows for the most complete representation of the viscoelastic behavior of blood vessels, since it includes the Maxwell fluid and Voigt solid as special cases. However, three independent parameters must be selected to define such a solid, while only two are needed for the Maxwell or Voigt model. For a thorough parametric analysis, the computational effort increases considerably with each additional parameter. Therefore, attention will be restricted to the Maxwell and Voigt models.

The decision as to whether the Maxwell or Voigt model is the more appropriate must be made on the basis of experimental evidence. Results of recent experiments[18] indicate that in the range from 50 to 200 cycles per second the damping per wavelength of type I waves in the thoracic aorta of anesthetized dogs is essentially independent of frequency. Assuming, as a first approximation, that the phase velocity c of type I waves is given by the Moens-Korteweg formula

$$c^2 = \frac{Eh}{2\rho_f a}$$

for all frequencies, it follows that in the viscoelastic case the damping per wavelength for the Voigt model in shear is given by

$$\frac{A_\lambda}{A_o} = \exp\left\{-2\pi\left[\frac{\sqrt{1+3\hat{\eta}^2\hat{\omega}^2}-1}{\sqrt{1+3\hat{\eta}^2\hat{\omega}^2}+1}\right]^{1/2}\right\} \tag{57}$$

while the Maxwell model yields

$$\frac{A_\lambda}{A_o} = \exp\left\{-2\pi\left[\frac{\sqrt{1+1/3\hat{\eta}^2\hat{\omega}^2}-1}{\sqrt{1+1/3\hat{\eta}^2\hat{\omega}^2}+1}\right]^{1/2}\right\}. \tag{58}$$

In these expressions A_o and A_λ are the wave amplitudes at $x = 0$ and $x = \lambda$, respectively, with λ denoting the wavelength. For large $\hat{\omega}$, A_λ/A_o approaches $\exp(-2\pi)$ for the Voigt model and 1.0 for the Maxwell model. From this we conclude that at high frequencies the Maxwell model predicts an extremely small attenuation, which is in contrast with experimental observations. It should be noted that the phase velocity c and A_λ/A_o have also been determined by solving the frequency equation for the viscoelastic shell using the Maxwell model. The results again show that the Maxwell model does not lead to damping characteristics and phase velocities which are in agreement with experimental evidence. On the other hand, as will be shown, the Voigt model reflects more realistic wave propagation characteristics. We have therefore restricted our parametric study of wave propagation to blood vessels whose shear deformation is governed by a Voigt model.

NORMALIZATION

In the elastic case we introduced as normalizing velocity

$$c_p = \left[\frac{E}{\rho_w(1-\nu^2)}\right]^{1/2} \tag{59}$$

Since, for viscoelastic material $\hat{E}$ and $\hat{\nu}$ are in general both complex functions of frequency, the above expression for c_p would lead to a complex velocity. We avoid this by introducing in lieu of the above definition a normalizing velocity

$$c_b = \left[\frac{\hat{E}_o}{\rho_w}\right]^{1/2} \tag{60}$$

where $\hat{E}_o$ is real and is equal to the value of the complex Young's modulus $\hat{E}$ taken for $\omega = 0$. In particular, for the Voigt model we have

$$c_b = \left[\frac{3E_o}{\rho_w}\right]^{1/2} \tag{61}$$

We additionally introduce the following dimensionless parameters:

$$\begin{aligned}
\hat{c}^2 &= c^2/c_b^2 \\
\hat{\omega}^2 &= \omega^2 a^2/c_b^2 \\
\hat{c}^{*2} &= c_f^2/c_b^2 \\
\hat{q}_1 &= T_{10}/3E_o h \\
\hat{q}_2 &= a\Delta p/3E_o h \\
\hat{\eta} &= \eta/(a\rho_w \sqrt{E_o/\rho_w})
\end{aligned} \tag{62}$$

It is interesting to note that in the expression for $\hat{\eta}$ the quantity $(E_o/\rho_w)^{1/2}$ has the dimension of a speed. Hence, $1/\hat{\eta}$ may be considered

to be a viscoelastic Reynold's number, in which the tube radius a is the characteristic length and $(E_o/\rho_w)^{1/2}$ the characteristic speed.

RESULTS OF VISCOELASTIC SHELL ANALYSIS

The frequency equation for the viscoelastic case interrelates eleven dimensionless parameters $\hat{\nu}$, s, h/a, $\bar{\rho}$, $\hat{q}_1$, $\hat{q}_2$, $\hat{\omega}$, $\hat{c}$, $\hat{c}^*$, $k_I a$, and $\hat{\eta}$. The first nine parameters are basically the same as in the elastic case, except that the five parameters $\hat{q}_1$, $\hat{q}_2$, $\hat{\omega}$, $\hat{c}$, and $\hat{c}^*$ differ by constant factors from q_1, q_2, $\bar{\omega}$, $\bar{c}$, and $\bar{c}^*$. In addition to these first nine parameters we now have also a measure of the wave attenuation in the form of $k_I a$, the imaginary part of the complex wave number, and the dimensionless coefficient of viscosity $\hat{\eta}$. It is convenient and more descriptive to present the effects of damping in the form of the amplitude ratio A_λ/A_o in lieu of $k_I a$. From equation (48) it follows immediately that A_λ/A_o is given by

$$A_\lambda/A_o = \exp[-2\pi \frac{k_I}{k_R}]. \tag{63}$$

Within the range of parameter values encountered in physiological problems, we again find that all but the three slowest modes are a direct consequence of fluid compressibility. Adhering to the same nomenclature as in the elastic case, we again identify these three slowest modes as waves of types I, II and III.

Discussion of Axisymmetric Waves

Figure 28 presents the non-dimensional axial phase velocity $\hat{c}$ for axisymmetric waves as a function of the non-dimensional viscosity

coefficient $\hat{\eta}$ ranging from 0 (elastic case) to 1.0. It should be recalled that type I waves have a displacement pattern that is predominantly radial in nature and therefore have associated with them considerably stronger pressure fluctuations than waves of type II and III. We note that as $\hat{\omega}$ approaches zero the phase velocity of each of the three types of waves approaches a limiting value which is independent of $\hat{\eta}$ and which is identical with the limiting value obtained in the elastic case.

For $\hat{\eta}\hat{\omega} \ll 1$ and $\frac{h}{a} \ll 1$ we can determine the phase velocities of type I waves approximately from

$$\hat{c}^2 \approx \frac{1}{(1-\nu^2)} \frac{\left[h/2\bar{\rho}a + \nu^2/(1 - 2\bar{\rho}\frac{a}{h})\right]}{\left(\sqrt{1 + 3\hat{\eta}^2\hat{\omega}^2} + 1\right)} . \tag{64}$$

From this it follows immediately that at very low frequencies the effects of viscoelasticity on dispersion of axisymmetric waves in a thin walled vessel is only of second order. This result is of particular significance since it predicts that the viscoelastic behavior of blood vessels will practically have no effect on the phase velocities at low frequencies. Therefore, one cannot expect to determine reliably the viscoelastic parameters of blood vessels on the basis of phase velocity measurements of pressure waves.

The frequency equation yields an exact expression for the phase velocities of type II waves, which can be written in the form

$$\hat{c}^2 = \frac{(1 + 3e^2)}{(1 + \nu)} \frac{(1 + 3\hat{\eta}^2\hat{\omega}^2)}{\left(\sqrt{1 + 3\hat{\eta}^2\hat{\omega}^2} + 1\right)} . \tag{65}$$

For type III waves no closed form expression can be given for the phase velocities. However, with the restriction $\hat{\eta}\hat{\omega} \ll 1$ we find approximately for the speeds of axisymmetric type III waves

$$\hat{c}^2 \approx \frac{1}{(1-\nu^2)} \frac{\left[1 - \nu^2/(1 - 2\bar{\rho}\frac{a}{h})\right]}{\left(\sqrt{1 + 3\hat{\eta}^2\hat{\omega}^2} + 1\right)} \tag{66}$$

As can be seen from Figure 28, type II and III waves become highly dispersive as $\hat{\eta}$ is increased from 0.0 to 1.0, although equations (65) and (66) indicate that the dispersion will be only of second order for small $\hat{\eta}\hat{\omega}$.

Figure 29 depicts the damping per wavelength of axisymmetric waves as a function of the frequency parameter $\hat{\omega}$ for $0.0 \leq \hat{\eta} \leq 1.0$. In the case of type I waves, the curves indicate that for $\hat{\omega} \geq 0.4$ the damping ratio A_λ/A_o is essentially independent of frequency, for all values of $\hat{\eta} \leq 1.0$. This property lends support to the appropriateness of the Voigt solid in shear as a model for the viscoelastic behavior of the vessel wall, since recent wave propagation experiments in the thoracic and abdominal aorta of anesthetized dogs have exhibited similar damping characteristics.[18] In this connection it should be emphasized that the experimental data referred to here includes the contribution of blood viscosity and radiation of energy into the vascular bed to the attenuation of waves in addition to the dissipation in the wall due to its viscoelasticity. A comparison of our theoretical results with experimental data from Reference 18 suggests that $\hat{\eta}$ is less than 0.5 over the frequency range of 50 to 200 cycles per second. This contrasts with $\hat{\eta} \approx 5$ implied by Reference 15 for low frequency waves in the abdominal aorta of dogs.

At very low frequencies type II and type III waves are not as heavily damped as those of type I but are more heavily damped when $\hat{\omega} \geq 0.4$. For waves of type II the amplitude ratio A_λ/A_o can be given in closed form as

$$\frac{A_\lambda}{A_o} = \exp\left\{-2\pi\left[\frac{(1 + 3\hat{\eta}^2\hat{\omega}^2)^{1/2} - 1}{(1 + 3\hat{\eta}^2\hat{\omega}^2)^{1/2} + 1}\right]^{1/2}\right\} \tag{67}$$

No such closed form expression for A_λ/A_o can be given for type I and III waves. However, when $\hat{\eta}\hat{\omega} \ll 1.0$, the damping ratio for all three types can be approximated by

$$\frac{A_\lambda}{A_o} \approx \exp(-\sqrt{3\pi\hat{\eta}\hat{\omega}}) \approx 1 - \sqrt{3\pi\hat{\eta}\hat{\omega}}\,. \tag{68}$$

From equation (68) we conclude that, for small $\hat{\eta}\hat{\omega}$, the damping ratio decreases linearly with $\hat{\eta}$ or $\hat{\omega}$.

The mode shapes for axisymmetric waves are nearly independent of $\hat{\eta}$ for $\hat{\eta} \leq 1.0$, as is evident from Figure 30. Only the radial components of type III waves show any noticeable change with $\hat{\eta}$. Changes in the type I mode shapes are so small as to fall within the plotting accuracy of the curves.

Figure 31 depicts the phase velocities of axisymmetric type I, II and III waves for $\hat{\eta} = 0.5$ and for four values of the axial tethering parameter $\hat{q}_1$. While dispersion of type I waves due to tethering is only significant at higher frequencies, we find that tethering affects the speed of waves of type II and III primarily at lower frequencies. From Figure 32, it is seen that axial tethering has a marked effect on the magnitude of the damping of type I waves for $\hat{\eta} = 0.5$. When

$\hat{q}_1 = 0.2$ the attenuation per wavelength at high frequencies is less than half of that for $\hat{q}_1 = 0$. This serves to emphasize that viscoelastic parameters extracted from data pertaining to high frequency pressure waves may be seriously in error if vessel tethering is not considered. The effect of tethering on the mode shapes of axisymmetric waves is negligible, as can be seen from Figure 33.

The results of the effects of a transmural pressure on the dispersion, mode shapes and attenuation of axisymmetric waves are illustrated in Figures 34, 35 and 36. We note that the effects on the wave propagation characteristics of a transmural pressure and an axial stretch are quite similar in nature. This is to be expected, since the vessel was assumed to be fixed at its ends, which means that an internal pressure Δp will introduce a corresponding axial stress of magnitude $\nu \Delta p a/h$.

The thickness ratio h/a significantly affects the phase velocities of type I waves, as in the elastic case, but leaves the speed of type II and type III waves nearly unchanged, as can be seen from Figure 37. According to Figure 38, the damping ratio A_λ/A_o is remarkably insensitive to variations in h/a for all three types of waves. Similarly, we find no significant changes in the mode shapes for different values of h/a.

Discussion of Non-Axisymmetric Waves

In the case of vessels with an elastic wall material, it was shown earlier that cut-off frequencies exist for non-axisymmetric waves of types I, II and III, with the sole exception of type I waves with $s = 1$. If the vessel wall is composed of an incompressible viscoelastic material, whose shear deformation is governed by the Voigt model, we no longer find

cut-off frequencies in the classical sense. Non-axisymmetric waves are now theoretically being propagated at all frequencies. However, as will be seen, the amplitude ratio A_λ/A_o of waves propagating near and below the corresponding elastic cut-off frequency is so small that the experimental verification of their existence would be a question of sensitivity of the transducers utilized. For practical purposes one might therefore consider introducing a cut-off frequency on the basis of a minimal observable wave amplitude.

Discussion of waves with $s = 1$.

For $s = 1$ the phase velocities of type I waves exhibit only mild dispersion when $\hat{\eta}$ varies between 0 and 1.0, as can be seen from Figure 40. On the other hand, the speed of waves of type II and III are strongly dependent on $\hat{\eta}$ and $\hat{\omega}$. Except for $\hat{\eta} = 0$, cut-off frequencies no longer exist for type II and type III waves, although this is not readily apparent from Figure 40. Considering, however, the variation of the mode shapes with frequency, as illustrated in Figure 42, we note that waves are indeed being propagated below the elastic cut-off frequency for all values of $\hat{\eta}$ covered in our parametric study. We also see that the mode shape of type I waves is practically unaltered by increasing $\hat{\eta}$ from 0 to 1.0, while the type II and type III mode shapes exhibit great sensitivity to changes in $\hat{\eta}$.

According to Figure 41, type I waves exhibit attenuation properties similar to those of axisymmetric type I waves, i.e., the attenuation per wavelength is again essentially independent of frequency for $\hat{\omega} \gg 0.4$. In contrast to this, even comparatively small values of $\hat{\eta}$ lead to a

strong attenuation per wavelength as compared with the axisymmetric case.

Discussion of waves with $s = 2$

From the results given in Figure 43, we again note that the speed of propagation of type I waves is only mildly affected by changes in $\hat{\eta}$ between 0 and 1.0. The phase velocities of type II and III waves on the other hand are strongly dependent on the viscoelasticity of the vessel wall. Propagation of all three types of waves below the elastic cut-off frequencies is again possible but damping per wavelength below cut-off is so high that they can be ignored.

From Figure 45 it follows that type II and III mode shapes exhibit strong dependence on the parameter $\hat{\eta}$ for all $\hat{\omega} \leq 4.0$, while the mode shape for $0 \leq \hat{\eta} \leq 1.0$ is indistinguishable from that of the elastic case $(\hat{\eta} = 0)$.

Figures 46 through 48 illustrate the sensitivity of both $\hat{c}$ and A_λ/A_o to axial tethering when $\hat{\eta} = 0.5$. Near the elastic cut-off frequency, type I phase velocities may double in magnitude as $\hat{q}_1$ is increased from 0 to 0.2. Likewise, the amplitude ratio may grow by more than a factor of two with the same change in tethering. The sensitivity of the phase velocities and damping characteristics of type II and III waves to changes in axial stretch may be equally pronounced, but for practical purposes unimportant in view of the heavy damping. From Figure 48, we see that mode shapes show no significant dependence on $\hat{q}_1$ except at low frequencies.

The effects of a transmural pressure on phase velocities, damping characteristics and mode shapes of $s = 2$ waves are summarized in Figures 49, 50 and 51 for $\hat{\eta} = 0.5$. The dispersive nature of these waves is essentially similar to that of the elastic case, except for the existence of waves below the elastic cut-off frequency. The amplitude ratio A_λ/A_o of type I waves increases markedly with rising transmural pressure, while the absolute changes in the amplitude ratio of type II and III waves may be termed insignificant.

The results plotted in Figures 52 through 54 illustrate the influence of changes in the thickness ratio h/a on the propagation characteristics of $s = 2$ waves for $\hat{\eta} = 0.5$. Variations in the thickness ratio have a strong influence on the phase velocities of waves of type I. Except near the elastic cut-off frequencies, the phase velocities of type I waves vary approximately as $(h/a)^{1/2}$. On the other hand, Figures 53 and 54 demonstrate that the damping characteristics and mode shapes of such waves are only moderately affected by variations in h/a. Waves of type II and III show only unimportant changes in their characteristics with respect to changes in h/a except below the elastic cut-off frequencies. It becomes clear, however, from Figure 53, that these changes are of no practical significance because of the severe damping.

CONCLUSIONS

From our dispersion curves we conclude that a realistic model for the dynamic behavior of blood vessels should include the effects of the transmural pressure and the axial stretch. The propagation of pressure pulses similar to those generated by the heart appears to involve primarily

symmetric waves of type I since waves of type II are not connected with intraluminal pressure fluctuations and waves of type III exhibit only very small pressure perturbations. Qualitative agreement is obtained with recent experiments on dissipation of high frequency waves in blood vessels by assuming that the vessel wall material is incompressible but behaves as a Voigt solid in shear. The phase velocities of type I axisymmetric waves are only mildly affected by such viscoelastic behavior, so that it will be difficult to obtain accurate estimates of the viscoelastic parameters of the vessel wall on the basis of type I phase velocity measurements only. The dissipation of waves, however, exhibits a strong dependence on the viscoelastic properties of the vessel wall. Moreover, the dissipation decreases substantially with increasing axial stretch or transmural pressure, especially at high frequencies. Consequently, the reliable determination of the viscoelasticity of the vessel wall from experiments involving high frequency wave propagation must take into consideration the effects of axial stretch and transmural pressure. Considering the striking dispersive properties of non-axisymmetric waves, their experimental verification would offer deeper insight into the viscoelastic behavior of arteries and veins. The effects of the compressibility of the blood are insignificant for waves with frequencies below 1000 cycles per second.

REFERENCES

1. McDonald, D. A., Blood Flow in Arteries, Edward Arnold Ltd., London, 1960.

2. Fox, E. A. and Saibel, Edward, Attempts in the Mathematical Analysis of Blood Flow, Trans. Soc. Rheol. VII, 1963, pp. 25-31.

3. Klip, Willem, Velocity and Damping of the Pulse Wave, Martinus Nijhoff, The Hague, 1962.

4. Womersley, J. R., An Elastic Tube Theory of Pulse Transmission and Oscillatory Flow in Mammalian Arteries, WADC Technical Report TR 56-614, Wright Air Development Center, Ohio, Jan. 1957.

5. Attinger, E. O., Ed., Pulsatile Blood Flow: Proceedings, Blakiston Division, McGraw Hill Book Co., New York, 1964.

6. Lin, T. C. and Morgan, G. W., Wave Propagation through Fluid Contained in a Cylindrical, Elastic Shell, J. Acoust. Soc. Am., 28, 1956, pp. 1165-1176.

7. Gazis, D. C., Three-Dimensional Investigation of the Propagation of Waves in Hollow Circular Cylinders. I. Analytical Foundation, J. Acoust. Soc. Am., 31, 1959, pp. 568-573.

8. Greenspon, J. E., Vibrations of Thick and Thin Cylindrical Shells Surrounded by Water, J. Acoust. Soc. Am., 33, 1961, pp. 1321-1328.

9. Anliker, Max and Raman, K. R., Korotkoff Sounds at Diastole – A Phenomenon of Dynamic Instability of Fluid-Filled Shells, Int. J Solids Structures, 2, 1966, pp. 467-491.

10. Atabek, H. B. and Lew, H. S., Wave Propagation through a Viscous Incompressible Fluid Contained in an Initially Stressed Elastic Tube, Biophysical Journal, 6, 1966, pp. 481-503.

11. Flügge, W., Stresses in Shells, Springer-Verlag, Berlin, 1962.

12. Landowne, Milton, A Method Using Induced Waves to Study Pressure Propagation in Human Arteries, Circulation Research, Vol. V, Nov. 1957, pp. 594-601.

13. Landowne, Milton, Characteristics of Impact and Pulse Wave Propagation in Brachial and Radial Arteries, J. Appl. Physiol. 12(I), 1958, pp. 91-97.

14. Peterson, Lysle H., The Dynamics of Pulsatile Blood Flow, Circulation Research, Vol. II, March 1964, pp. 127-139.

15. Bergel, D. H., The Dynamic Elastic Properties of the Arterial Wall, J. Physiol., 156, 1961, pp. 458-469.

16. McDonald, D. A. and Gessner, Urs, Wave Attenuation in Viscoelastic Arteries, Proceedings of the First International Conference on Hemorheology, Pergamon Press, Oxford, 1966.

17. Hardung, V., Propagation of Pulse Waves in Viscoelastic Tubings, Handbood of Physiology, Circulation, Vol. 1, American Physiological Society, 1962, pp. 107-135.

18. Anliker, Max, Histand, M., Ogden, E. and Westbrook, R. M., Direct Measurement of Dissipation of Waves in Arteries and Veins, Proceedings of the Annual Conference on Engineering in Medicine and Biology, Vol. 8, 1966.

19. Jones, E., Oscillatory, Axially Symmetric Motion of an Elastic Tube Containing a Streaming Newtonian Fluid, Proceedings of the 1966 Divisional Meeting of the Division of Fluid Dynamics, American Physical Society, Stanford, California, Nov. 1966.

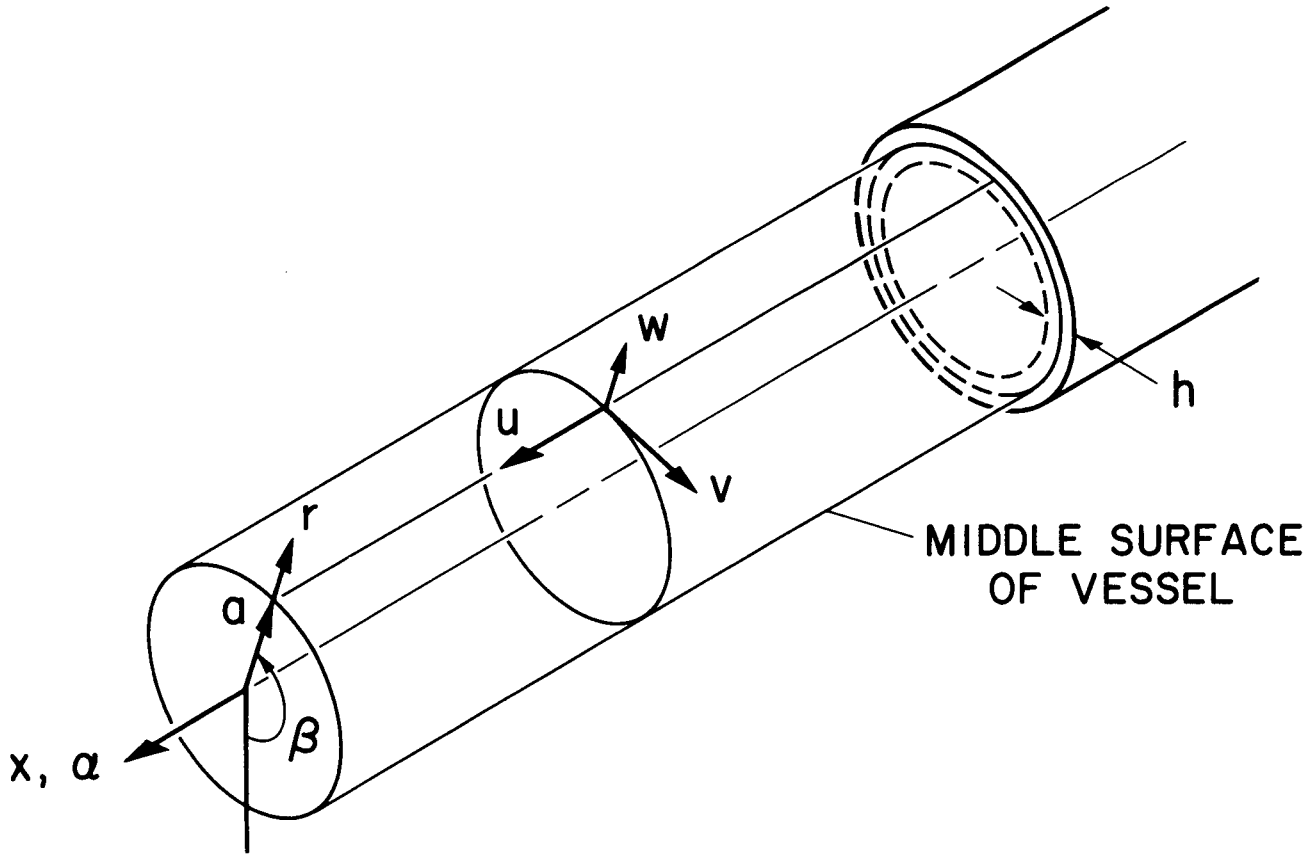

Figure 1. Coordinate System

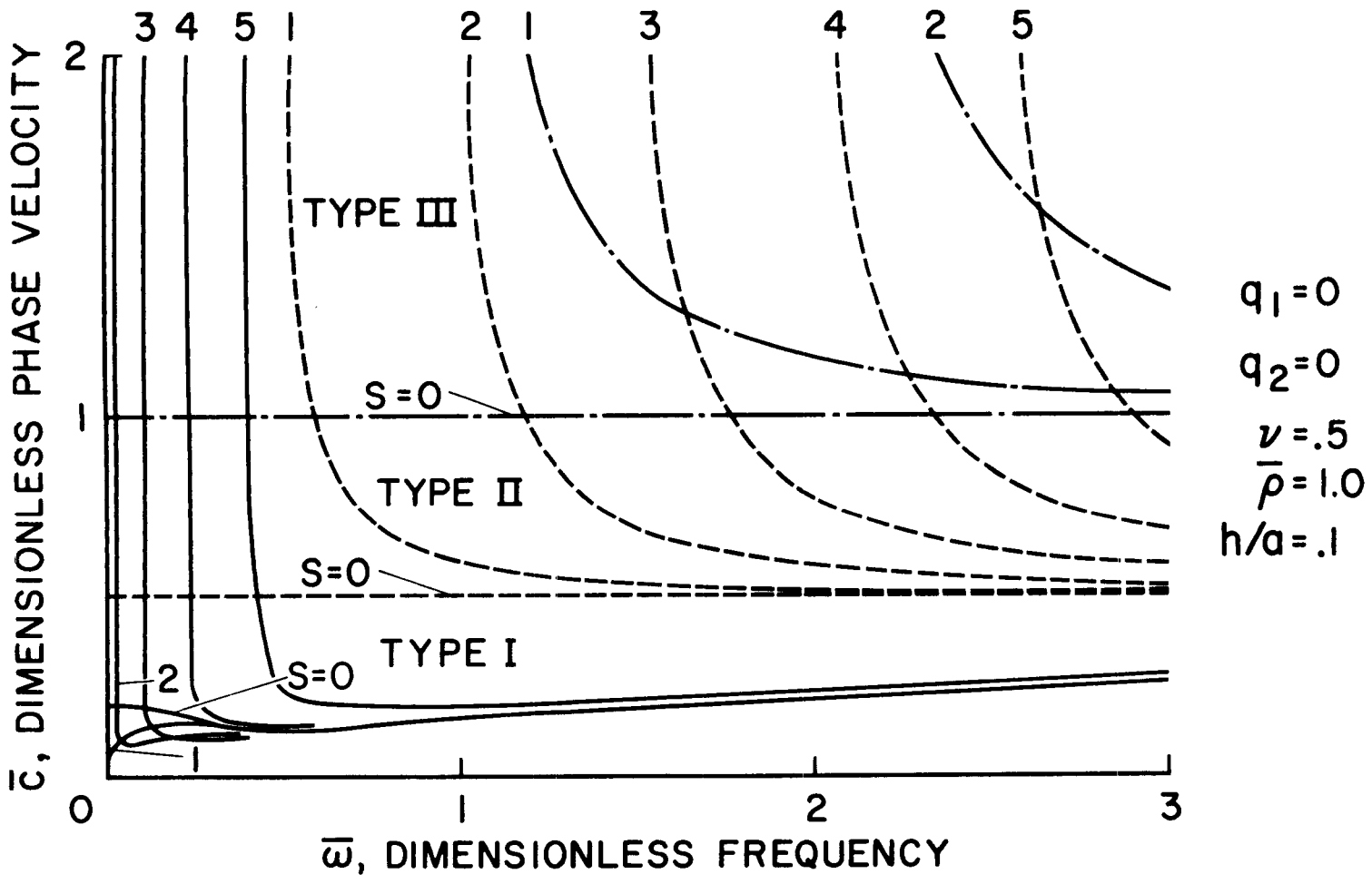

Figure 2. Elastic Shell. Dispersion Curves of the Slowest Waves at Zero Transmural Pressure and Zero Axial Stretch. Solid Lines - Type I. Dotted Lines - Type II. Chain Dots - Type III. Numbers Refer to the Circumferential Wave Number s

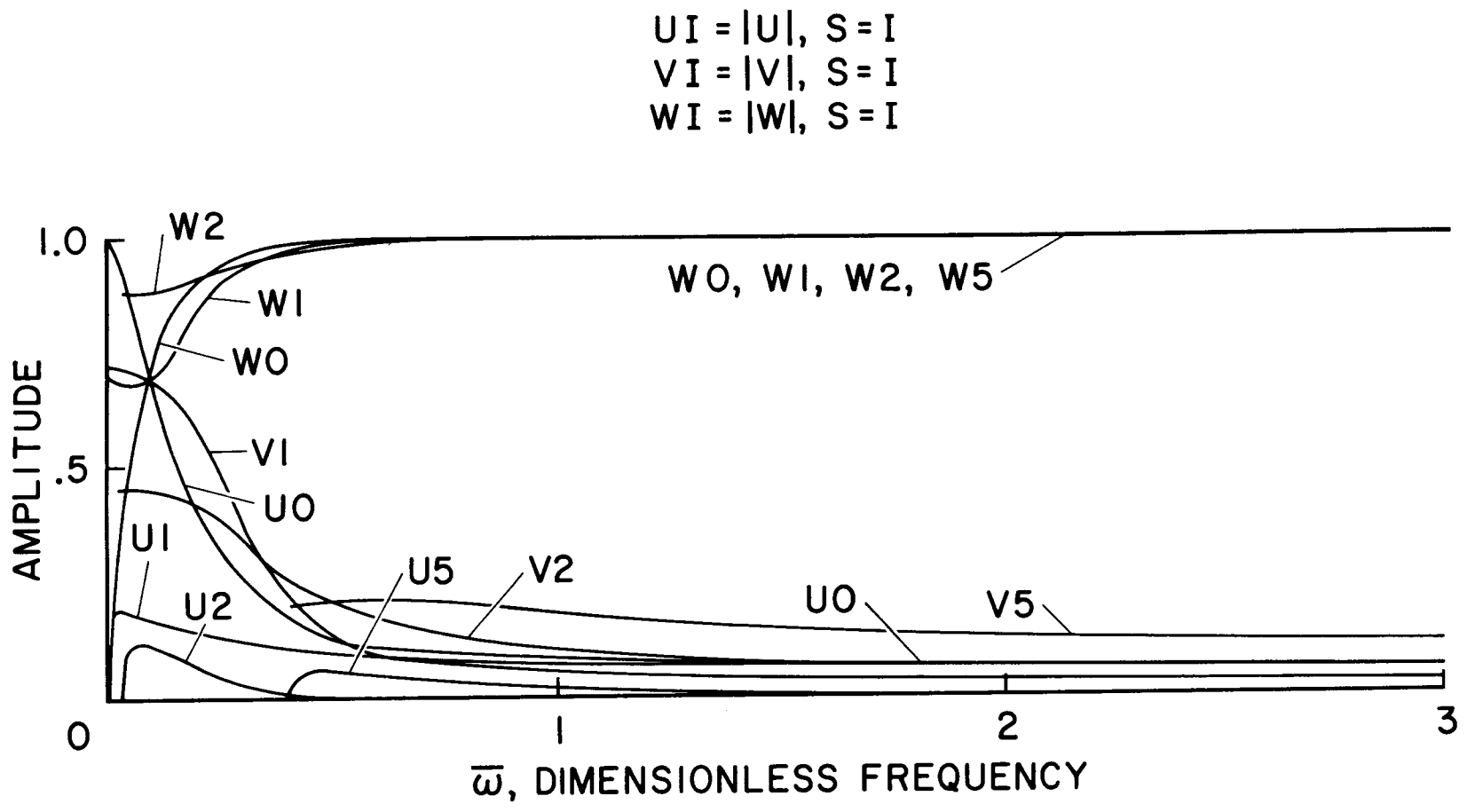

Figure 3. Elastic Shell. Mode Shapes of Type I Waves at Zero Transmural Pressure and Zero Axial Stretch

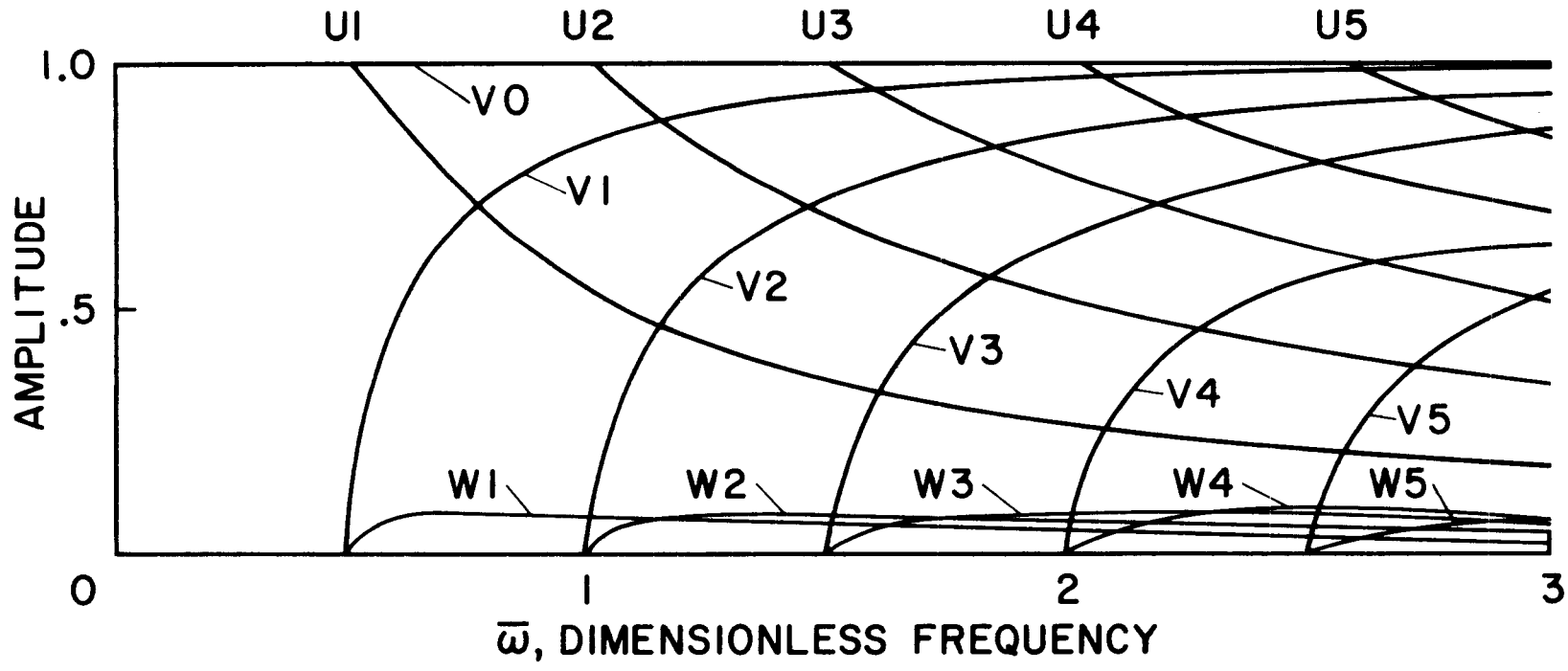

Figure 4. Elastic Shell. Mode Shapes of Type II Waves at Zero Transmural Pressure and Zero Axial Stretch

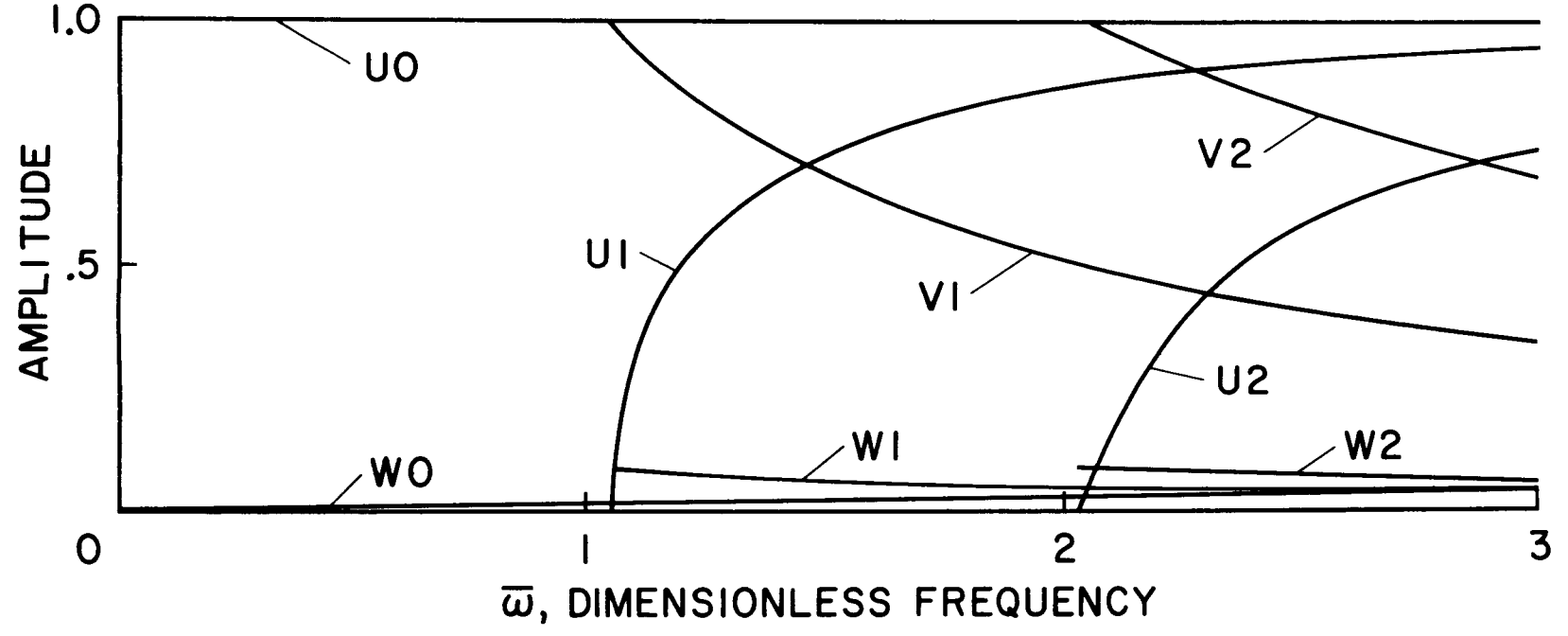

Figure 5. Elastic Shell. Mode Shapes of Type III Waves at Zero Transmural Pressure and Zero Axial Stretch

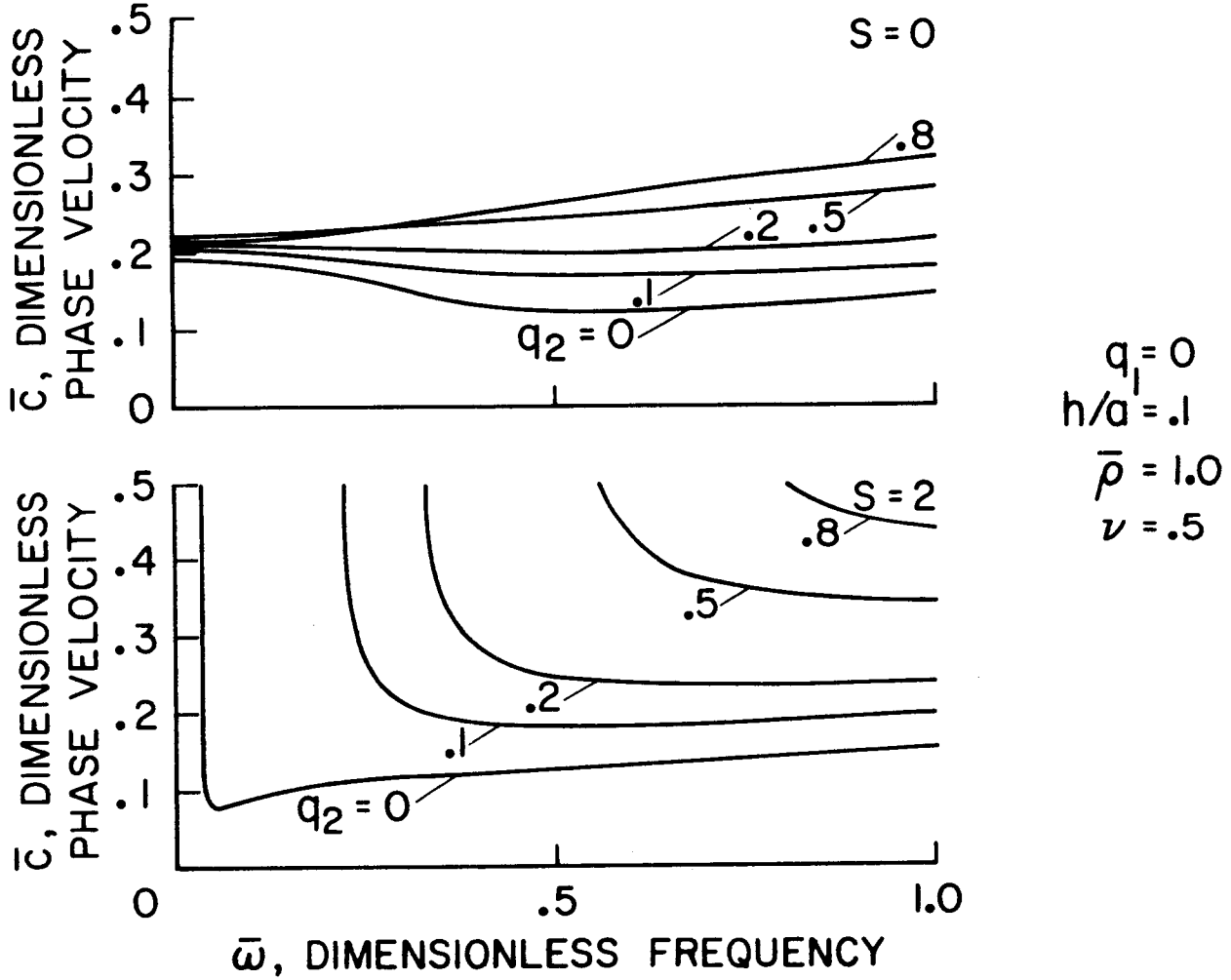

Figure 6. Elastic Shell. Dispersion Curves of Type I Waves for Various Transmural Pressures and Zero Axial Stretch

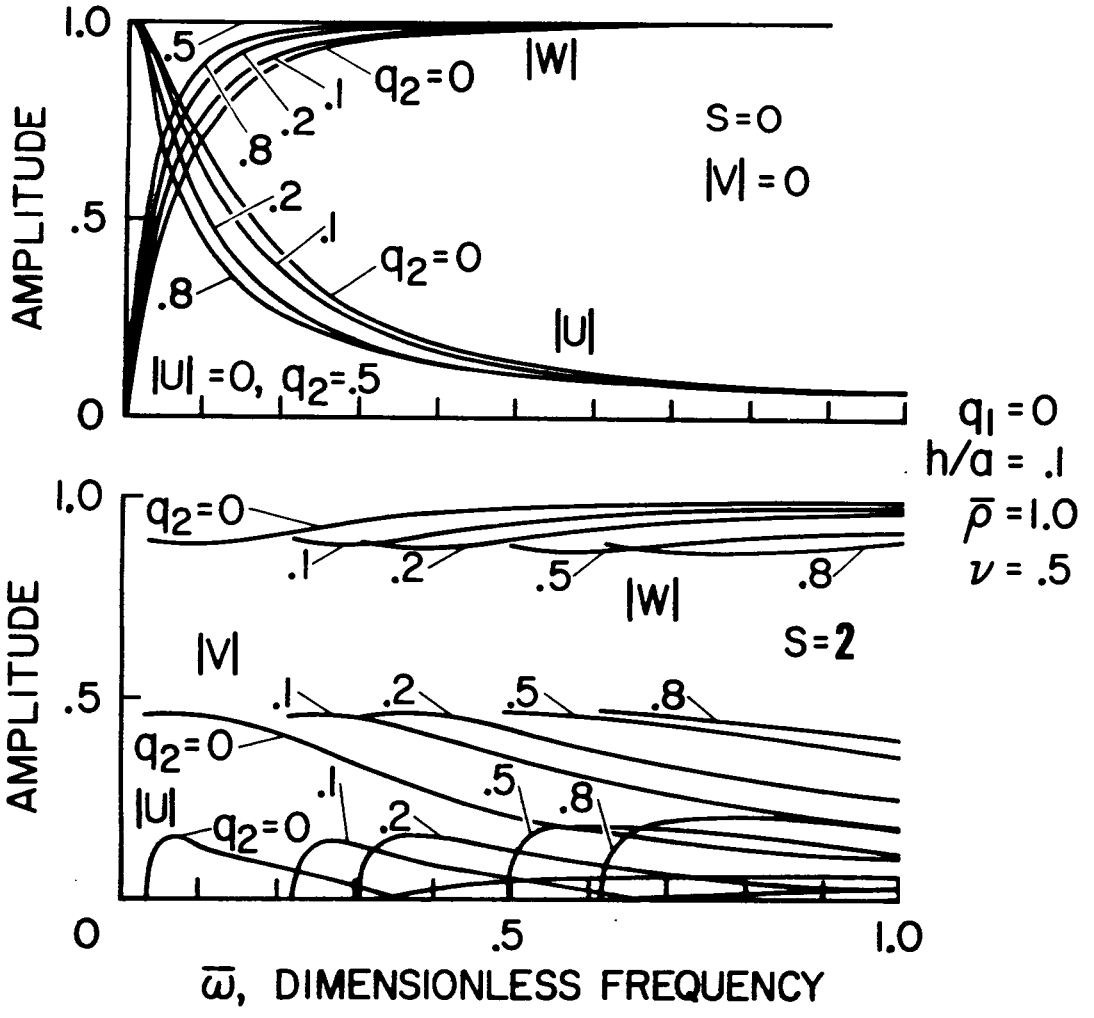

Figure 7. Elastic Shell. Mode Shapes of Type I Waves for Various Transmural Pressures and Zero Axial Stretch

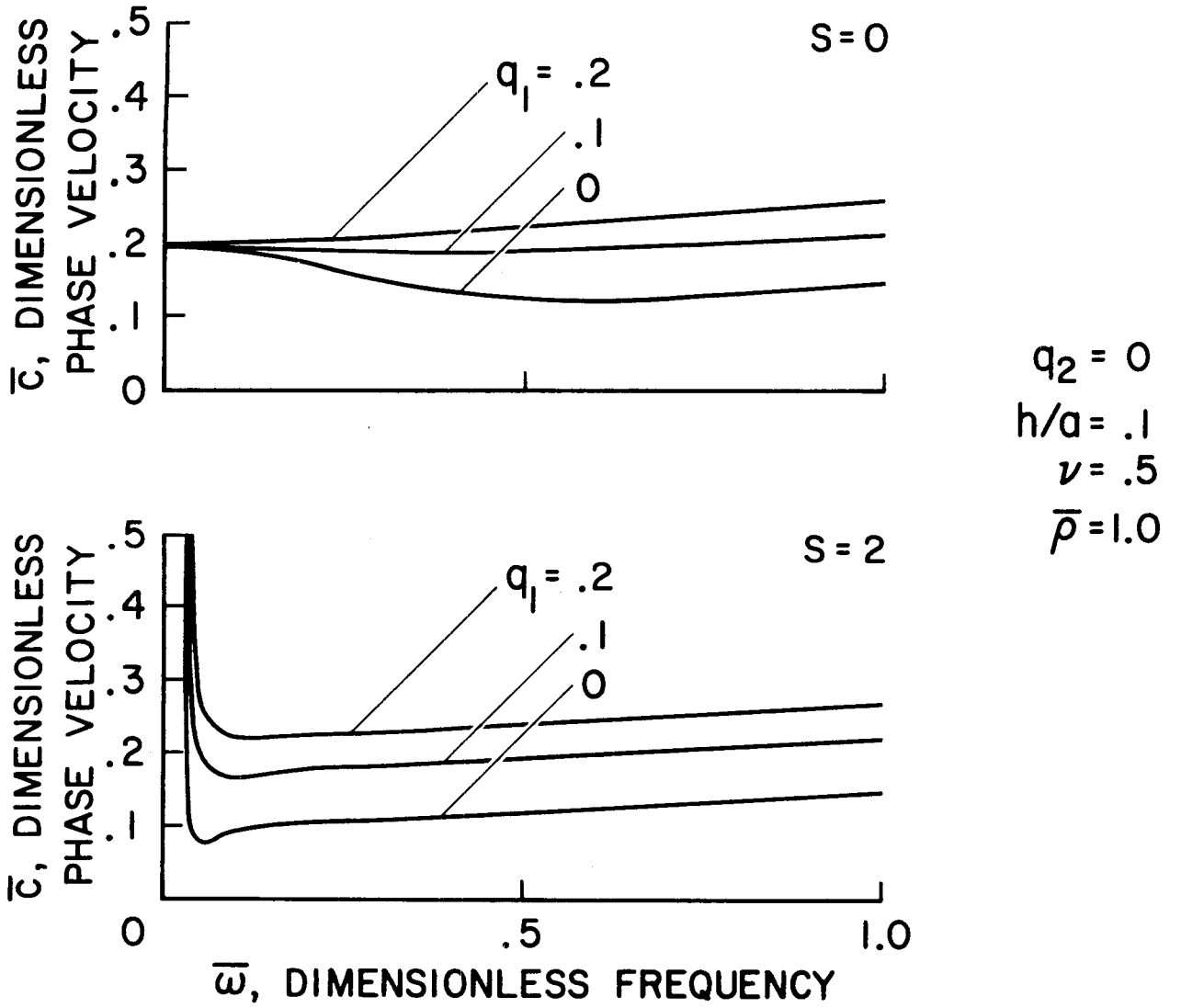

Figure 8. Elastic Shell. Dispersion Curves of Type I Waves for Various Axial Stretches and Zero Transmural Pressure

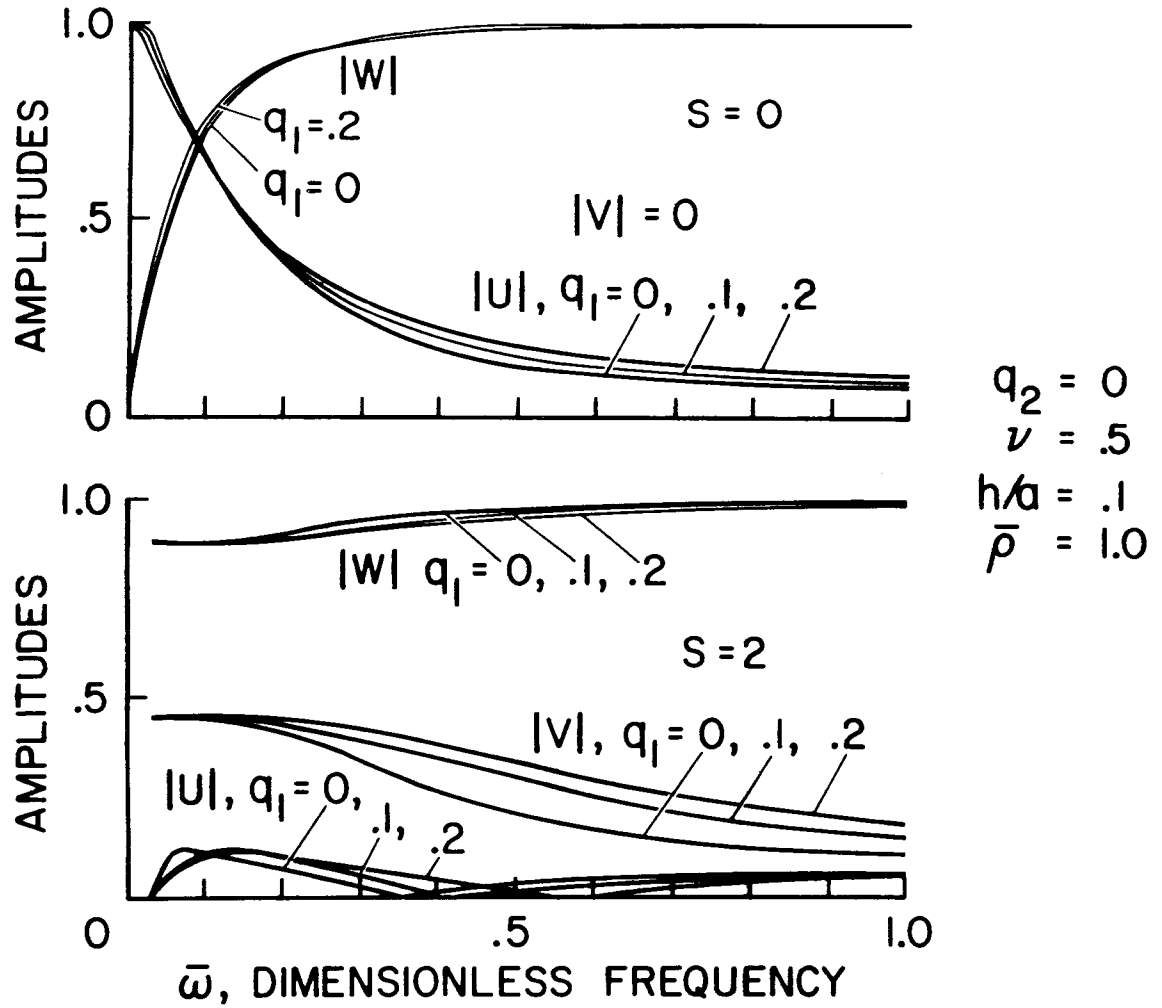

Figure 9. Elastic Shell. Mode Shapes of Type I Waves for Various Axial Stretches and Zero Transmural Pressure

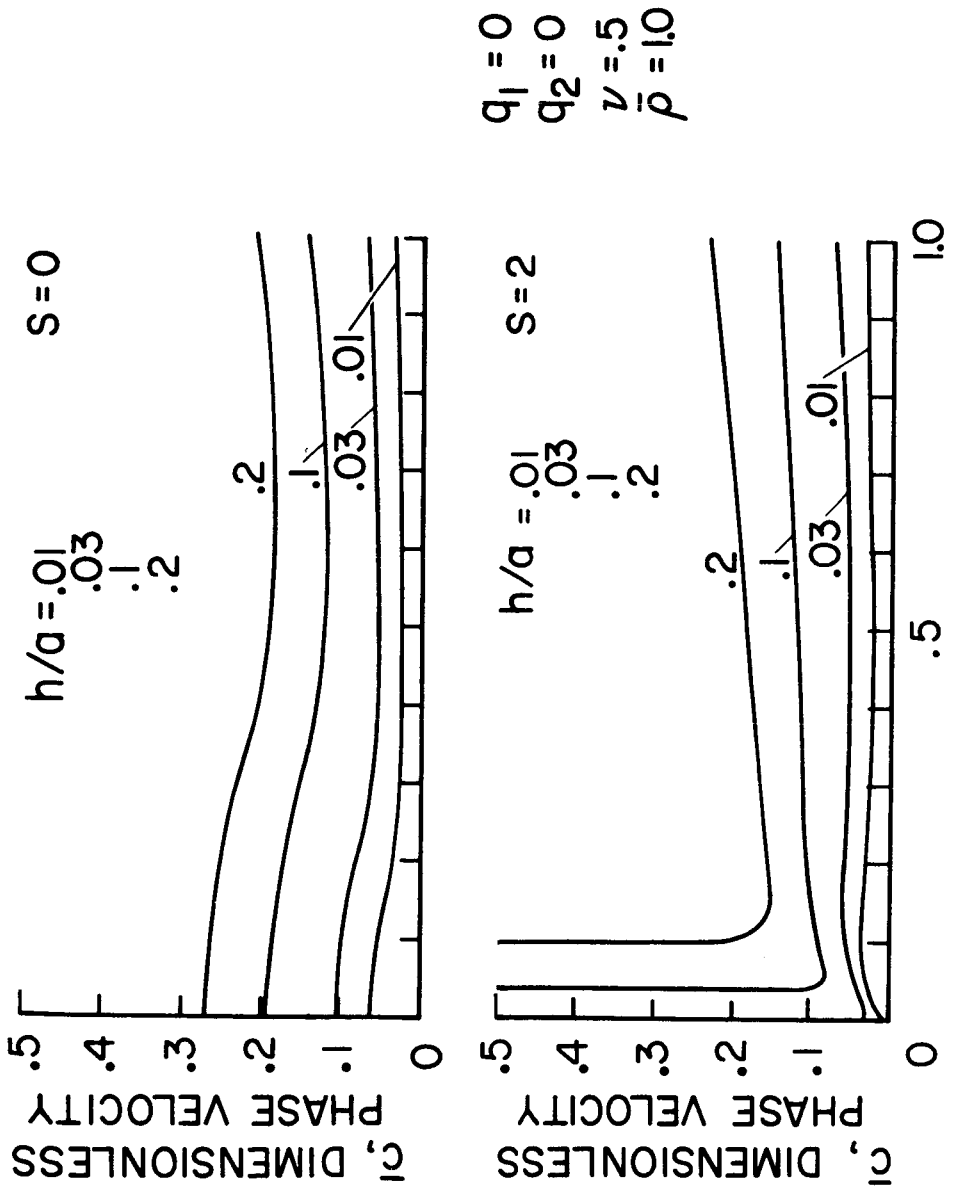

Figure 10. Elastic Shell. Dispersion Curves of Type I Waves for Various Wall Thickness to Radius Ratios at Zero Transmural Pressure and Zero Axial Stretch

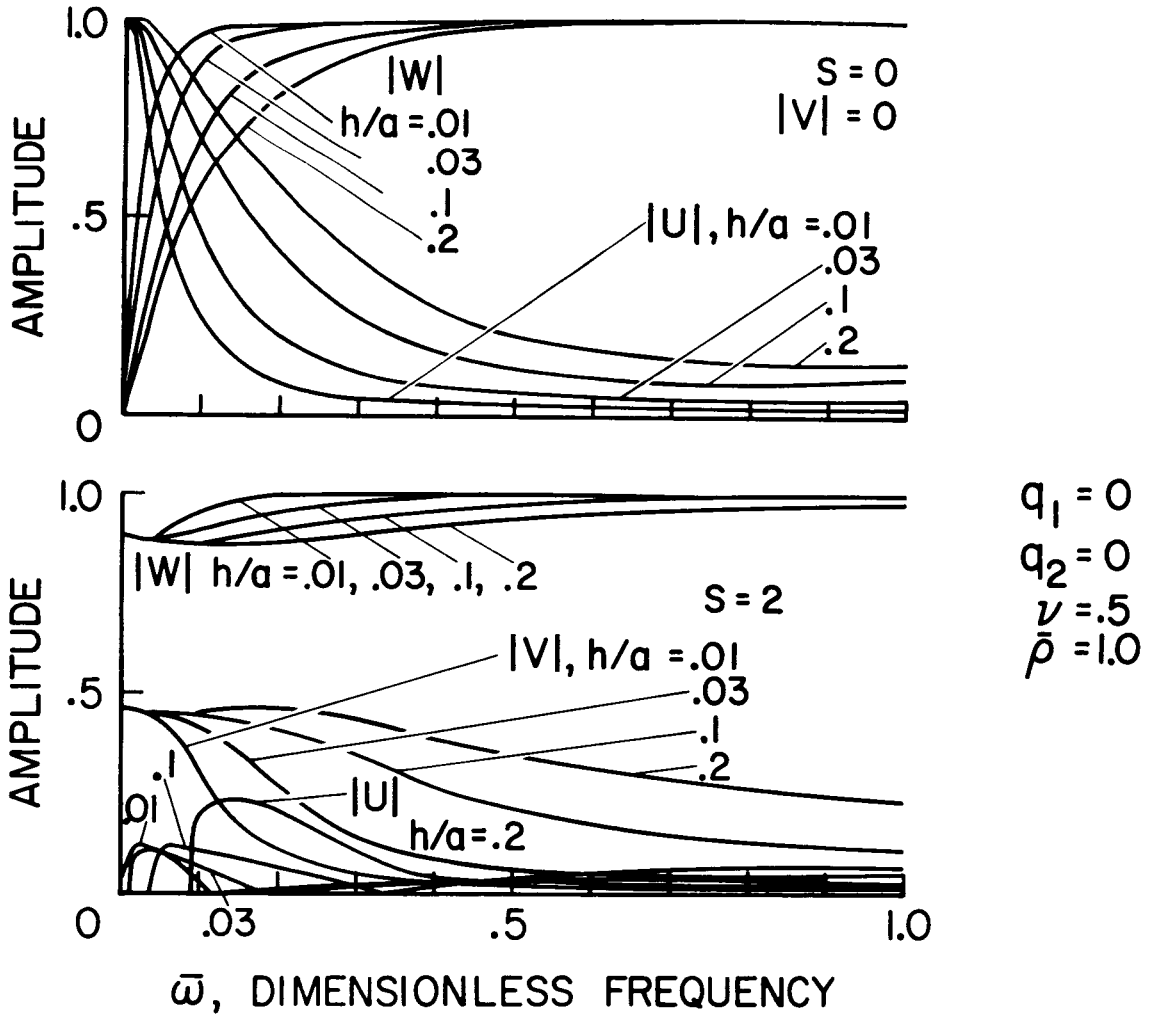

Figure 11. Elastic Shell. Mode Shapes of Type I Waves for Various Wall Thickness to Radius Ratios at Zero Transmural Pressure and Zero Axial Stretch

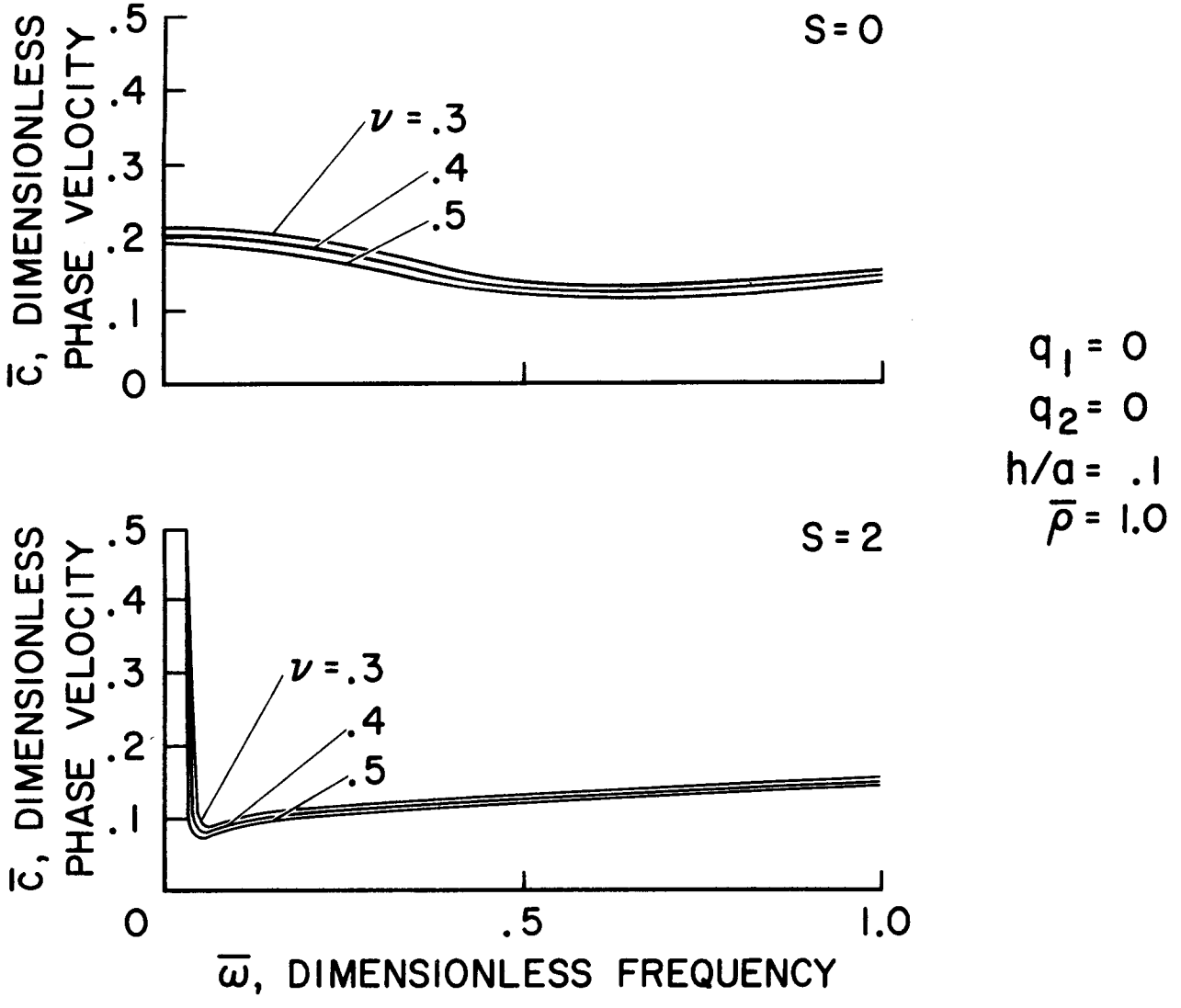

Figure 12. Elastic Shell. Dispersion Curves of Type I Waves for Various Poisson's Ratios at Zero Transmural Pressure and Zero Axial Stretch

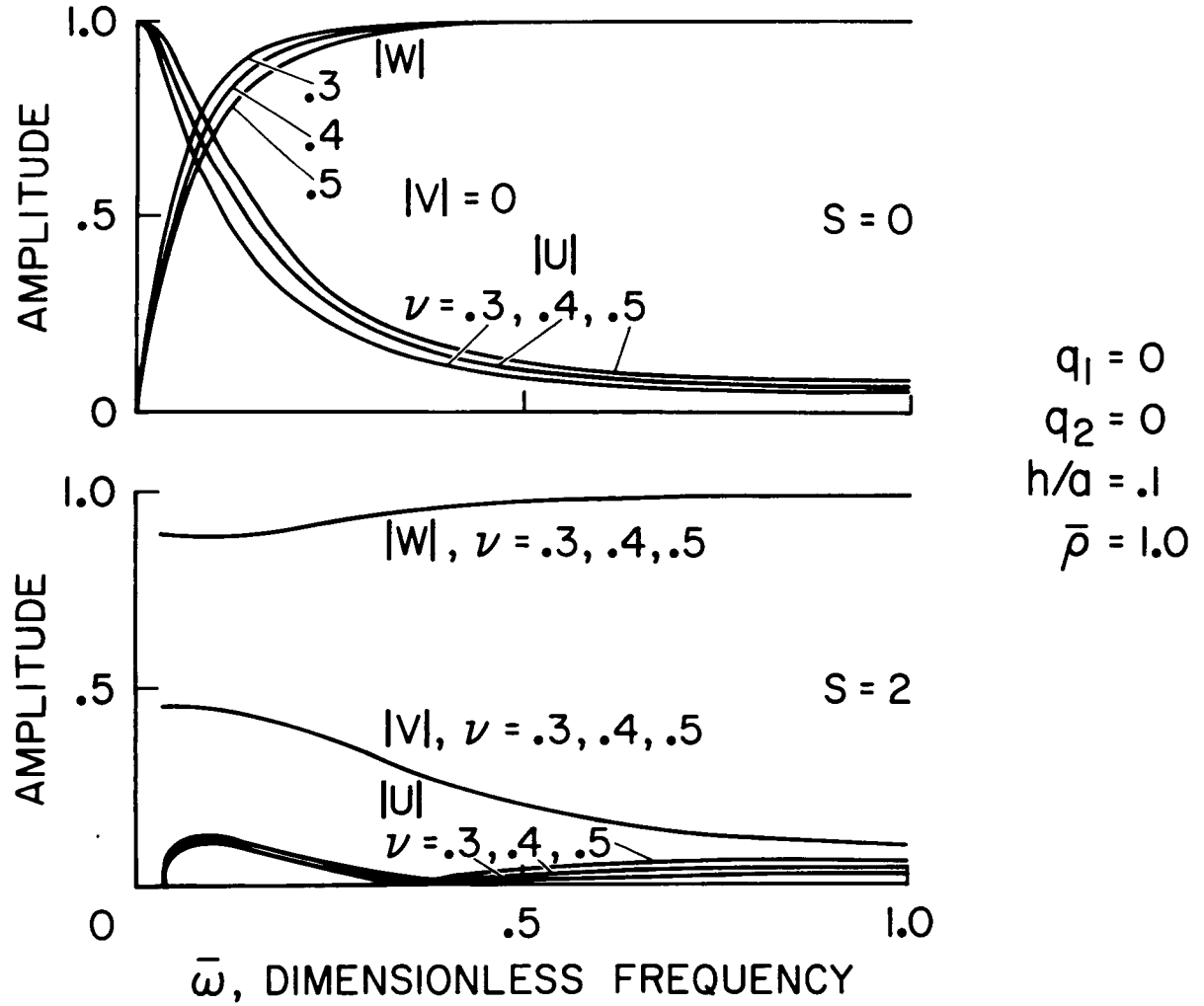

Figure 13. Elastic Shell. Mode Shapes of Type I Waves for Various Poisson's Ratios at Zero Transmural Pressure and Zero Axial Stretch

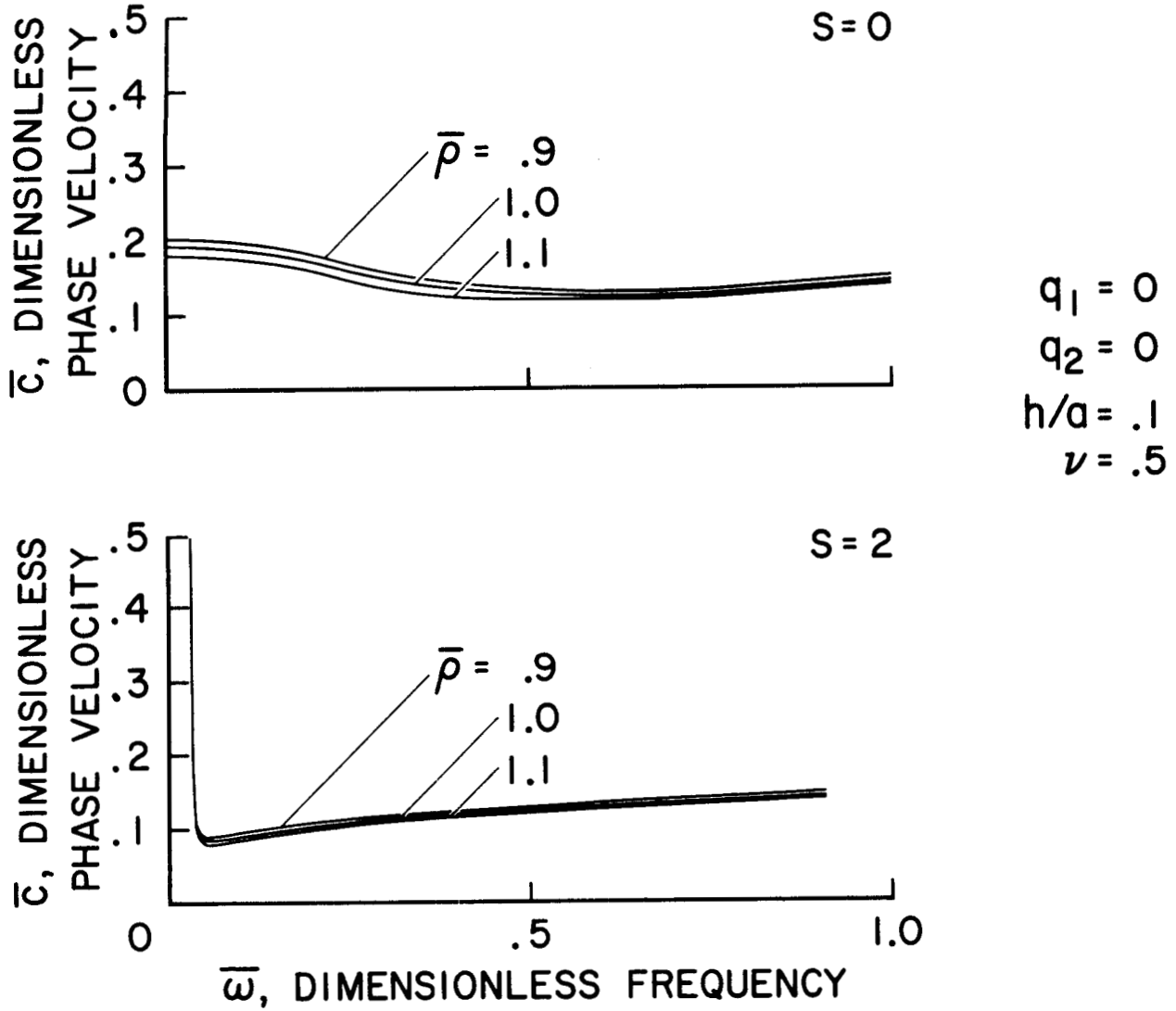

Figure 14. Elastic Shell. Dispersion Curves of Type I Waves for Various Density Ratios at Zero Transmural Pressure and Zero Axial Stretch

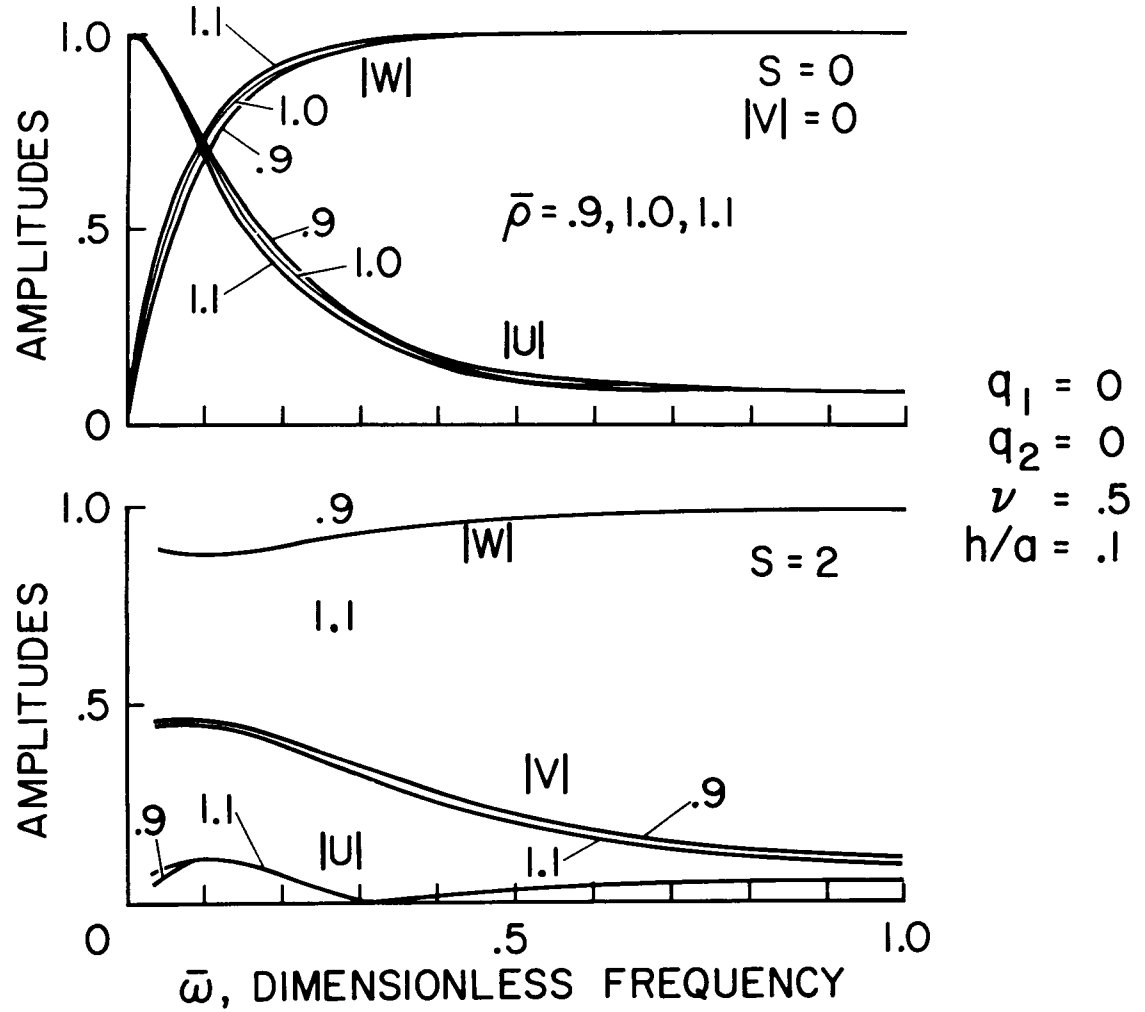

Figure 15. Elastic Shell. Mode Shapes of Type I Waves for Various Density Ratios at Zero Transmural Pressure and Zero Axial Stretch

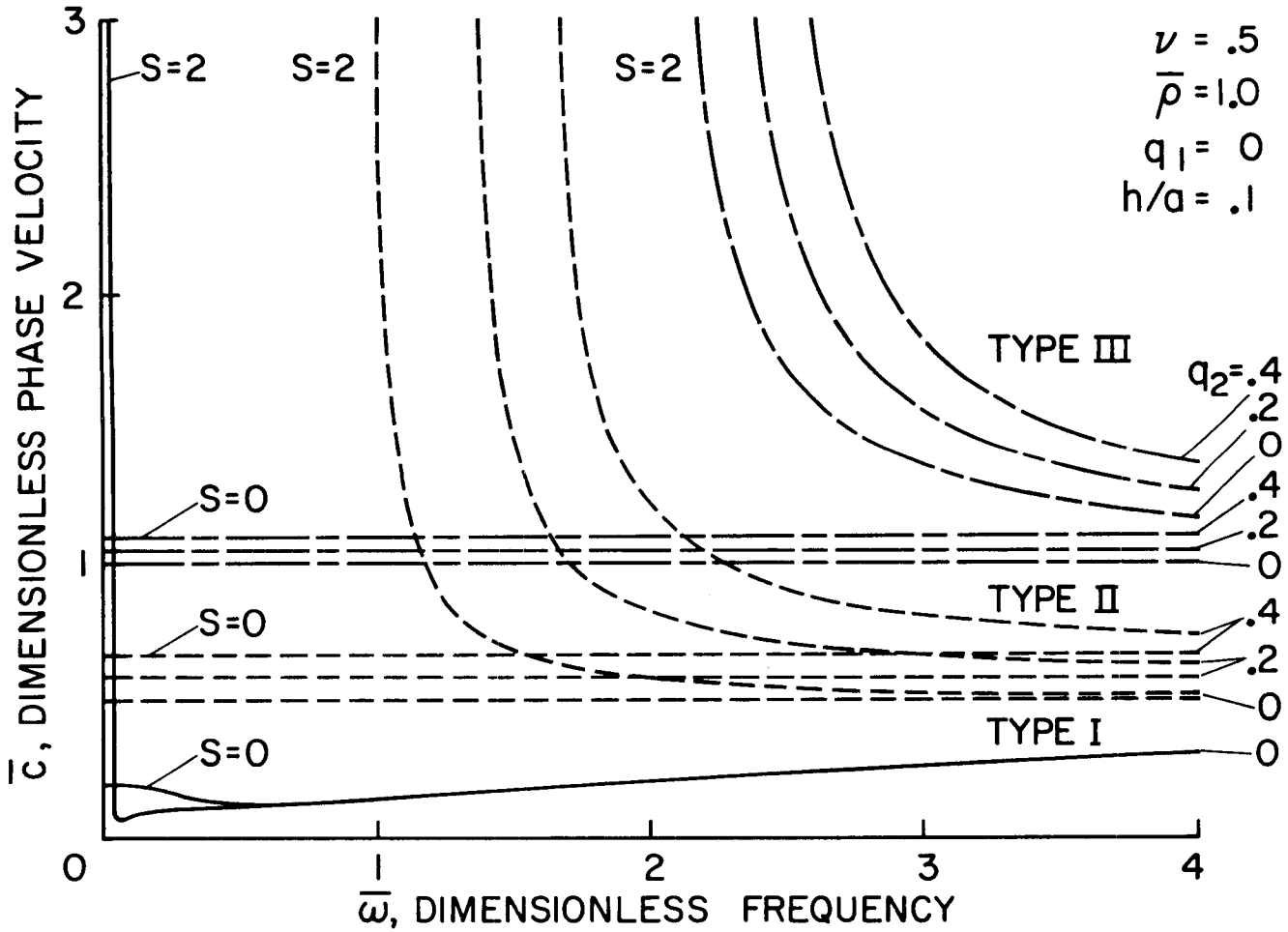

Figure 16. Elastic Shell. Dispersion Curves of Type II and Type III Waves for Various Transmural Pressures and Zero Axial Stretch. Type I Curves at Zero Transmural Pressure and Zero Axial Stretch Presented for Reference Only

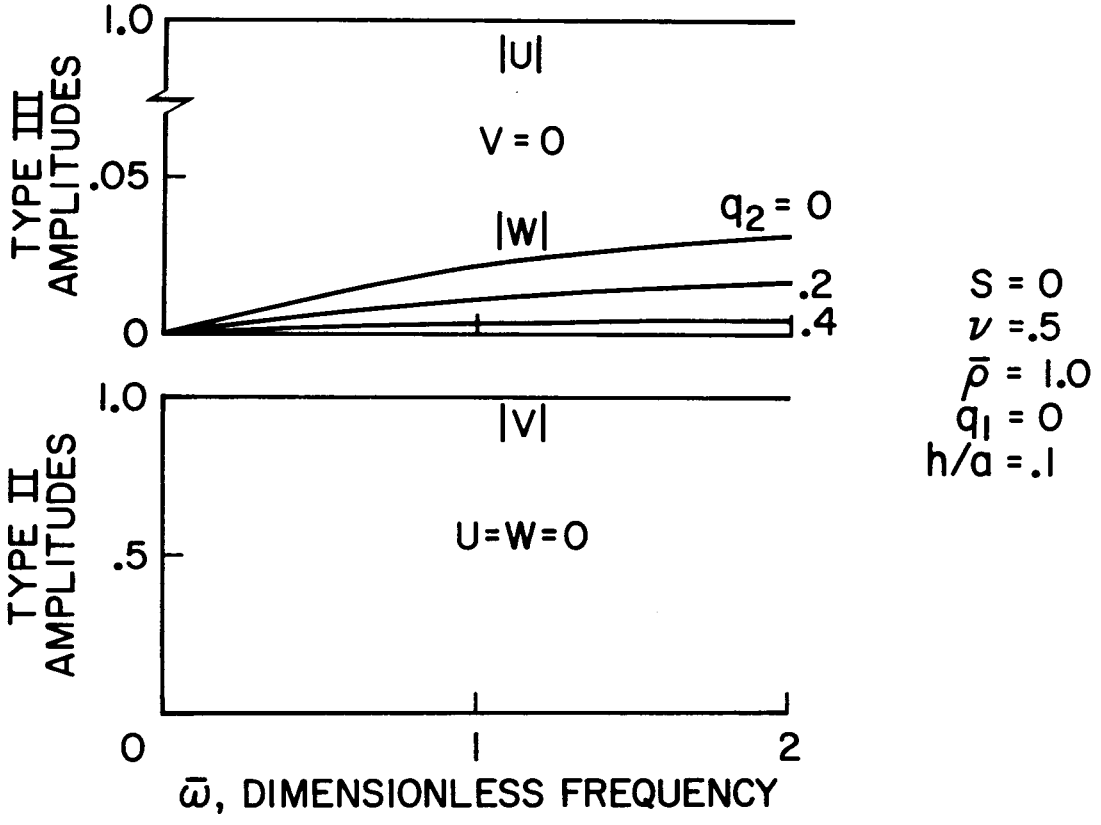

Figure 17. Elastic Shell. Mode Shapes of Axisymmetric Type II and Type III Waves for Various Transmural Pressures and Zero Axial Stretch

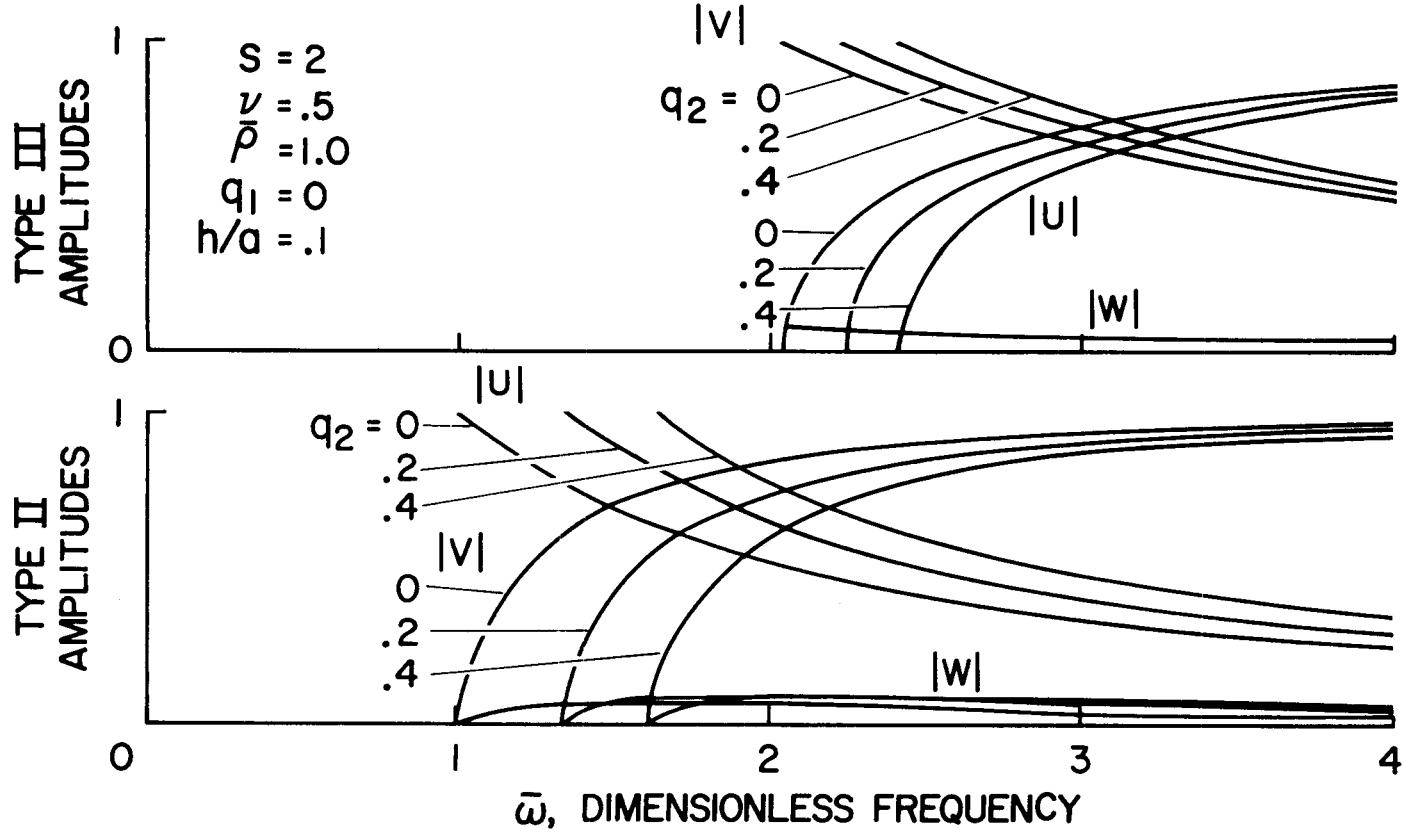

Figure 18. Elastic Shell. Mode Shapes of Non-Axisymmetric Type II and Type III Waves for Various Transmural Pressures and Zero Axial Stretch

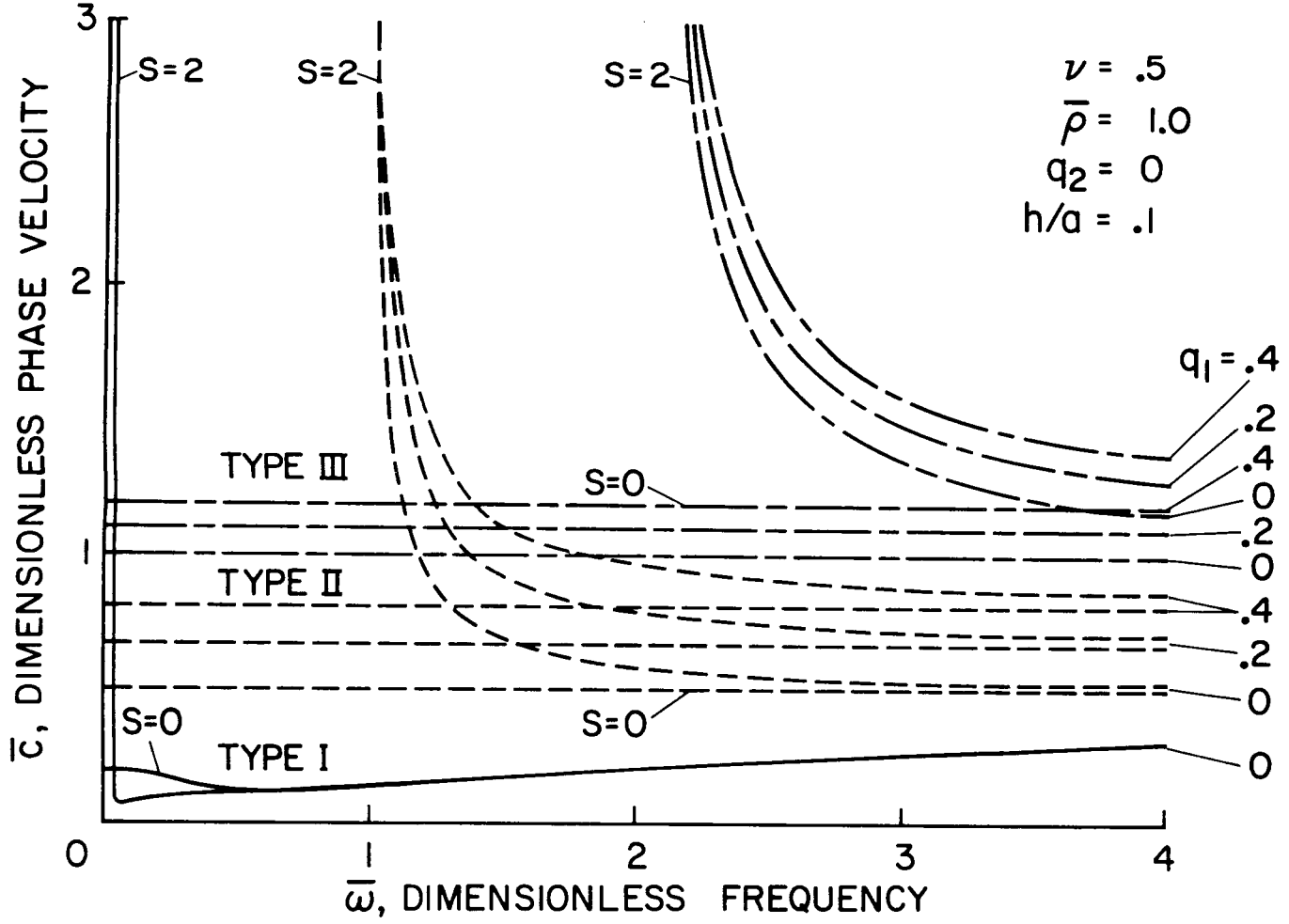

Figure 19. Elastic Shell. Dispersion Curves of Type II and Type III Waves for Various Axial Stretches and Zero Transmural Pressure. Type I Curves at Zero Transmural Pressure and Zero Axial Stretch Presented for Reference Only

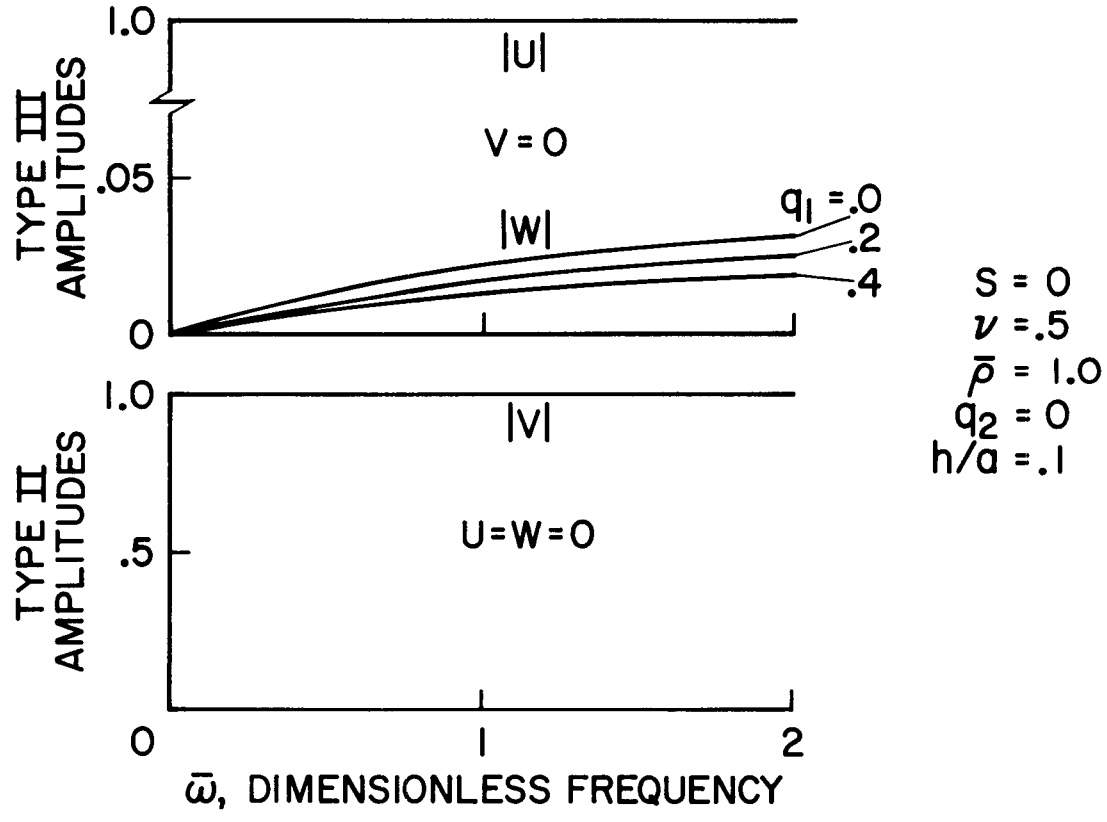

Figure 20. Elastic Shell. Mode Shapes of Axisymmetric Type II and Type III Waves for Various Axial Stretches and Zero Transmural Pressure

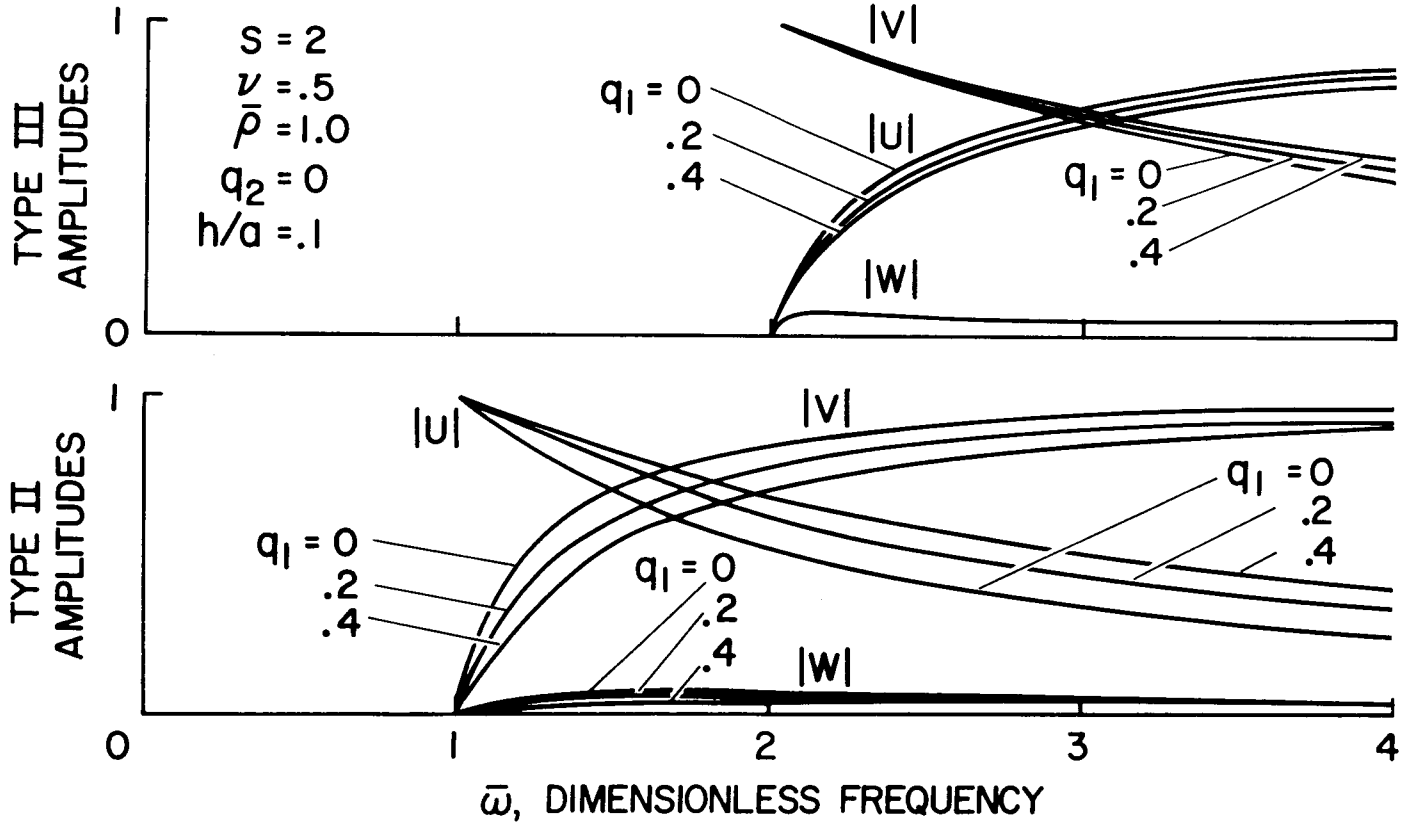

Figure 21. Elastic Shell. Mode Shapes of Non-Axisymmetric Type II and Type III Waves for Various Axial Stretches and Zero Transmural Pressure

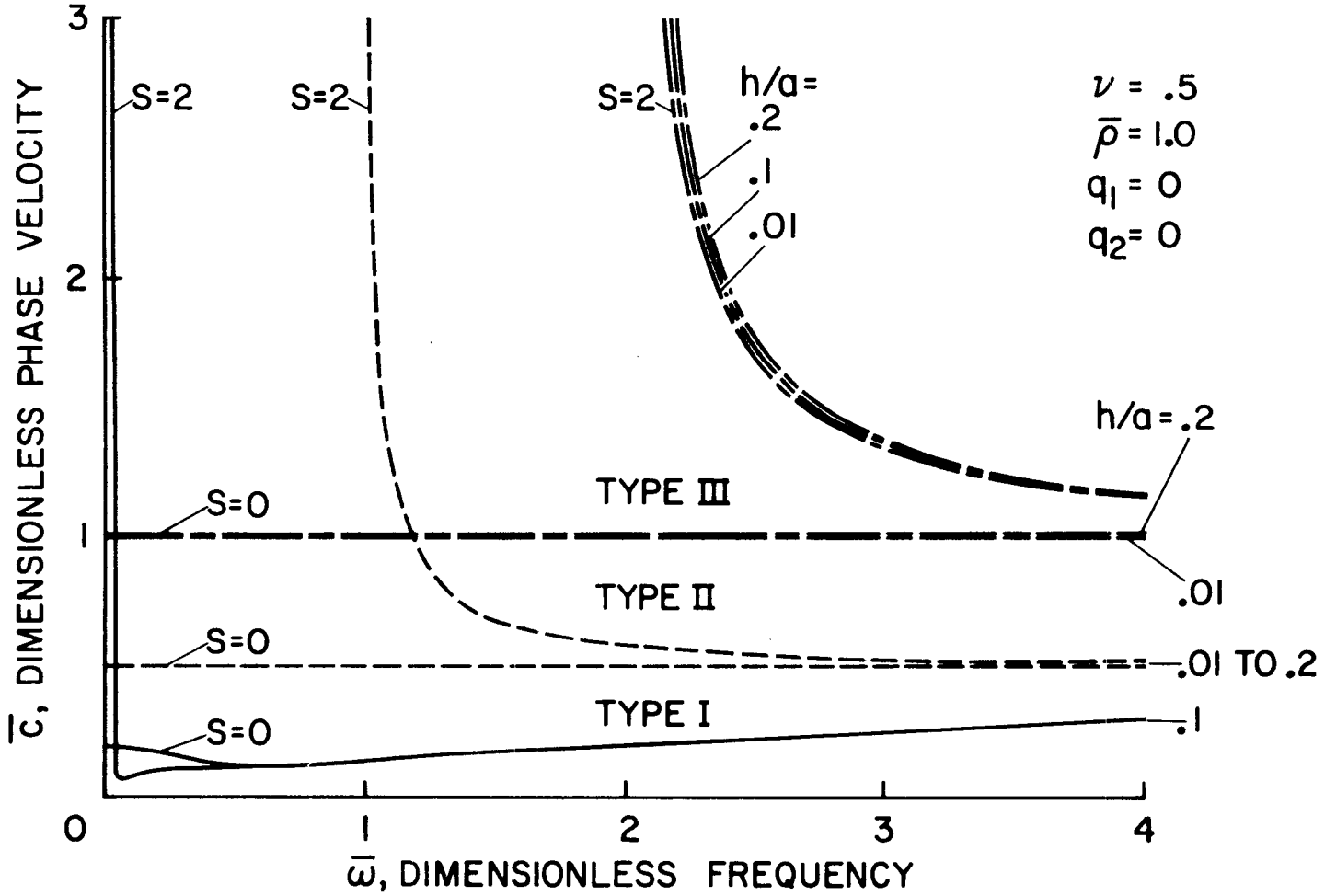

Figure 22. Elastic Shell. Dispersion Curves of Type II and Type III Waves for Various Wall Thickness to Radius Ratios at Zero Transmural Pressure and Zero Axial Stretch

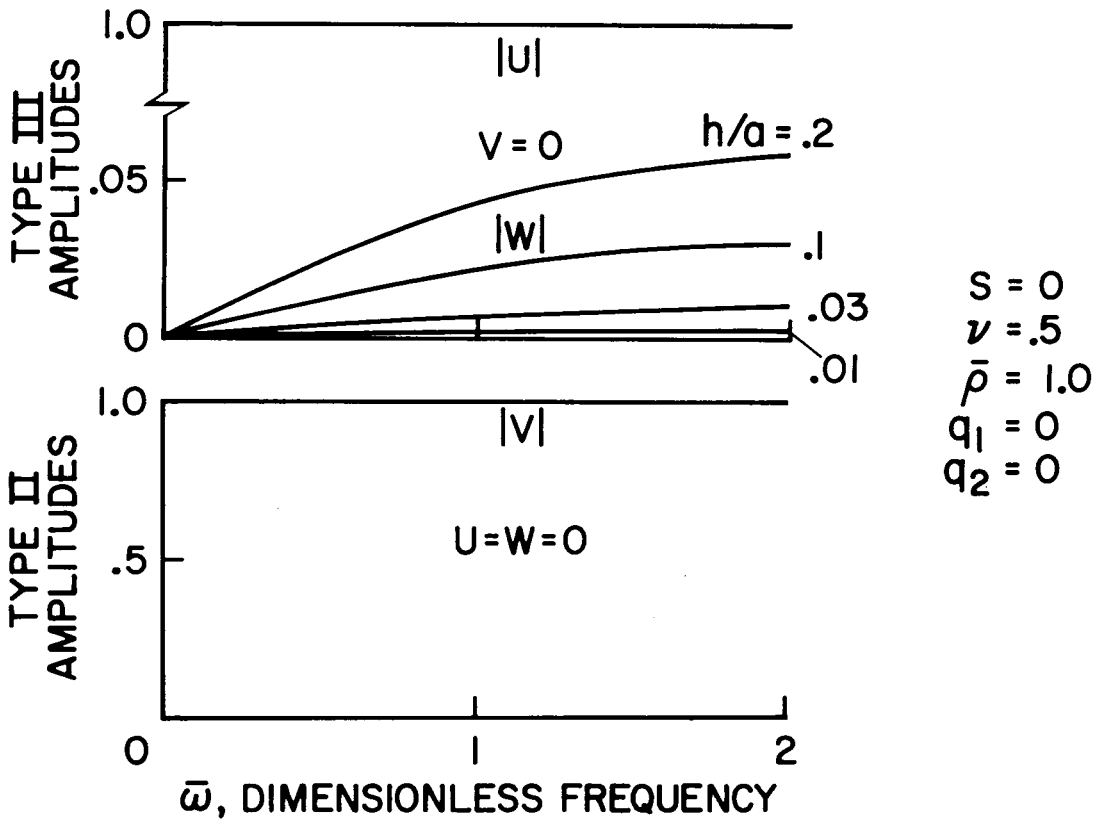

Figure 23. Elastic Shell. Mode Shapes of Axisymmetric Type II and Type III Waves for Various Wall Thickness to Radius Ratios at Zero Transmural Pressure and Zero Axial Stretch

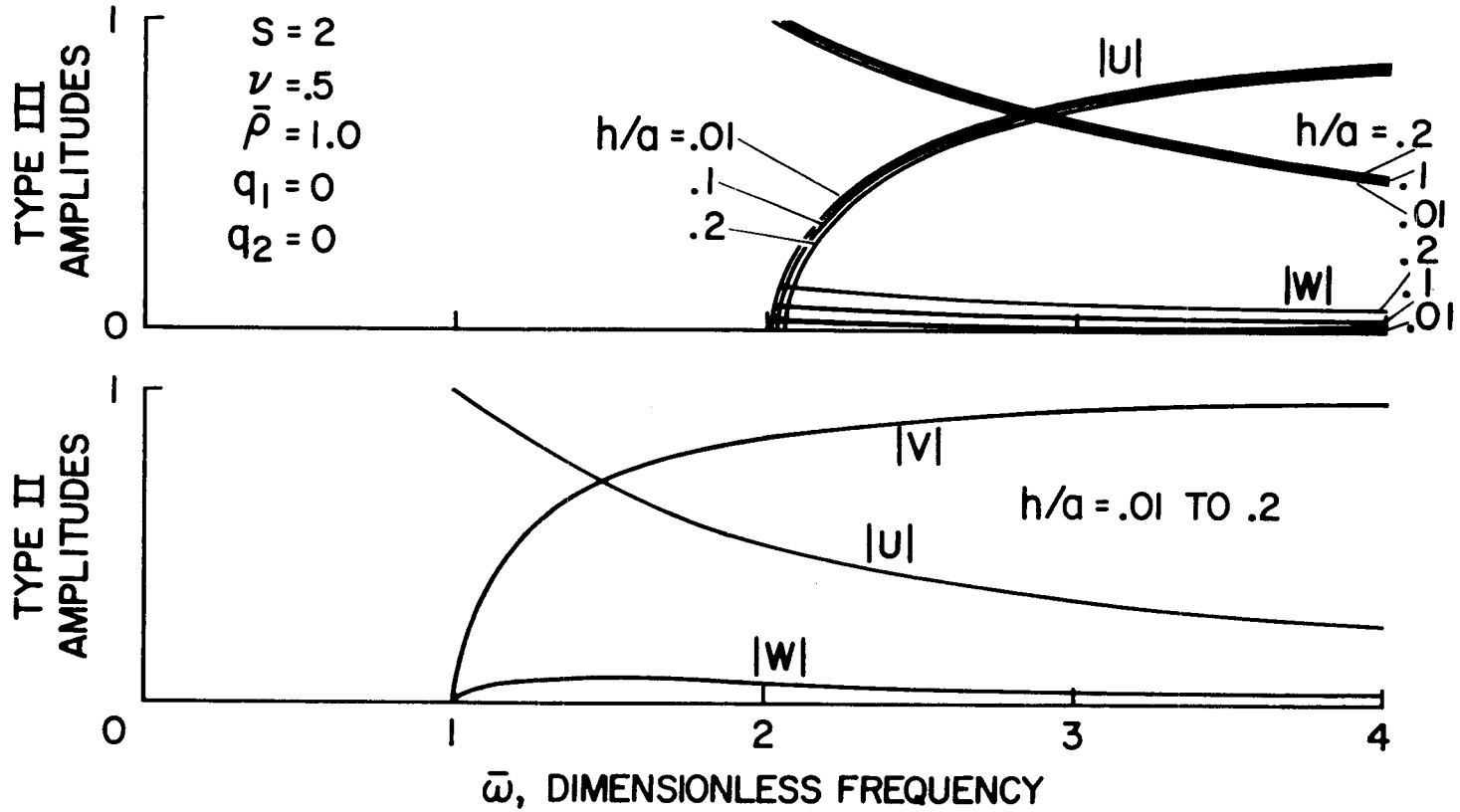

Figure 24. Elastic Shell. Mode Shapes of Non-Axisymmetric Type II and Type III Waves for Various Wall Thickness to Radius Ratios at Zero Transmural Pressure and Zero Axial Stretch

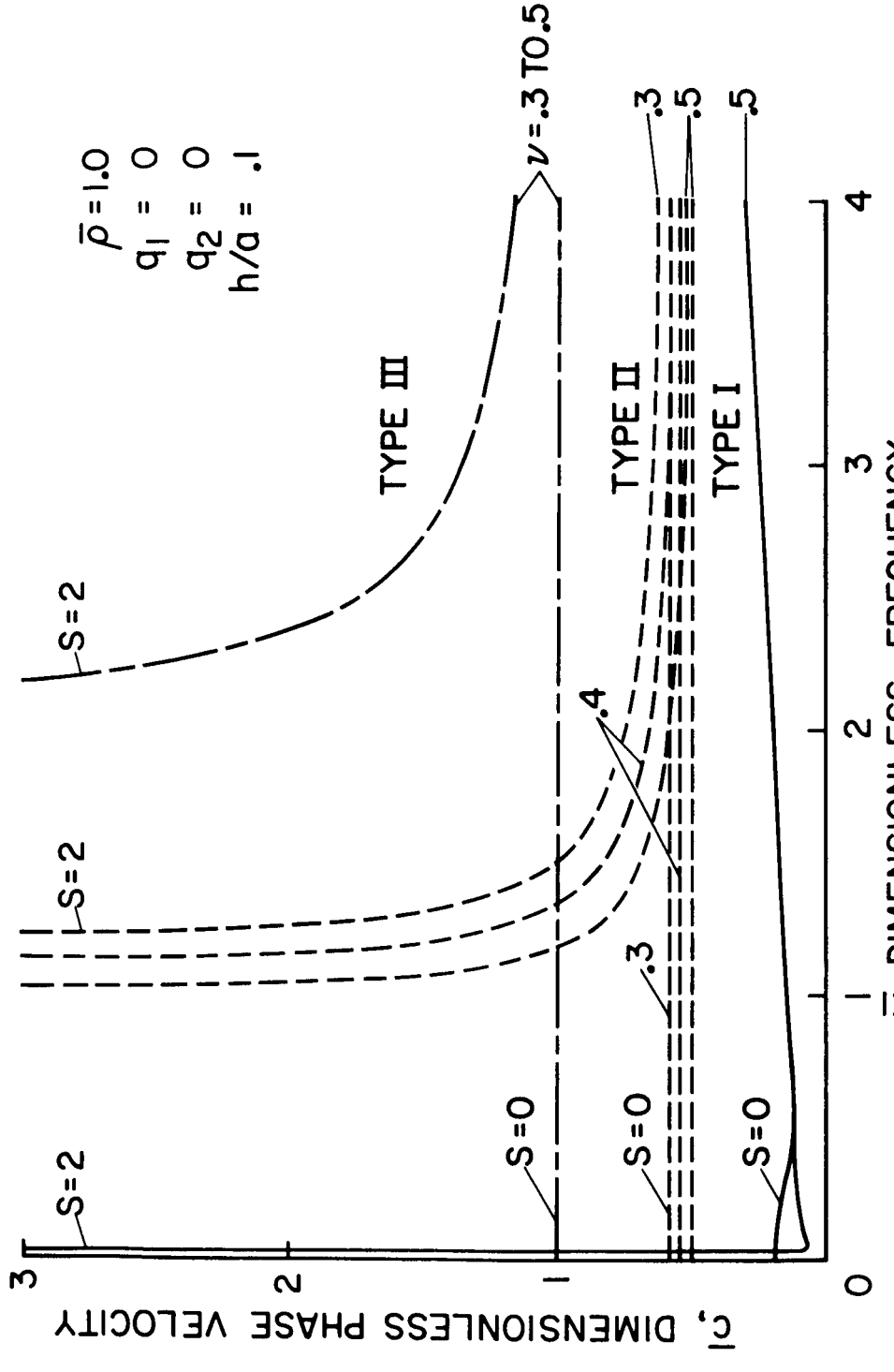

Figure 25. Elastic Shell. Dispersion Curves of Type II and Type III Waves for Various Poisson's Ratios at Zero Transmural Pressure and Zero Axial Stretch

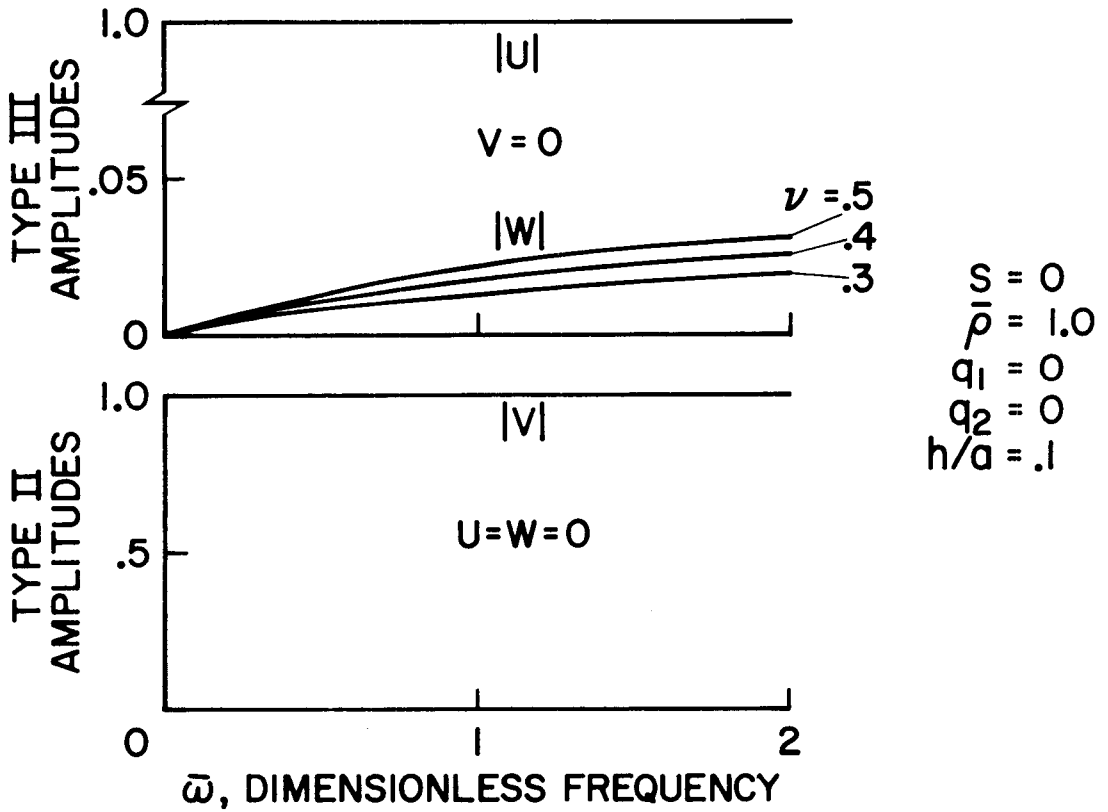

Figure 26. Elastic Shell. Mode Shapes of Axisymmetric Type II and Type III Waves for Various Poisson's Ratios at Zero Transmural Pressure and Zero Axial Stretch

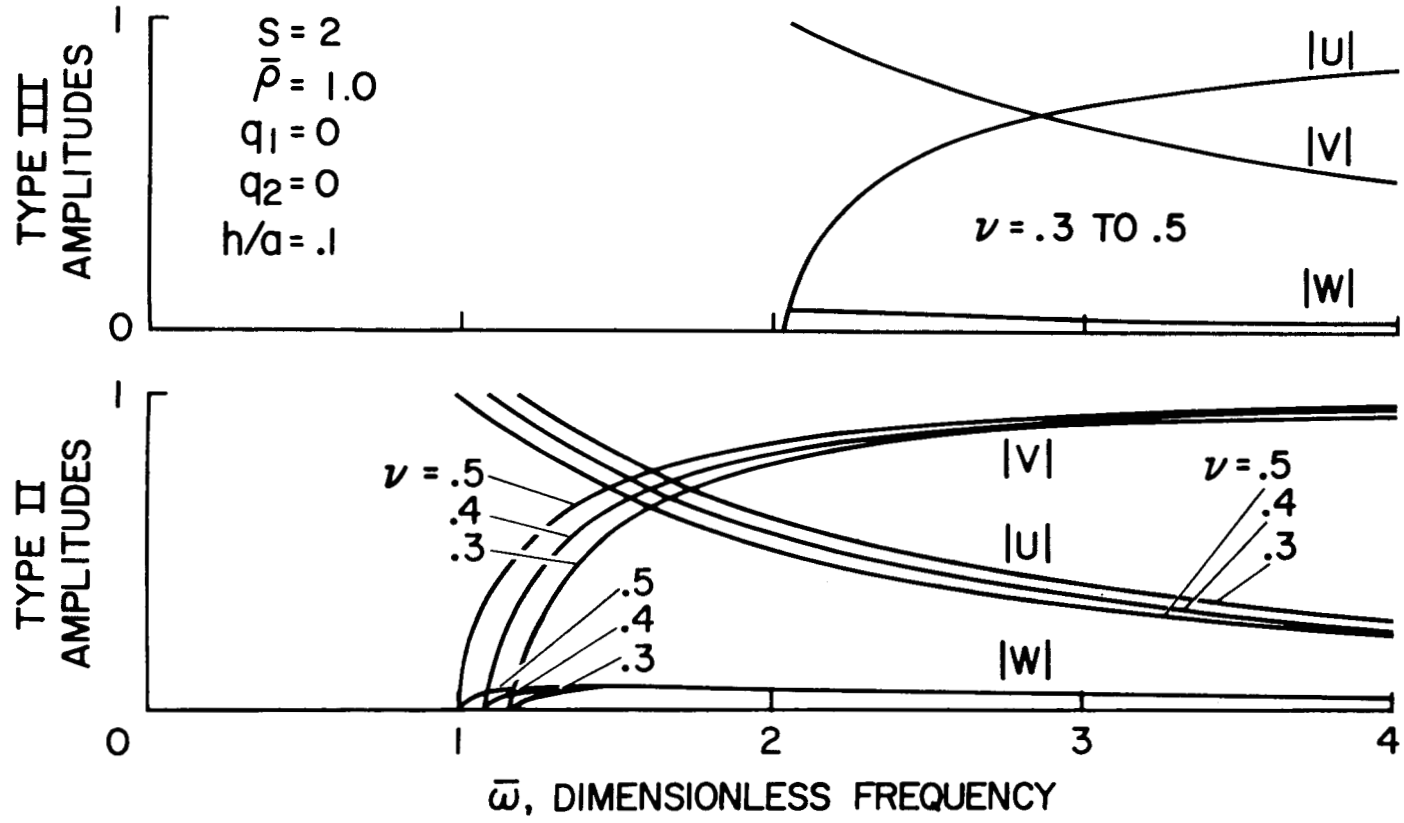

Figure 27. Elastic Shell. Mode Shapes of Non-Axisymmetric Type II and Type III Waves for Various Poisson's Ratios at Zero Transmural Pressure and Zero Axial Stretch

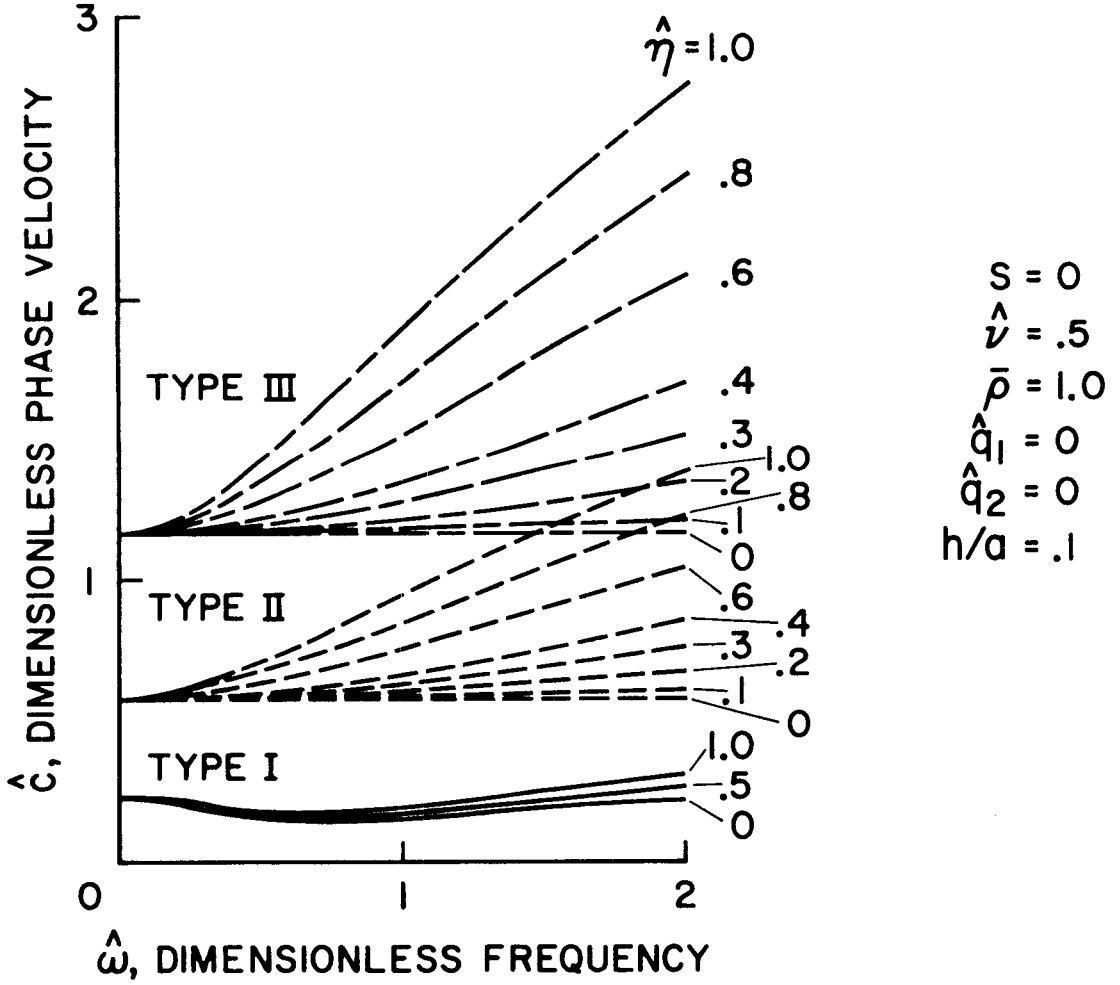

Figure 28. Viscoelastic Shell. Dispersion Curves of Axisymmetric Type I, II and III Waves for Various Values of the Dimensionless Viscosity Coefficient of the Vessel Wall. Transmural Pressure and Axial Stretch are Both Equal to Zero

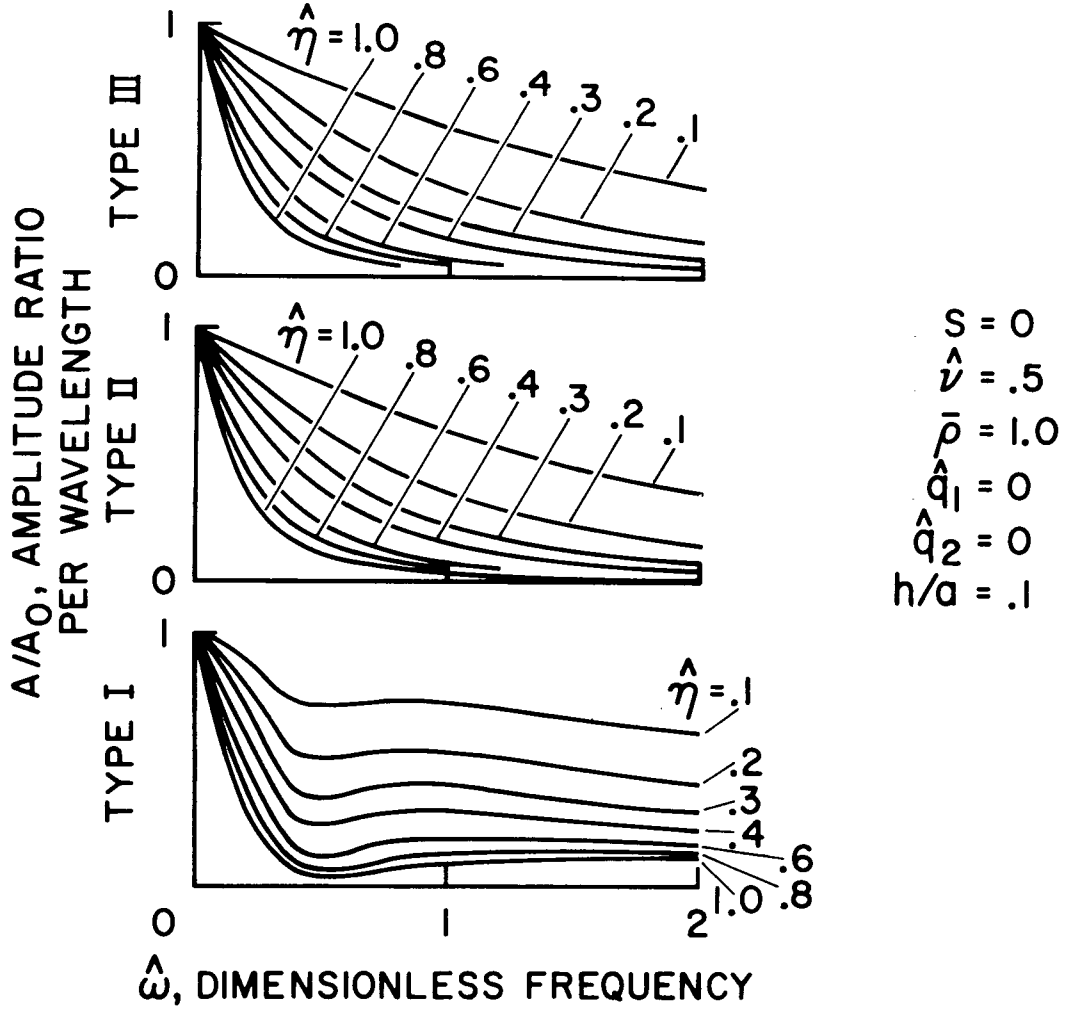

Figure 29. Viscoelastic Shell. Amplitude Ratio Curves of Axisymmetric Type I, and III Waves for Various Values of the Dimensionless Viscosity Coefficient of the Vessel Wall. Transmural Pressure and Axial Stretch are Both Equal to Zero

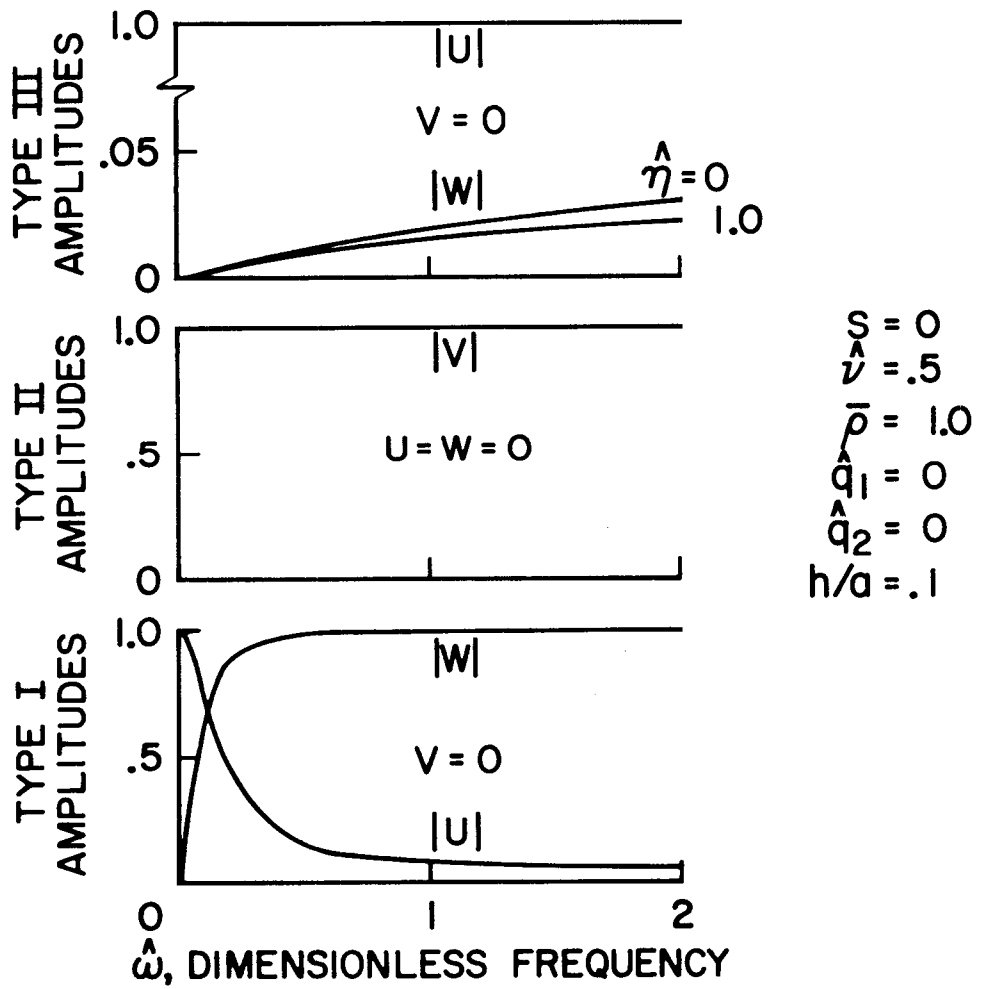

Figure 30. Viscoelastic Shell. Mode Shapes of Axisymmetric Type I, II and III Waves for Various Values of the Dimensionless Viscosity Coefficient of the Vessel Wall. Transmural Pressure and Axial Stretch are Both Equal to Zero

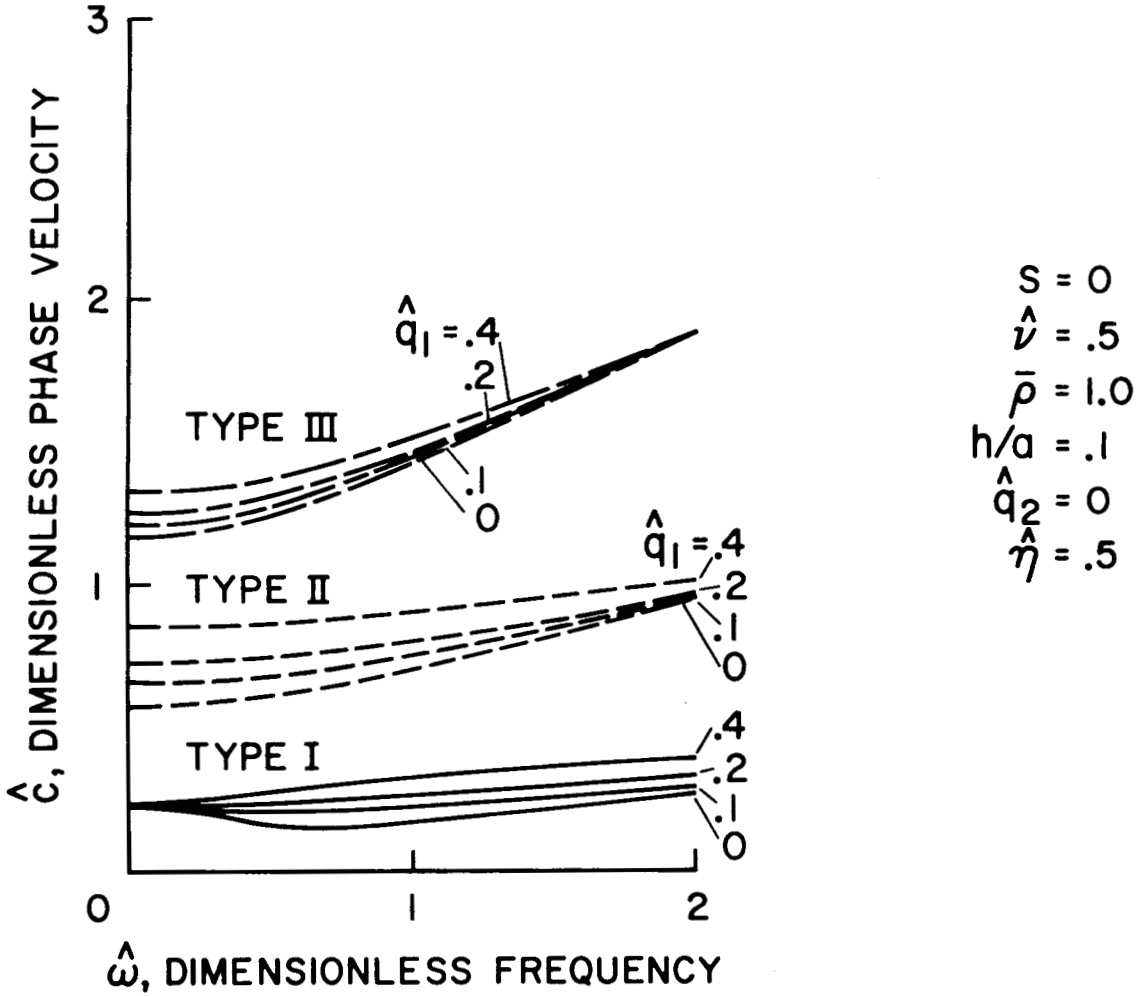

Figure 31. Viscoelastic Shell. Dispersion Curves of Axisymmetric Type I, II and III Waves for Various Axial Stretches, Zero Transmural Pressure and Dimensionless Wall Viscosity Coefficient $\hat{\eta}$ = 0.5

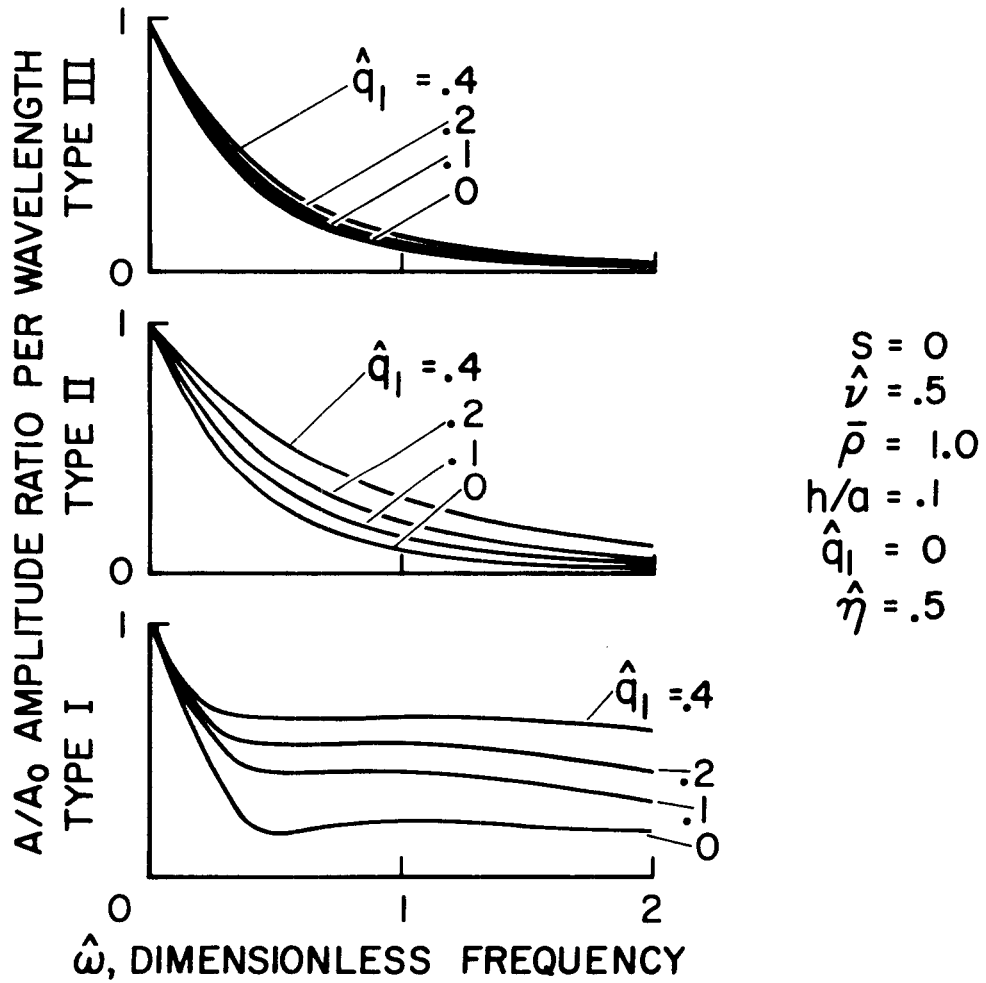

Figure 32. Viscoelastic Shell. Amplitude Ratio Curves of Axisymmetric Type I, II and III Waves for Various Axial Stretches, Zero Transmural Pressure and Dimensionless Wall Viscosity Coefficient $\hat{\eta} = 0.5$

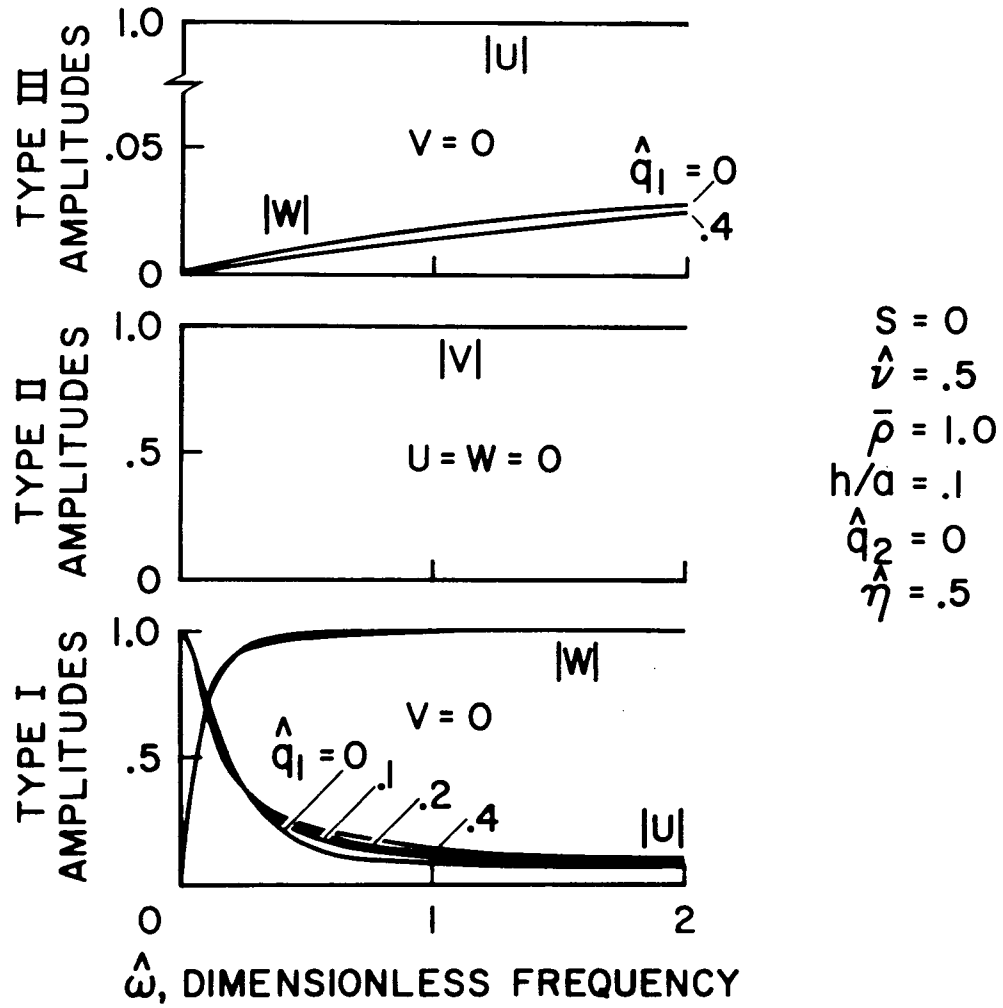

Figure 33. Viscoelastic Shell. Mode Shapes of Axisymmetric Type I, II and III Waves for Various Axial Stretches, Zero Transmural Pressure and Dimensionless Wall Viscosity Coefficient $\hat{\eta} = 0.5$

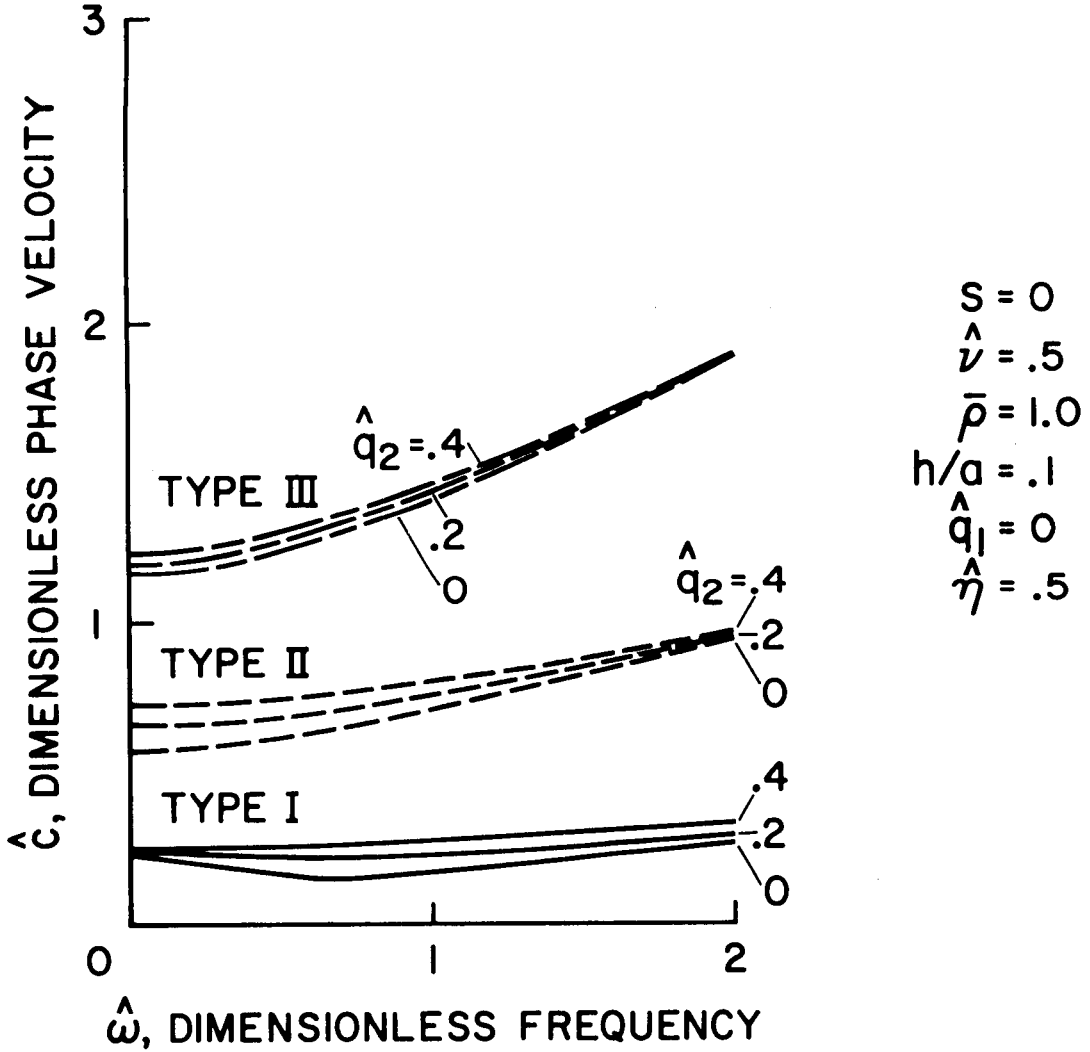

Figure 34. Viscoelastic Shell. Dispersion Curves of Axisymmetric Type I, II and III Waves for Various Transmural Pressures, Zero Axial Stretch and Dimensionless Wall Viscosity Coefficient $\hat{\eta} = 0.5$

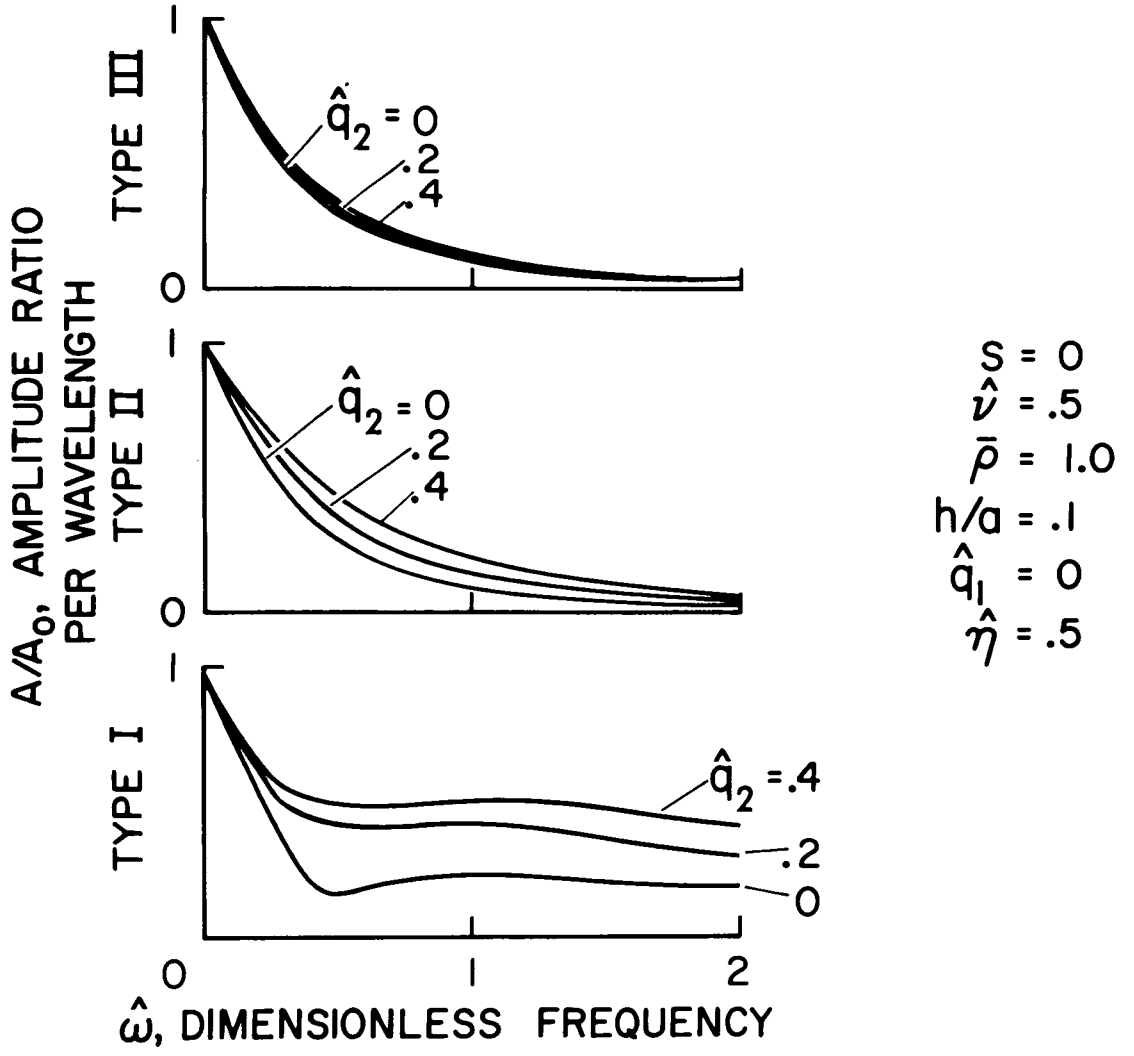

Figure 35. Viscoelastic Shell. Amplitude Ratio Curves of Axisymmetric Type I, II and III Waves for Various Transmural Pressures, Zero Axial Stretch and Dimensionless Wall Viscosity Coefficient $\hat{\eta} = 0.5$

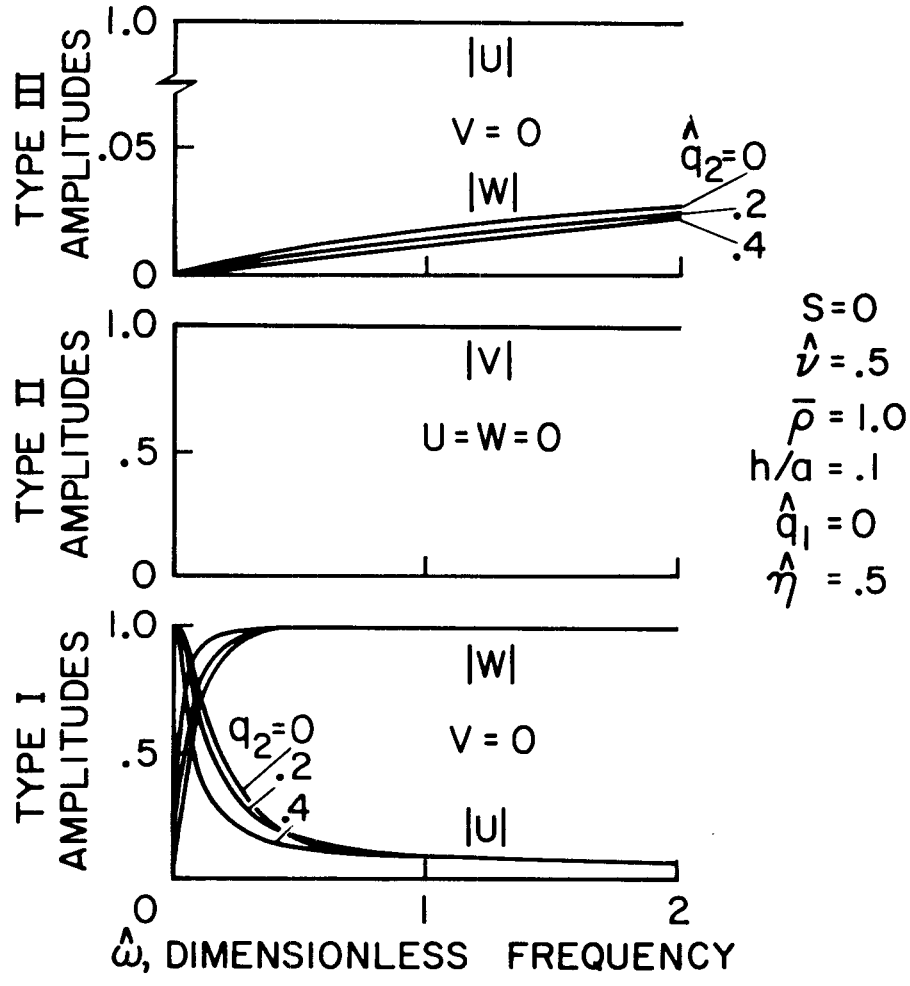

Figure 36. Viscoelastic Shell. Mode Shapes of Axisymmetric Type I, II and III Waves for Various Transmural Pressures, Zero Axial Stretch and Dimensionless Wall Viscosity Coefficient $\hat{\eta} = 0.5$

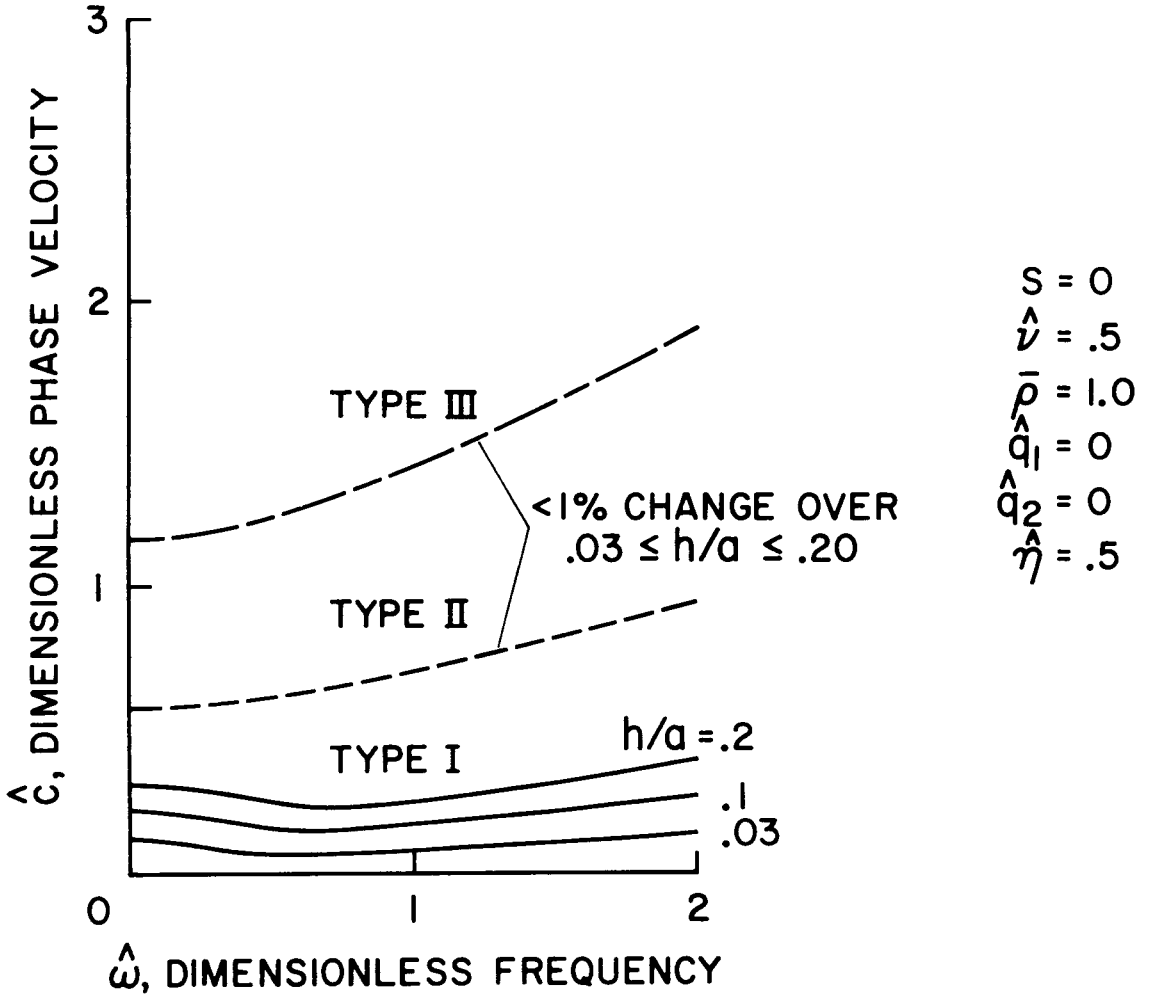

Figure 37. Viscoelastic Shell. Dispersion Curves of Axisymmetric Type I, II and III Waves for Various Wall Thickness to Radius Ratios at Zero Transmural Pressure, Zero Axial Stretch and Dimensionless Wall Viscosity Coefficient $\hat{\eta} = 0.5$

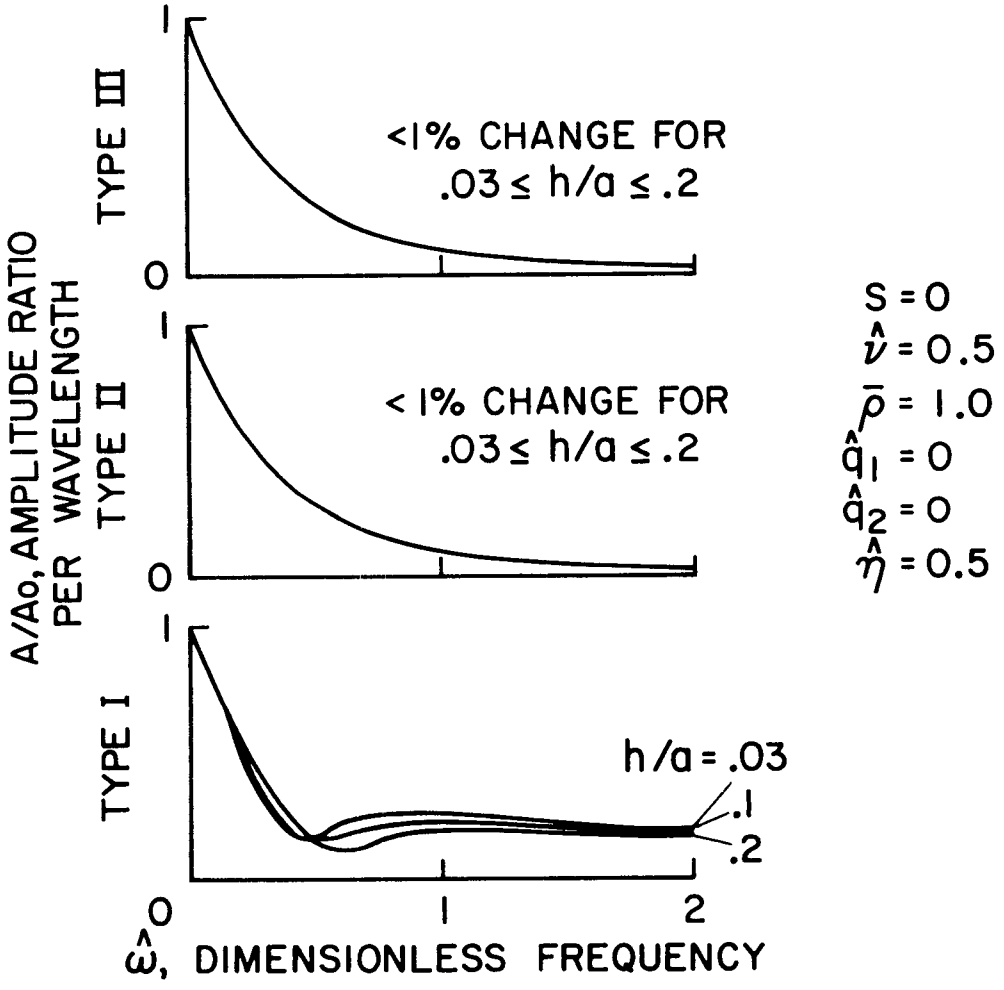

Figure 38. Viscoelastic Shell. Amplitude Ratio Curves of Axisymmetric Type I, II and III Waves for Various Wall Thickness to Radius Ratios at Zero Transmural Pressure, Zero Axial Stretch and Dimensionless Wall Viscosity Coefficient $\hat{\eta} = 0.5$

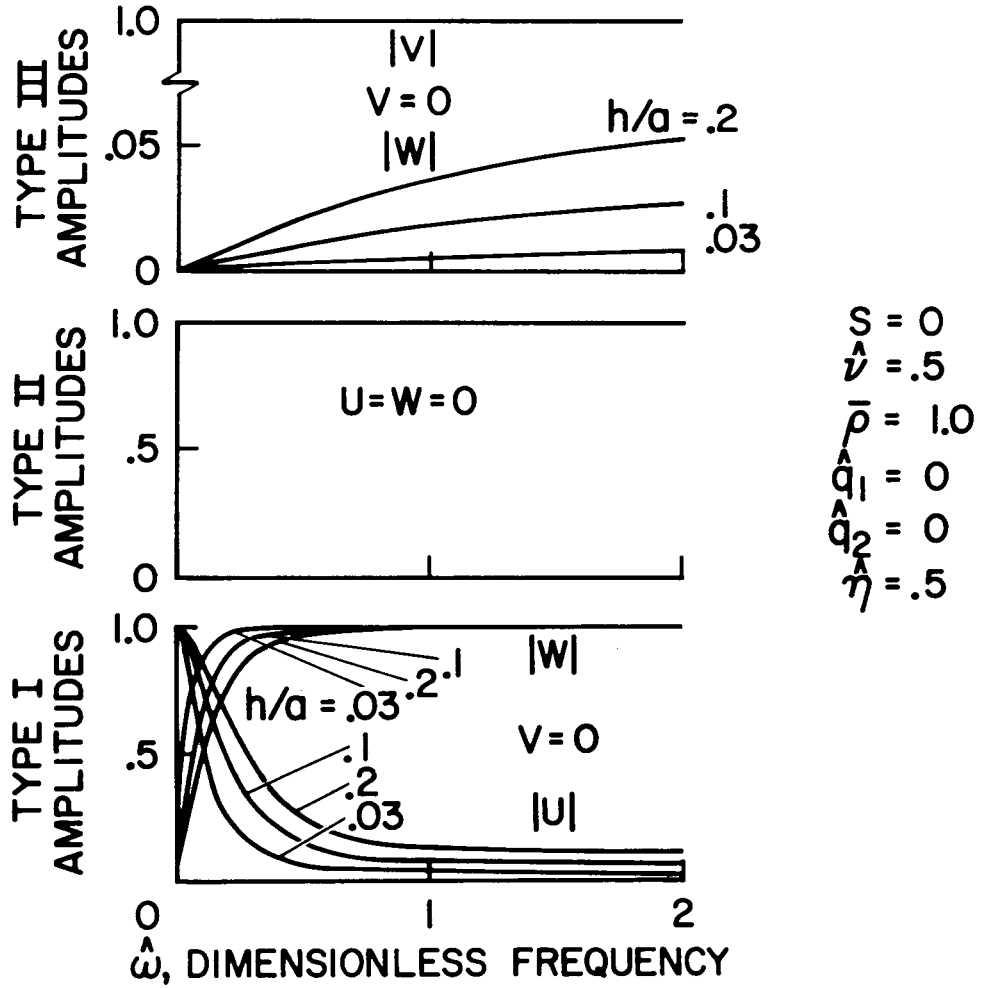

Figure 39. Viscoelastic Shell. Mode Shapes of Axisymmetric Type I, II and III Waves for Various Wall Thickness to Radius Ratios at Zero Transmural Pressure, Zero Axial Stretch and Dimensionless Wall Viscosity Coefficient $\hat{\eta} = 0.5$

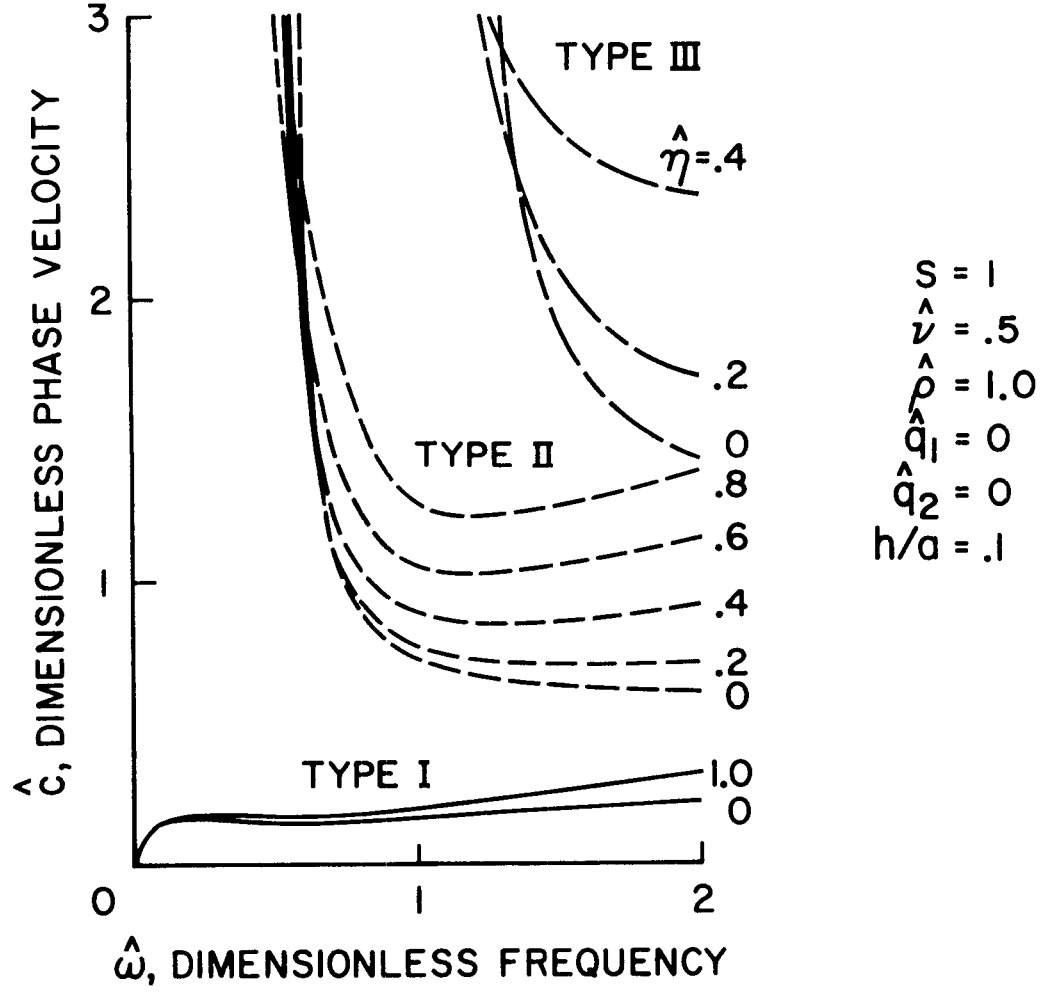

Figure 40. Viscoelastic Shell. Dispersion Curves of Non-Axisymmetric (s = 1) Type I, II and III Waves for Various Values of the Dimensionless Viscosity Coefficient of the Vessel Wall. Transmural Pressure and Axial Stretch are Both Equal to Zero. Below the Elastic Cut-Off Frequencies, $\hat{c} > 3.0$ for Type II and Type III Waves

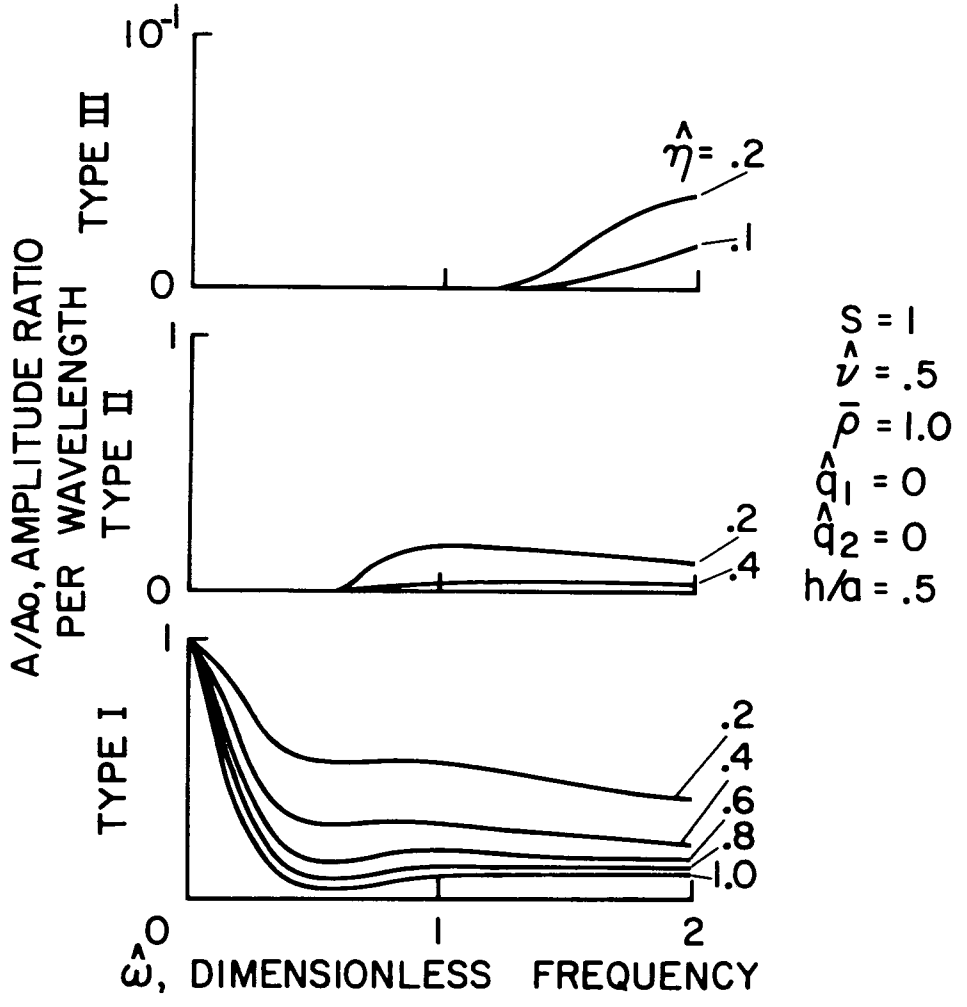

Figure 41. Viscoelastic Shell. Amplitude Ratio Curves of Non-Axisymmetric (s = 1) Type I, II, and III Waves for Various Values of the Dimensionless Viscosity Coefficient of the Vessel Wall. Transmural Pressure and Axial Stretch are Both Equal to Zero

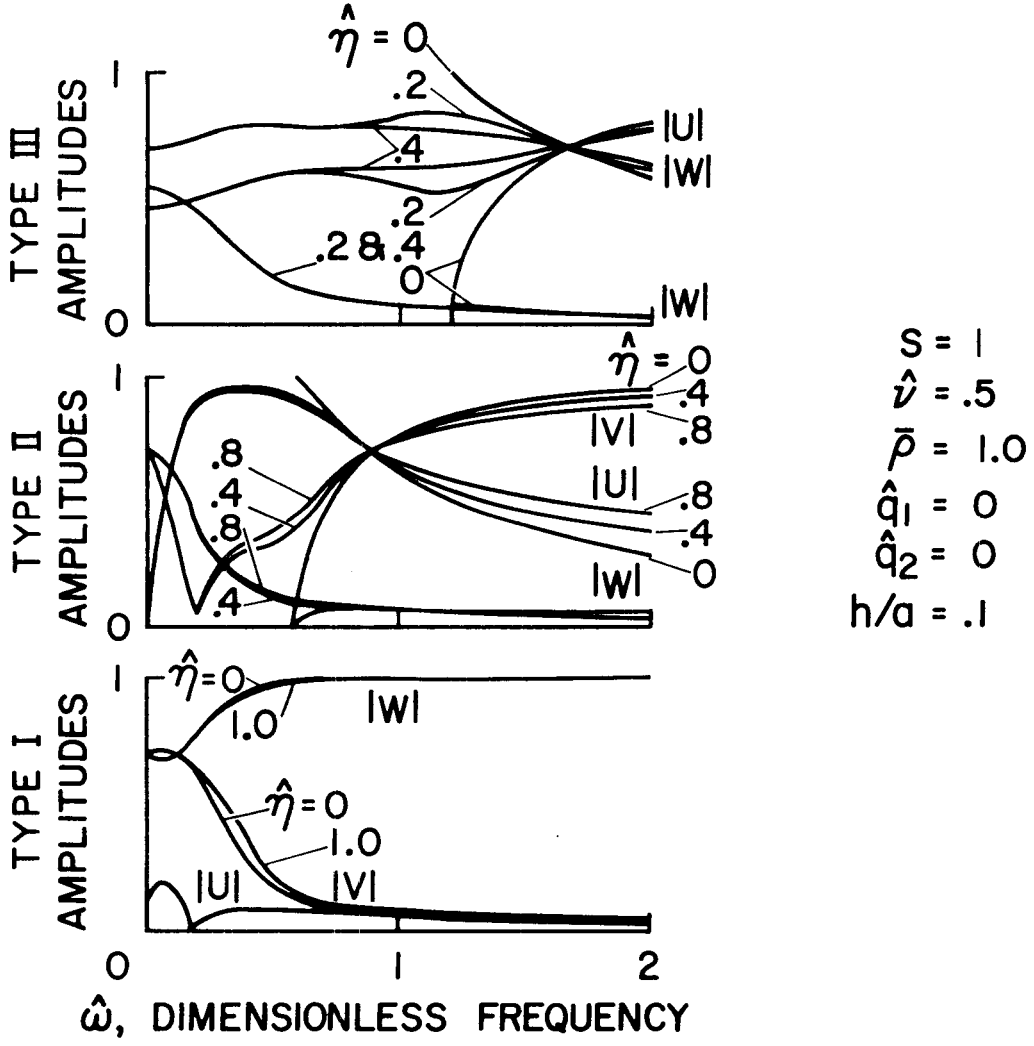

Figure 42. Viscoelastic Shell. Mode Shapes of Non-Axisymmetric (s = 1) Type I, II, and III Waves for Various Values of the Dimensionless Viscosity Coefficient of the Vessel Wall. Transmural Pressure and Axial Stretch are Both Equal to Zero

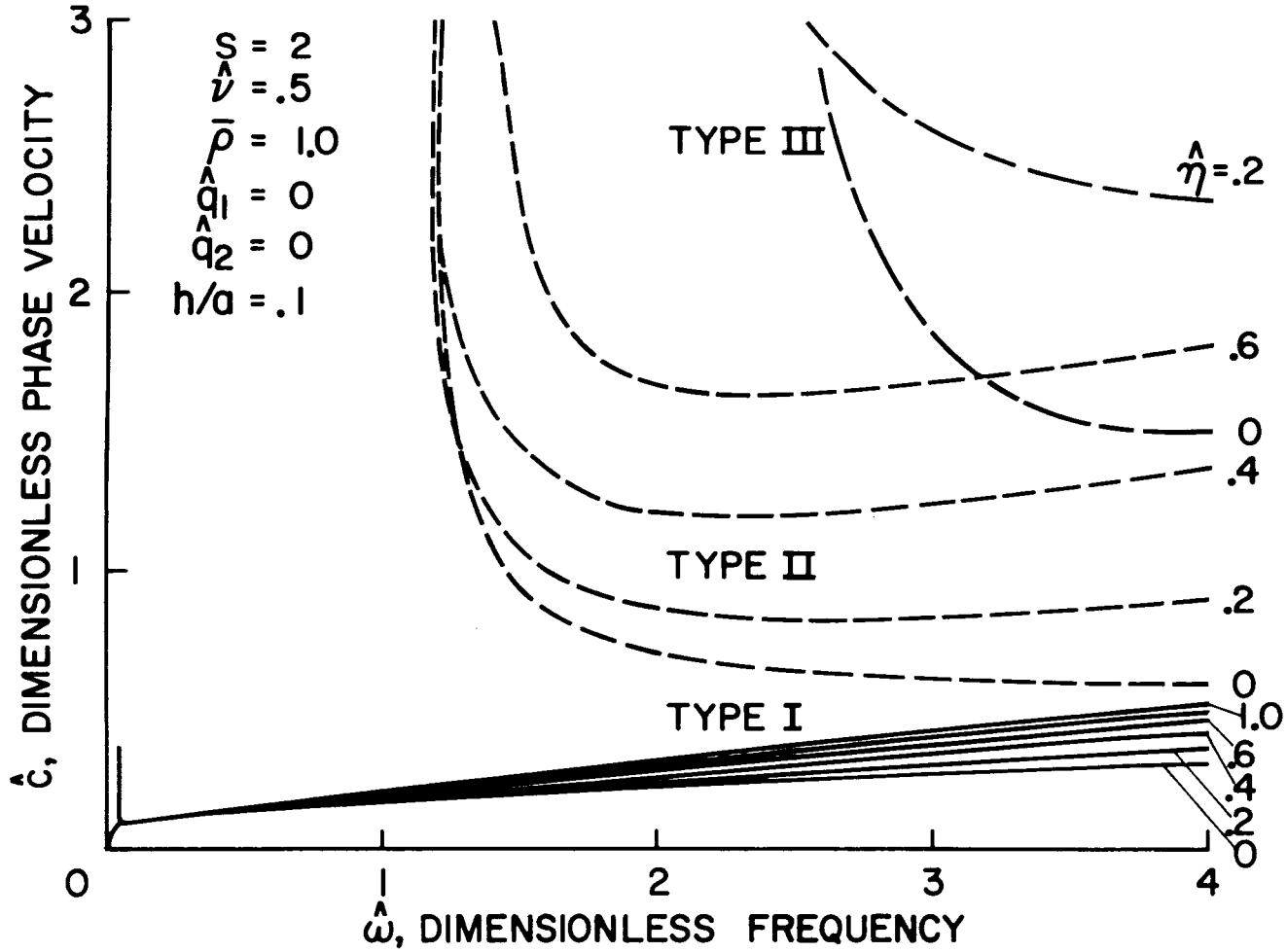

Figure 43. Viscoelastic Shell. Dispersion Curves of Non-Axisymmetric (s = 2) Type I, II and III Waves for Various Values of the Dimensionless Viscosity Coefficient of the Vessel Wall. Transmural Pressure and Axial Stretch are Both Equal to Zero. Below the Elastic Cut-Off Frequencies, $\hat{\omega} > 3.0$ for Type II and Type III Waves

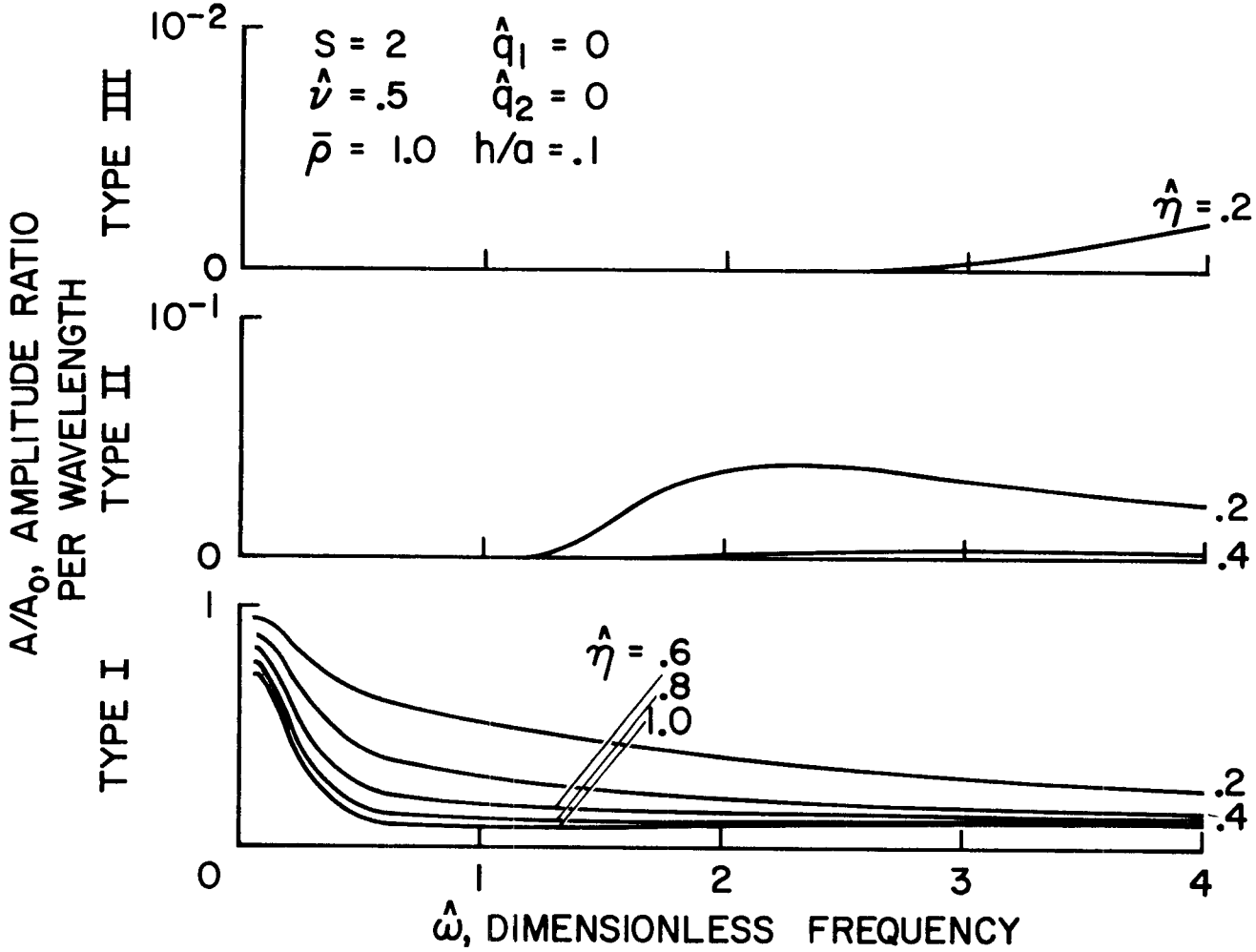

Figure 44. Viscoelastic Shell. Amplitude Ratio Curves of Non-Axisymmetric (s = 2) Type I, II, and III Waves For Various Values of the Dimensionless Viscosity Coefficient of the Vessel Wall. Transmural Pressure and Axial Stretch are Both Equal to Zero

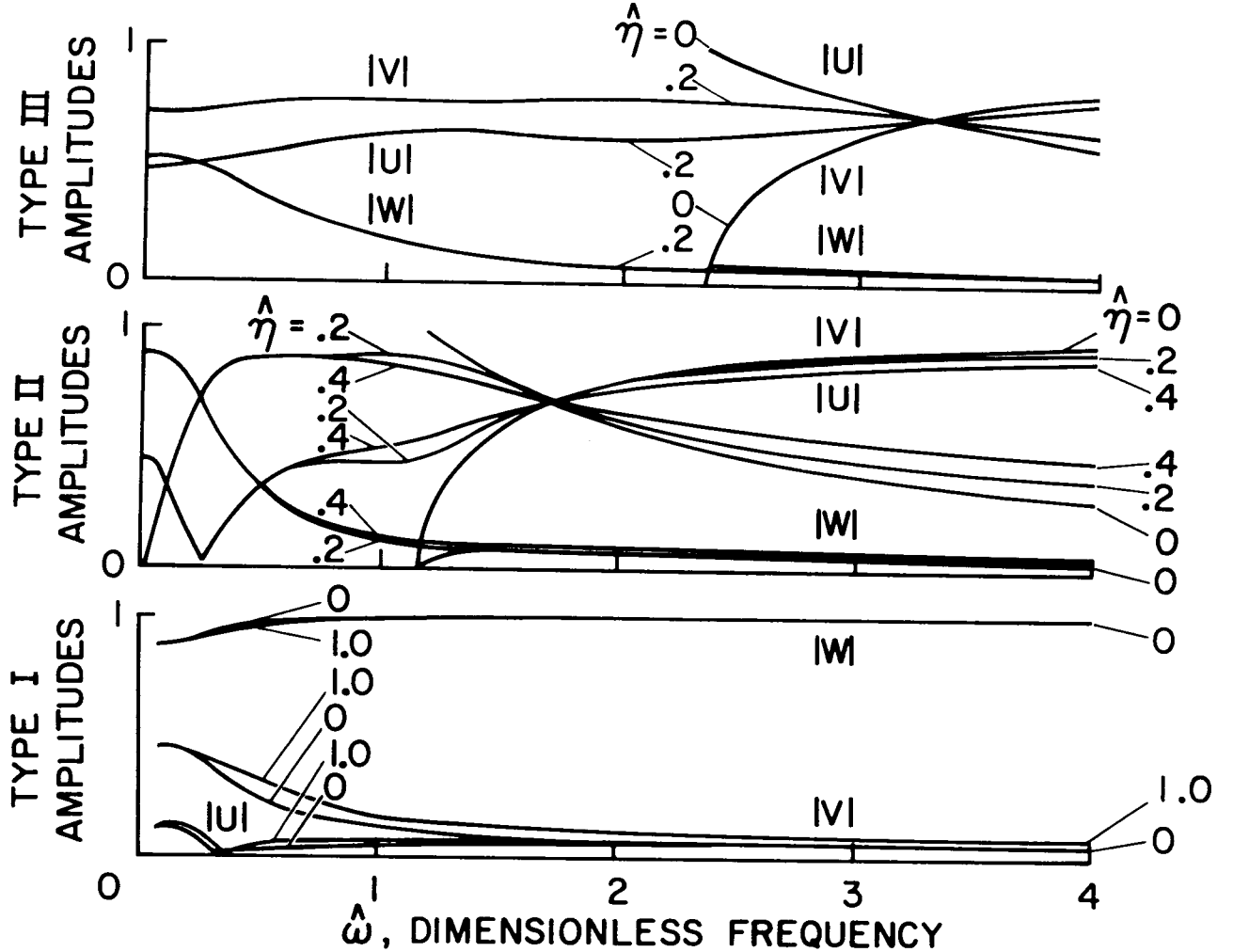

Figure 45. Viscoelastic Shell. Mode Shape Curves of Non-Axisymmetric (s = 2) Type I, II and III Waves for Various Values of the Dimensionless Viscosity Coefficient of the Vessel Wall. Transmural Pressure and Axial Stretch are Both Equal to Zero, with h/a = 0.1, $\bar{\rho}$ = 1.0 and $\hat{\nu}$ = 0.5

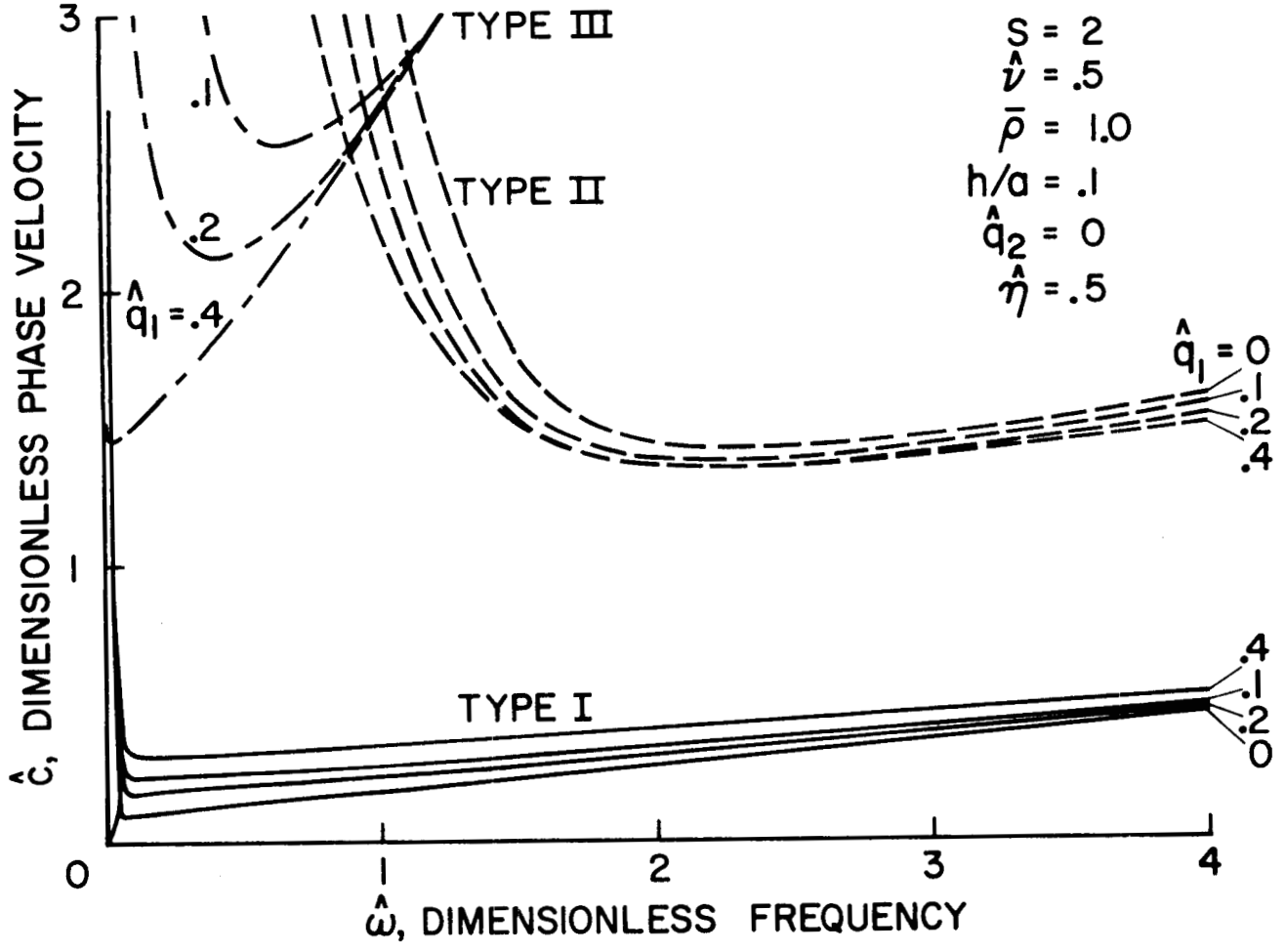

Figure 46. Viscoelastic Shell. Dispersion Curves of Non-Axisymmetric (s = 2) Type I, II and III Waves for Various Axial Stretches, Zero Transmural Pressure and Dimensionless Wall Viscosity Coefficient $\hat{\eta}$ = 0.5. Below the Elastic Cut-Off Frequencies, c > 3.0 for Type II and Type III Waves

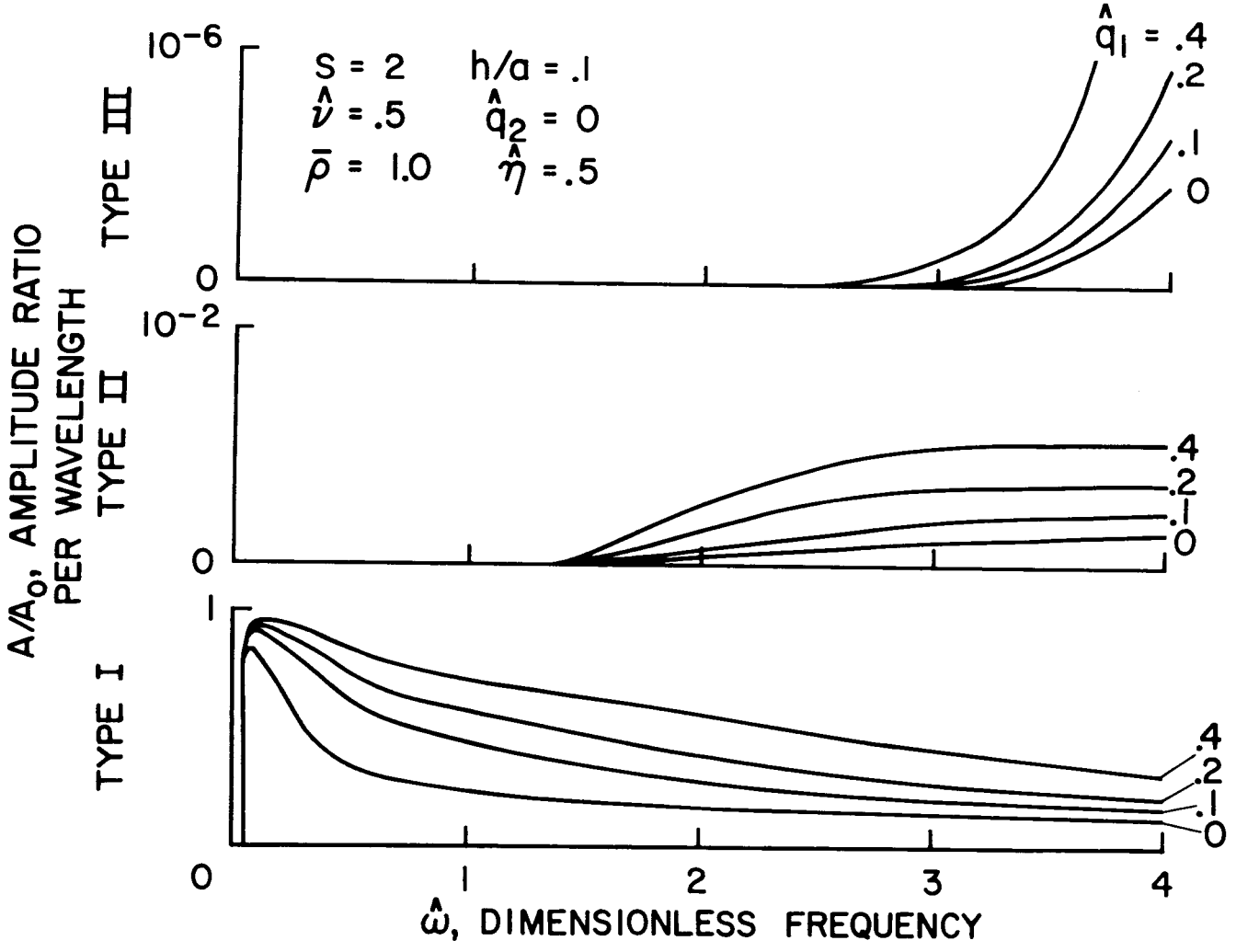

Figure 47. Viscoelastic Shell. Amplitude Ratio Curves of Non-Axisymmetric (s = 2) Type I, II and III Waves for Various Axial Stretches, Zero Transmural Pressure and Dimensionless Wall Viscosity Coefficient $\hat{\eta}$ = 0.5

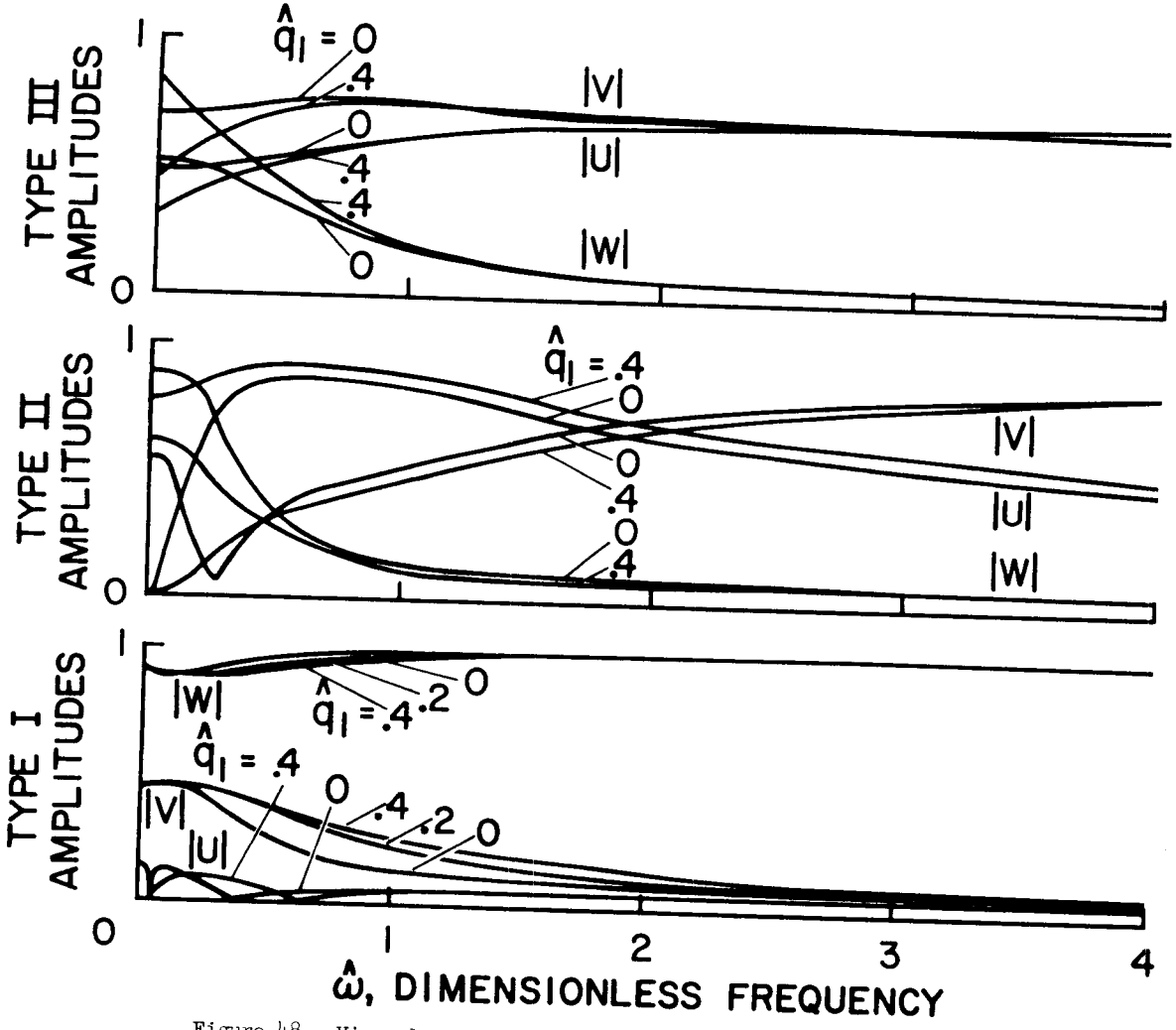

Figure 48. Viscoelastic Shell. Mode Shapes of Non-Axisymmetric (s = 2) Type I, II and III Waves for Various Axial Stretches, Zero Transmural Pressure and Dimensionless Wall Viscosity Coefficient $\hat{\eta} = 0.5$, with $h/a = 0.1, \bar{\delta} = 1.0$ and $\hat{\nu} = 0.5$

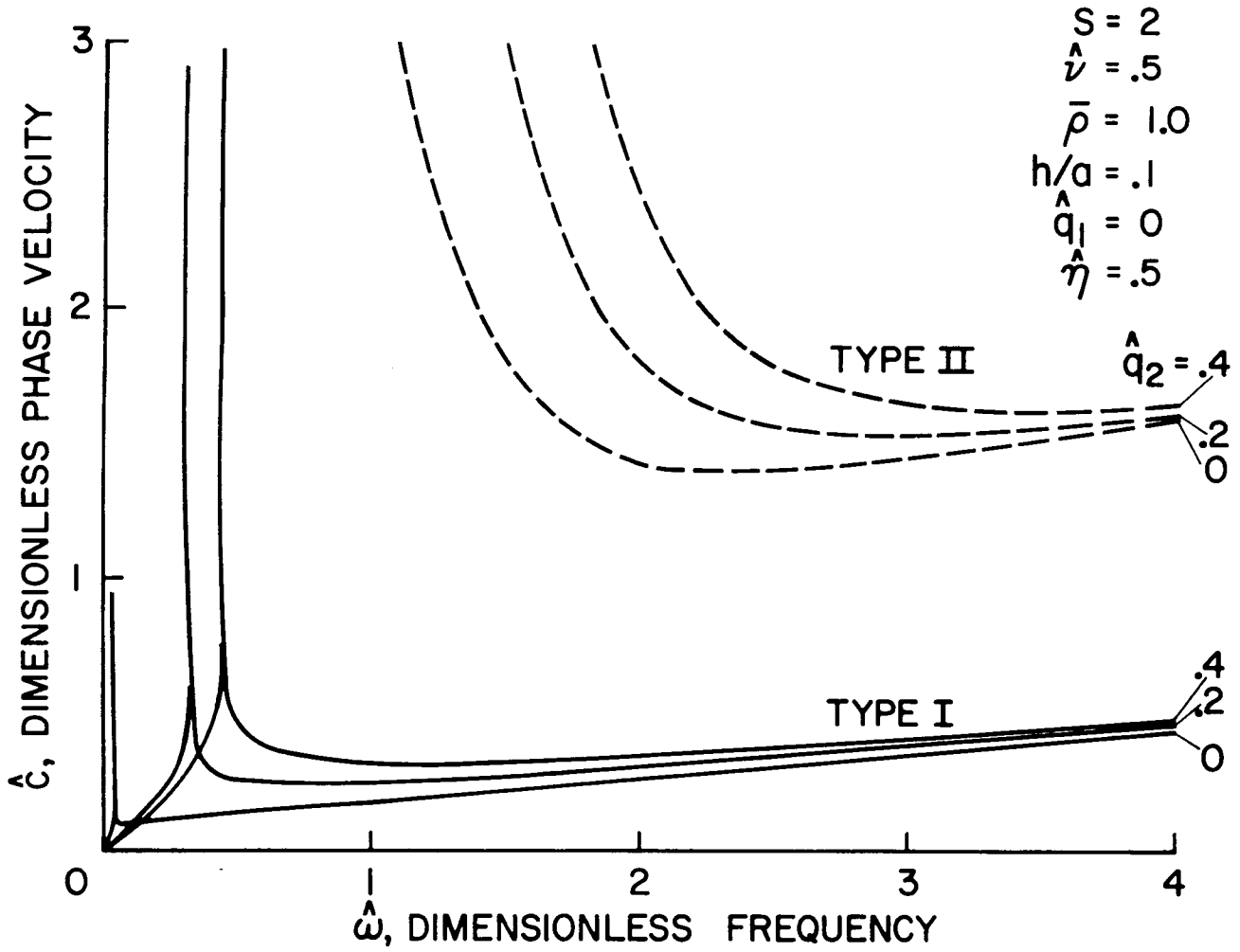

Figure 49. Viscoelastic Shell. Dispersion Curves of Non-Axisymmetric (s = 2) Type I, II and III Waves for Various Transmural Pressures, Zero Axial Stretch and Dimensionless Wall Viscosity Coefficient $\hat{\eta}$ = 0.5. Below the Elastic Cut-Off Frequencies, $\bar{c}$ > 3.0 for Type II and Type III Waves

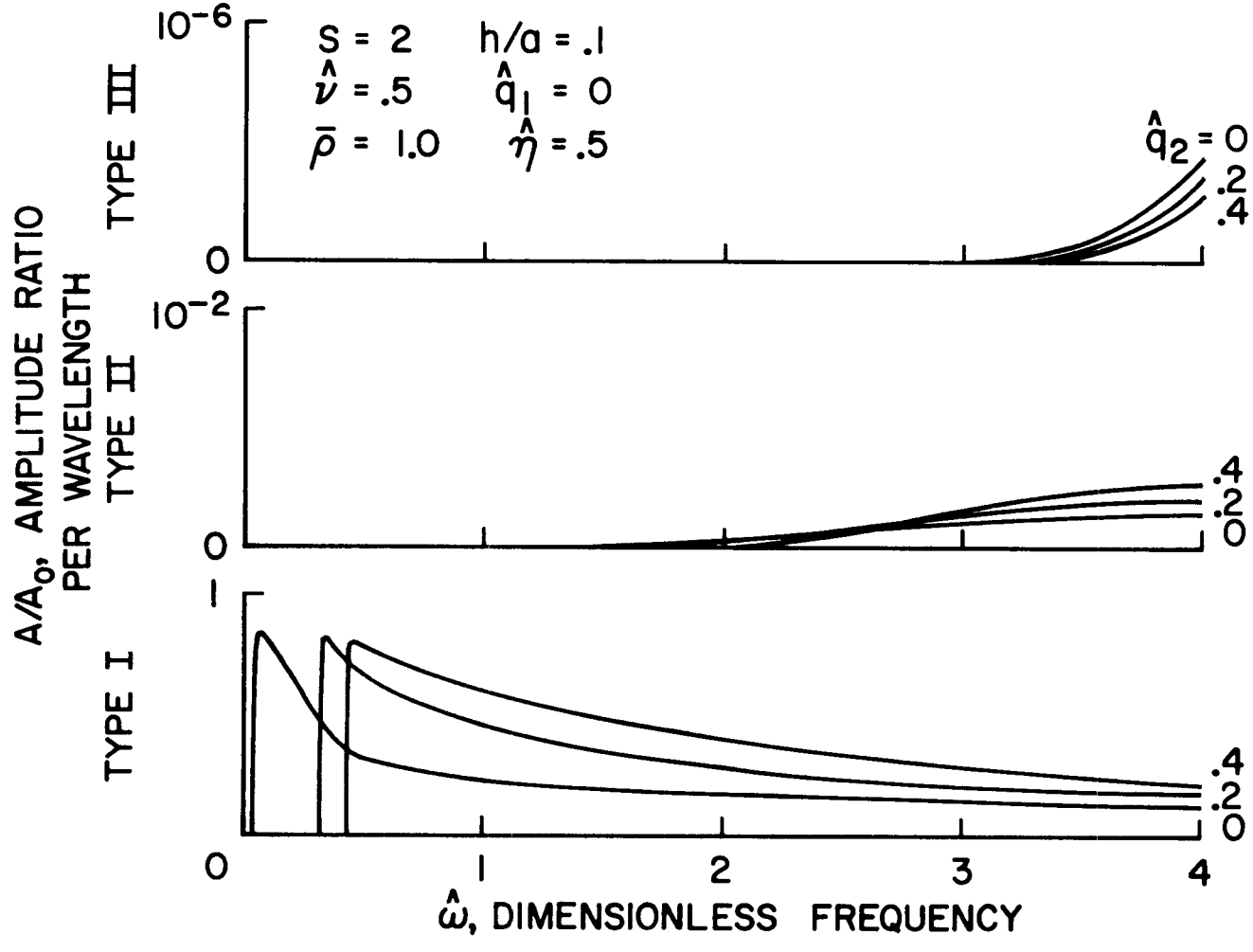

Figure 50. Viscoelastic Shell. Amplitude Ratio Curves of Non-Axisymmetric (s = 2) Type I, II and III Waves for Various Transmural Pressures, Zero Axial Stretch and Dimensionless Wall Viscosity Coefficient $\hat{\eta}$ = 0.5

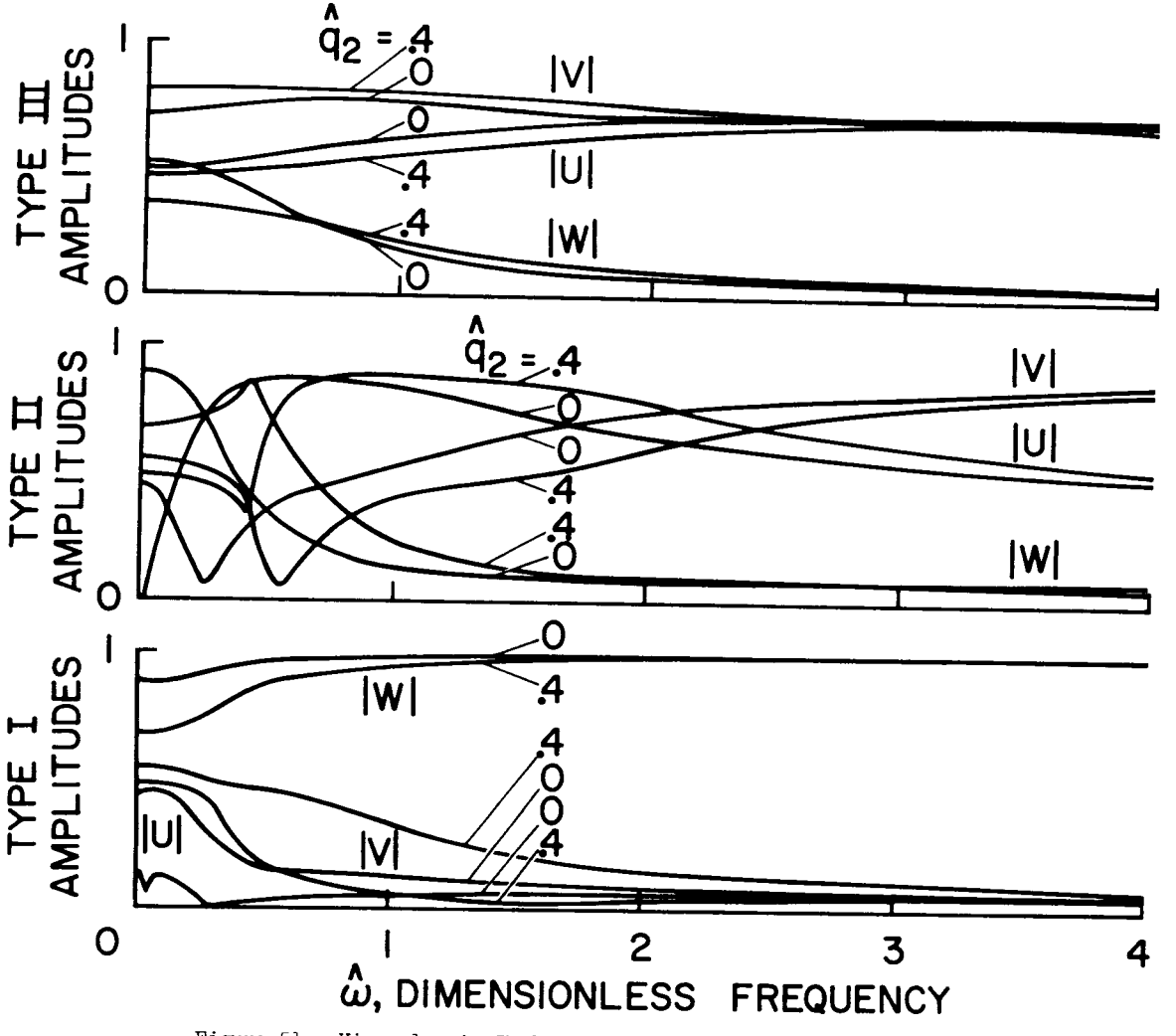

Figure 51. Viscoelastic Shell. Mode Shapes of Non-Axisymmetric (s = 2) Type I, II and III Waves for Various Transmural Pressures, Zero Axial Stretch and Dimensionless Wall Viscosity Coefficient $\hat{\eta}$ = 0.5, with h/a = 0.1, $\bar{\beta}$ = 1.0 and $\hat{\nu}$ = 0.5

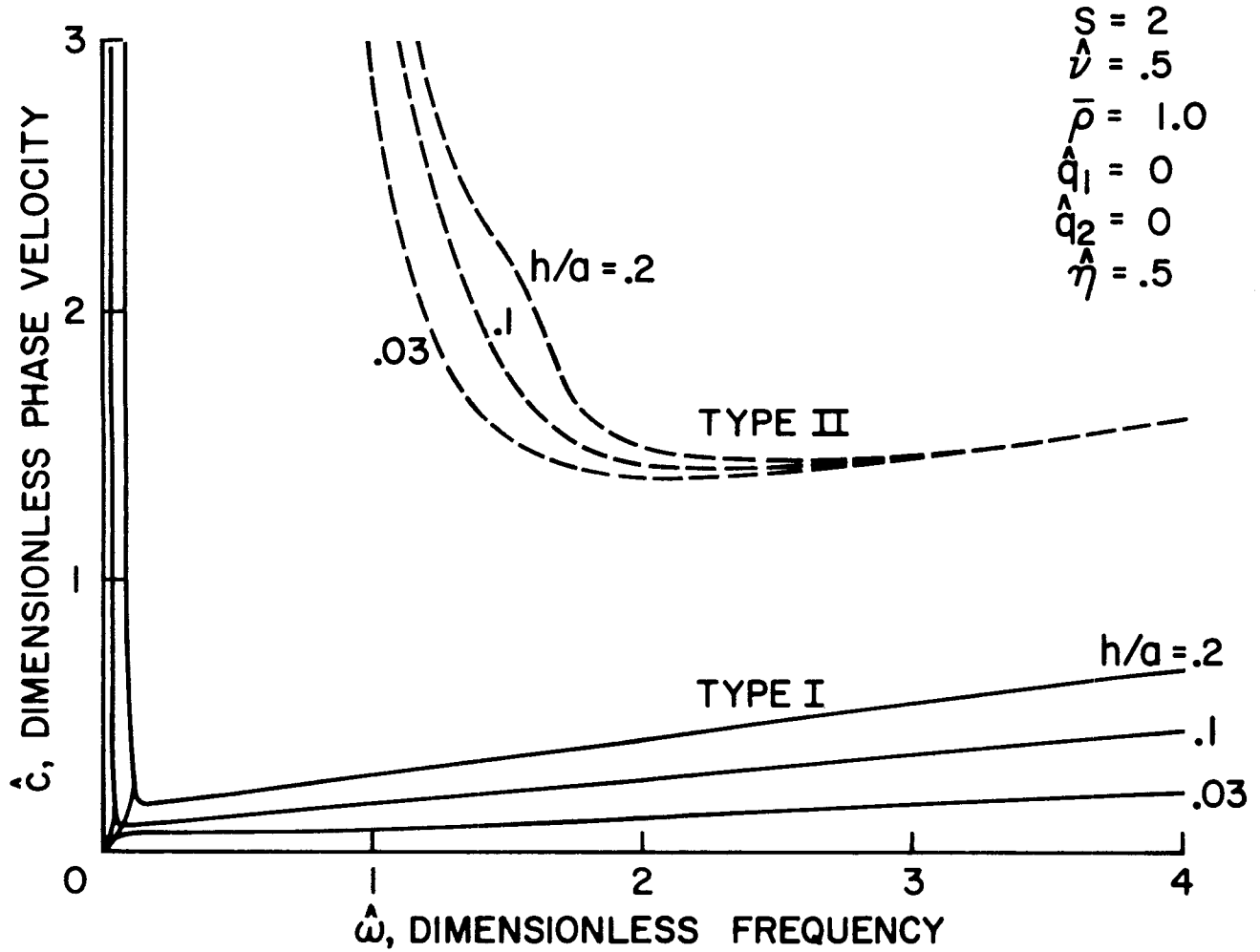

Figure 52. Viscoelastic Shell. Dispersion Curves of Non-Axisymmetric (s = 2) Type I, II and III Waves for Various Wall Thickness to Radius Ratios at Zero Transmural Pressure, Zero Axial Stretch and Dimensionless Wall Viscosity Coefficient $\hat{\eta}$ = 0.5. Below the Elastic Cut-Off Frequencies, $\bar{c} > 3.0$ for Type II and Type III Waves

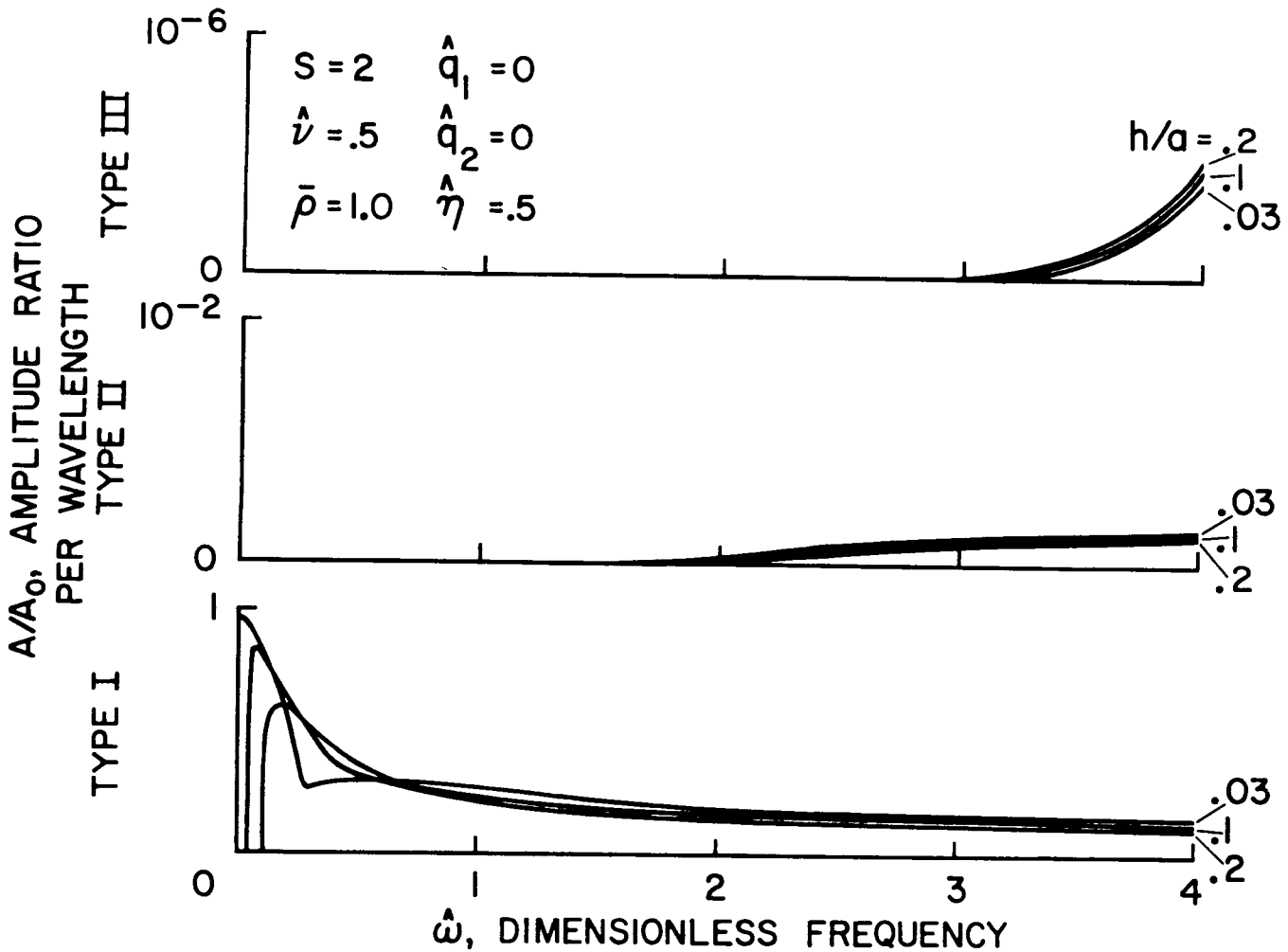

Figure 53. Viscoelastic Shell. Amplitude Ratio Curves of Non-Axisymmetric (s = 2) Type I, II and III Waves for Various Wall Thickness to Radius Ratios at Zero Transmural Pressure, Zero Axial Stretch and Dimensionless Wall Viscosity Coefficient $\hat{\eta} = 0.5$

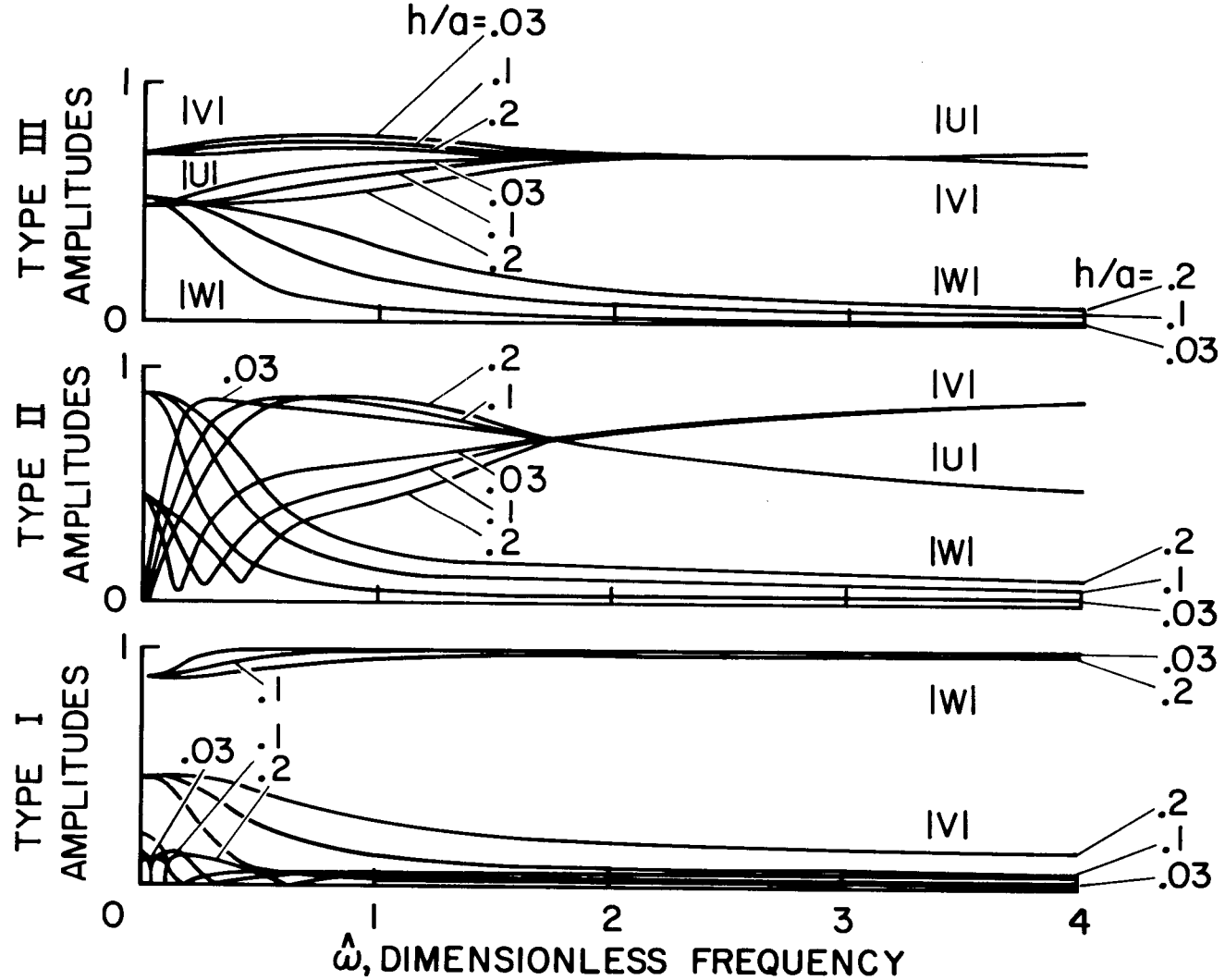

Figure 54. Viscoelastic Shell. Mode Shapes of Non-Axisymmetric (s = 2) Type I, II and III Waves for Various Wall Thickness to Radius Ratios at Zero Transmural Pressure, Zero Axial Stretch and Dimensionless Wall Viscosity Coefficient $\hat{\eta} = 0.5$, with h/a = 0.1, $\tilde{\rho} = 1.0$ and $\hat{\nu} = 0.5$